THESIS

STRENGTH AND CONSOLIDATION BEHAVIOUR OF REMOLDED REDBED CLAYSTONE FROM THE MAE MOH LIGNITE MINE

Submitted by

Abhishek Dongol

Department of Civil and Environmental Engineering

In partial fulfillment of the requirements

For the Degree of Master of Science

Colorado State University

Fort Collins, Colorado

Fall 2024

Master's Committee:

Advisor: Christopher Bareither
Co-Advisor: Kuo-Chieh Chao

Joseph Scalia IV
Sean Gallen

ABSTRACT

STRENGTH AND CONSOLIDATION BEHAVIOR OF REDBED CLAYSTONE FROM THE MAE MOH LIGNITE MINE, LAMPANG

The objective of this study was to evaluate the strength and consolidation behavior of remolded Redbed claystone within a critical state framework. In 2018, a slope failure occurred in the northwestern waste rock pile at the Mae Moh Lignite mine in Thailand. A hypothesis of the failure was the slaking of the claystone at the base of the piles resulted in substantial strength loss relative to the intact blocky mass of the as-placed claystone waste rock. Consolidated undrained (CU) triaxial compression tests were conducted on 38-mm-diameter samples of remolded and intact specimens of the claystone. Remolded specimens were prepared from slurry and consolidated to form normally consolidated clay specimens. One dimensional consolidation tests were conducted on remolded and intact claystone specimens prepared in a similar manner. The remolded specimens exhibited contractive, strain-softening behavior in undrained shear typical of normally consolidated clays with effective friction angles ranging between 20° and 21° (M = 0.8). The intact claystone exhibited stiff, dilative behavior in undrained compression with higher shear strength parameters (M = 1.11-1.66). One dimensional consolidation tests on remolded specimens yielded only virgin compression, whereas similar tests on in-tact specimens yielded only negligible recompression. The claystone transitioned from a strong, stiff, dilative material to a soft, contractive soil with a drastic reduction in strength and an increase in compressibility. A modified Cam Clay model was parameterized from the triaxial and consolidation results to model the shear behavior of remolded Redbed claystone. The model predictions showed good agreement with observed laboratory test data, which supports the use of the model to in advanced stress-deformation modeling of the waste rock piles at Mae Moh Lignite Mine.

ACKNOWLEDGMENTS

Although the cover page bears my name, this thesis is the result of support of many individuals. First, my deepest gratitude and appreciation to my, Dr. Christopher Bareither, who has supported me in every facet of my master's research, whether it be logistics, lab work, brainstorming ideas or writing. This work would not have been in its current state if not for his support over the past year.

I would also like to extend my gratitude and appreciation to Dr. Geoff Chao. I am immensely grateful to you for igniting a passion in soil mechanics. Your lectures and the discussions we've had in AIT were very inspiring. You have helped me grow as a scholar and an engineer.

I am also grateful to Dr. Joseph Scalia, CSU, Dr Sean Gallen, CSU, and Dr Avirutt Puttiwongrak, AIT for serving on my thesis committee.

A note of thanks to Mr. Apipat Chaiwan, Ms. Ananya Chaladthanyakit and the slope stability team at Mae Moh for facilitating our field visit in 2023 and helping in collecting and shipping samples of the claystone. I would also like to mention Ms. Peetiya Nidhinandhana for her guidance in the initial phases of this research.

Thank you Kittisak (Whale) for managing the shipment of the claystones from Thailand to the U.S. and Sam for helping in transporting the samples to CSU.

Thank you, GTE family for all the good times, tours, and parties. Thank you, Khun Au and P Apple for all the administrative support.

Sam, Rayson and Emily; there was never a dull moment in the office, thank you all for always keeping things lively.

Lastly, I would like to thank my family for always having my back, for supporting me through the tough times and celebrating my wins. Your blessings and unwavering support have made me who I am today.

TABLE OF CONTENTS

LIST OF TABLES

LIST OF FIGURES

Chapter 1 - Introduction

1.1. Background of the Study

Slope instability issues have been a recurring problem since 1984 within the waste rock piles at Mae Moh Lignite Mine, Lampang, Thailand. Waste rock piles are large man-made structures composed primarily of the rock and soil that exist between the coal seams at the mine and have no economic value. Waste rocks comprise of fragmented rock with particle sizes ranging from fine sand to boulders, depending upon formation characteristics and extraction methods. At the Mae Moh Mine, the primary waste rock is claystone derived from four distinct lithologies: Redbed Claystone from the Huai Luang formation, and overburden, inter-burden, and under-burden Claystones from the Na Khaem formation.

The stability of the northwestern waste rock piles has posed considerable challenge to the mine, with a large landslide occurring in 2018. Forensic investigations have indicated that a layer of weak material formed within the waste rock due to slaking of the claystone may have been the cause of failure. More specifically, these past studies suggest that undrained loading of the weak layer at the base of the waste rock pile could be the instability trigger. Thus, the evaluation of waste rock pile stability in the forensic analyses as well as for current site operations require a broader understanding of the undrained shear behavior of the slaked waste rock.

Slaking of the parent claystones within the waste rock piles may ultimately reduce the rock to a remolded, normally consolidated soil composed of the constituent clay particles. Breakdown of the claystone at the base of the pile has been hypothesized as the culprit for the waste rock pile slumps. Previous studies at Asian Institute of Technology (AIT) (eg., Nidhinandana, 2022, Zaman, 2023) have attempted to evaluate the stability of the dumps based on shear strength and hydraulic properties.

However, more advanced modeling of landslide mechanisms requires information on the stress-deformation behavior of the claystone. To address this gap in knowledge, mechanical properties, and behavior of slaked Redbed claystone were evaluated under a critical state framework.

1.2. Problem Statement

A large-scale slope failure occurred in 2018 in the northwestern waste rock pile at Mae Moh Lignite Mine. From previous studies, slaking of the waste rock was shown to have an impact on the stability of the dumps. A detailed strength characterization of the intact waste rock and remolded state has not been conducted. This analysis is informative to the evaluation of the current landslide and any future works regarding the waste dump.

This thesis focuses on the strength characteristics and the stress-strain behavior of a normally consolidated clay formed due to slaking of the parent waste rock. This research includes testing of slaked Redbed claystone of the Huai Luang formation as well as intact claystone specimens for comparison.

1.3. Objectives and Scope of Work

The objective of this study was to evaluate the strength and consolidation behavior of the Redbed claystone when slaked and remolded. According to work by Nidhinandana, (2022), Redbed claystone exhibited the highest slaking potential and highest reduction in shear strength among the various waste rock at the Mae Moh Mine. From their studies, the basal layer of the dump was hypothesized to be composed of material with strength comparable to that of slaked Redbed claystone. The operating history of the mine also indicates that Redbed Claystone constitutes the major volume of the base of the waste dump. Thus, this thesis focused on laboratory testing of undrained shear and consolidation behavior of remolded slaked Redbed (RB) claystone.

The scope of this research included the following:

- Review existing literature and documents regarding the slope failures at the waste dumps in Mae Moh Lignite Mine;
- Collect samples of the Redbed claystone from the site;
- Conduct consolidated undrained triaxial compression tests on intact and remolded samples of slaked claystone;
- Conduct one-dimensional consolidation tests on intact and remolded samples of slaked claystone; and
- Evaluate strength-deformation characteristics of the claystone within the framework of critical state soil mechanics.

Chapter 2 - Literature Review

2.1. Mine Waste

Mine waste is the biproduct of mining operations. Along with valuable material from mines (example: metal ores, coals, minerals etc.), unwanted materials such as rock, soil, and non-valuable minerals are also extracted. The two most common and abundant uneconomical materials (i.e., mine wastes) are waste rock and tailings. Waste rocks are larger sized material that are generated in the primary stages of mining such as excavation and blasting, to access the ore body. Waste rock can include stripped soil, partly weathered rock overburden, and / or non-ore bearing rock blasted and removed to access the ore body. Blight (2011) defines tailings as the fine-grained remnants leftover after crushing and extracting the minerals from their ores.

2.1.1. Mine Waste Rock

Waste rocks are unmineralized rocks, and rocks with low mineral grades. The host rock and the rocks surrounding the ore body determine the characteristics of the waste rock. Although waste rock consists of competent and durable particles (with sizes ranging from 2m to silt and clay sized particles), weaker material can also be present which are a cause of stability concerns. (Daniel, 1993).

Large volumes of overburden and inter-burden rocks and sediments are extracted in the process of coal mining. Coal mining often is done by draglines due to the continuous nature of coal beds. Coal wastes are typically sedimentary rocks consisting of sandstones and/or shales. The mine spoils are frequently reclaimed as mine develops. (Daniel, 1993).

2.1.2. Mine Tailings

Tailings refers to the residual material left over after the extraction of economic products through milling and processing. Ground rock and effluents from the mineral extraction process make up tailings. The processing methods can vary, involving techniques such as mechanical sorting,

crushing, grinding, and subsequent physical or chemical processes. Essentially, tailings comprise all the constituents of the original ore except for the primary extracted metal or mineral.

2.2. Mine Waste Storage

The methods to store mine waste vary depending on whether they are tailings or waste rock. Waste rock are stacked in piles or dumps whereas tailings are stored in impoundments that typically require natural and/or constructed containment (e.g., embankments).

2.2.1. Waste Rock Dumps

The waste rock generated from mining operations are typically stored by forming piles where the waste rocks are dumped and spread over a large area. These waste rocks are stockpiled at a site that is typically close to the active mine. According to Zevgolis (2018), waste rock piles are composed of dry overburden material as bi-product of mining operations to access the ore body.

Figure 2-1 shows the configurations of waste rock piles according to their disposal methods and Table 2-1 lists the characteristics associated with disposal method. Waste dumps are categorized according to the disposal method and topography of the disposal terrain. If waste rock is dumped over an advancing face, the method is termed top-down dumping. Bottom-up dumping involves dumping the waste rock on top of the existing level and spreading them by use of bulldozers or spreaders. The topography of the dumping area may be inclined or flat.

2.3. Failure Mechanisms of Waste Rock Piles

Slope failures in waste rock piles develop in slopes constructed too steeply above a certain height or because loading conditions were not appropriately accounted for in design (e.g., rise in the phreatic surface; low strength foundation materials; earthquake loading, etc.).

Figure 2-2 shows a cross-section of a "first-time failure " that occurred in a waste rock dump. The waste rocks at the dump ranged from 300 mm to particles <0.075 mm in size. A thin layer of clay

was present along the foundation of the rock pile. The failure was found to have occurred along a horizontal plane. At the toe of the waste rock pile, the waste rock was pushed horizontally and then upwards.

The geometry of a typical "first-time failure" in waste rock piles is shown in Figure 2-3. Based on physical model experiments, first-time failures were observed to involve formation of an active wedge that displaces the passive wedge along a horizontal plane in the foundation (G. E. Blight, 2009).

Waste dumps that are advanced over a failed section typically tend to fail again. A section of a dump that failed repeatedly is shown in Figure 2-4. It was observed that subsequent failures in a rockfill recur in the same position. As opposed to first-time failures, the failure surface is composed of multiple shear surfaces through the rockfill.

A schematic of a subsequent failure over a previously failed section is shown in Figure 2-5. The failure surface in this case is composed of alternating active and passive wedges and is much more complex than a first-time failure.

2.4. Claystone

Chemical weathering of igneous and metamorphic rocks form clay minerals whereas mechanical disintegration of hard rocks form silt particles which lithify to form mudrocks. Clay and silt sediments are transported and deposited by rivers into lakes and seas. As the sediments are gradually buried, the overburden and temperatures increase with depth result in compaction and hardening to form mudrocks (Kanji et al., 2020).

Common terms associated with fine grained sedimentary rocks are included in Table 2-2. The naming convention of mudrocks has been a matter of confusion in literature because of definitions that are inconsistent and changing with time (Potter et al., 2005). Considering the multitude of terms and differences between some terms being unclear (for example, siltstone versus mudstone),

establishing terminology that eliminates any confusion about the material one is working with is necessary.

Claystones are lithified and non-fissile mudrock. In order to be considered a claystone, the rock unit must consist of up to 50% clay (Aird, 2019). Claystone generally contains one of the following clay minerals: illite, smectite (montmorillonite), or kaolinite. In addition, claystones can contain smaller or larger proportions of chlorite and rare glauconite (Haldar & Tišljar, 2014). In this thesis, the term claystone is used to describe the clay bearing sedimentary rocks extracted from the Mae Moh Lignite Mine, Lampang, Thailand.

A common problem encountered in clay bearing rocks such as claystones is degradation in structure, strength, and durability due to weathering. Unweathered claystones are hard and stiff, but weathering can lead to significant loss in strength. Slaking, which is degradation due to alternate wetting and drying cycles of rocks, is a major contributor to the disintegration process.

According to Blatt (1982), about two thirds of the earth's stratigraphy and 60% of exposed sedimentary rocks at the surface of the earth are argillaceous rocks (e.g., Mudrocks and Shales). Natural slaking of argillaceous rocks lead to considerable challenges, most notably slope stability issues along highways(Gautam & Shakoor, 2013).

2.5. Slaking of clay bearing rocks

The degradation of argillaceous rocks due to slaking and weathering effects have been extensively studied in the past. According to Seedsman (1986), compression of entrapped air and osmotic swelling of expansive minerals are the two main mechanisms for slaking of clay shales associated with coal strata.

Slaking of clay-bearing rocks under natural conditions was studied by Gautam and Shakoor (2013). Five samples each of claystone, siltstone, mudstone, and shales were exposed to variable

climactic conditions ranging from cold winters to warm and humid summers in Ohio, USA over the course of a year. Slaking of each. Slaking of each rock type was quantified to determine the "disintegration ratio" proposed by Erguler and Shakoor (2009). The durability of claystone was found to the least followed by mudstones and then siltstones. Shales would display varying degrees of slaking based on their mineral composition. The slaking of claystones initiated on exposure to climatic conditions and disintegrated rapidly.

Landslides occurring in tertiary mudstones in Japan revealed that the mudrock bedrocks weathered into clay with time. Nakano (1967) made observations that rapid disintegration of the rocks occurs not just due to wetting but more so due to alternating cycle of wetting and drying. They have stated that mudstone may easily deteriorate, especially within the zone of fluctuating water vapor pressure or fluctuating groundwater level within geologically fractured zones.

Nunt-jaruwong (2006) did extensive studies on the Patonga Claystone in Sydney, Australia where that solid rocks were observed to breakdown within a matter of days on exposure to the atmosphere. Of the samples they tested, 67% yielded a jar slake index value of 1 as shown in Figure 2-6. A jar slake test is a qualitative test of slake-potential where intact pieces of rocks are immersed in water for 24 h and the condition is inspected visually. The Jar Slake Index (I_j) ranges from 1 to 6, and qualitative descriptions of I_j based on the behavior during test are detailed in Table 2-3. From the experiments by Nunt-jaruwong (2006), oven dry specimens displayed more disintegration, which was attributed to the fact that more air voids are available in dry samples that become pressurized by the capillary pressure when immersed in water.

Pineda et al. (2014) evaluated the degradation of Lilla claystone due to cycles of change in relative humidity.. They examined the progressive degradation of the mechanical properties of Lilla claystone. This situation of changing humidity is common in open excavation and tunnelling. The cyclic change in relative humidity led to irreversible volumetric changes followed by progressive

fissuring of the rock. In addition, the fissuring behavior was found to be faster when liquid water (as opposed to water vapor) was used to wet the claystone. The samples experienced loss in stiffness and tensile strength.

Botts (1986) has described the transitional behavior of clay shales, with four distinct stages of as:

1. Rock-like mass in which the strength was controlled primarily by the orientation of and strength along the intact fissures;
2. Partially softened rock-like mass with the strength controlled primarily by the strength and orientation of soft, filled fissures;
3. Highly softened mass consisting of a matrix of soft clay surrounding stiff, intact cores;
4. Fully softened, remolded clay

Czerewko and Cripps (2001) used a modified slaking test to evaluate the durability of mudrocks. Their test involved preparing 40 to 50 mm sided blocks of mudrock which were then dried at 60 °C for 72 h and then immersed in water. The samples were assessed regularly for up to 24 h. They then compared their results to the third cycle slake durability test. For most claystones, seatearths[1], and mudstones, a change in durability was observed between the first and third cycles.

A series of waste dump instabilities in coal mines in southwest Turkey was investigated by Ulusay et al. (1995). The waste rocks mostly consisted of marls, a sedimentary rock consisting of clay and lime. Amongst other factors, slaking of the waste rock was a contributing factor to the slope stability issues. Figure 2-7 shows the results of slake durability tests on the waste rock from the mines. In a slake durability test, the rock samples are subject to alternating cycles of wetting and oven drying.

[1] Seaterth is a british coal mining term used to refer to sedimentary rocks underlying coal seams.

Mass of rock retained after each cycle is recorded and the ratio between final and initial mass of rock is the durability index. The standard 2-cycle slake durability test on these marls yielded a value of 90%, which implies the rock had high durability according to the classification system proposed by Franklin and Chandra (1972) . However, the rocks did exhibit a considerable loss in structure after a third cycle of wetting and drying.

A series of slake durability tests were performed on red mudstones from a coal mine by Qi et al. (2015). The standard 2-cycle slake durability index for these mudstones was 7.19%, a durability classification of very low. Figure 2-8 shows the transition of the mudstones from intact rock to remolded clay over eight (8) cycles of wetting and drying. Wetting was observed to cause a more intense loss in structure than drying.

Bell et al. (1997) performed tests on fresh and weathered mudstones obtained from British coal mines. Breakdown of these mudstones were attributed to slaking and expansive clay minerals. It was found that at least two cycles of slake durability test is required to describe breakdown of mudrocks.

2.6. Strength Loss due to Slaking

The disintegration of mudstones due to slaking has been shown to produce a reduction in shear strength. Various studies have quantified loss via laboratory strength tests (e.g., direct shear or triaxial compression) and Mohr Coulomb strength parameters that include a cohesion intercept and internal angle of friction.

One of the earliest study was done by Chandler (1969), who evaluated changes due to weathering of mudstones. Chandler (1969) used the weathering scheme proposed by Skempton and Davis (1966) to characterize weathering from Zone I to IV, whereby zone I is unweathered mudstone and Zone IV is fully weathered where clay sized particles may account for up to 50% of the soil.

Chandler (1969) conducted consolidated drained and consolidated undrained triaxial compression tests as well as K_o (i.e., laterally constrained) consolidation tests. Relationships of deviator stress (i.e., difference between princip) and volumetric strain versus axial deformation in consolidated drained triaxial compression tests are shown in Figure 2-9. The fresh mudstones (Zone 1) showed a pronounced peak followed by strain softening to a residual value, which is similar behavior to an overconsolidated (OC) clay. In contrast, fully weathered mudstone (Zone IV) displayed stress strain behavior that was similar to a normally consolidated (NC) clay that has no defined peak strength. The reduction in strength is shown by the transition from Zone 1 to Zone 3 to Zone 4 in Figure 2-9.

Tests performed by Cripps (1987) on degraded Cretaceous mudrocks from sites of unstable slopes show properties of remolded clays with cohesion equal to or approaching zero. In addition, effective stress friction angles were less than the peak value for undisturbed clay and may approximate the fully softened strength. The "fully softened strength" is the strength of clay once weathering and degradation reduces the material (e.g., soil or mudrock) to a state devoid of any previous stress history and diagenesis. Further discussion on fully softened strength is presented subsequently.

According to Cripps and Taylor (1981), interparticle bonding are destroyed by unloading and weathering thus reducing mudrocks into an effectively remolded state. This degradation (or softening) is what ultimately leads to reduction in strength and deformation modulus. Weathering reduces the angle of internal friction to a fully softened value through the development of progressive small-scale failures in the weathering mudrock. Softening of mudrocks into normally consolidated clays occurs with disregard to the age and origin of the mudrocks.

Sharma et al. (2017) conducted direct shear tests on crushed mudstone where the wetting and drying could be simulated under stress in the shear box. The mudstones were found to exhibit considerable creep displacement during both wetting and drying phases under the constant shear stress conditions. It was observed that creep was more significant during the drying phases than in the

wetting phases. Creep displacement was found to accumulate with progressive wetting and drying cycles. The peak stress ratio was also observed to decrease with increasing wetting and drying cycles.

Wei et al. (2022) studied the reduction in shear strength and permeability of mudstones granules considering weathering processes. Direct shear tests were performed on samples that underwent wet-dry cycles. It was found that the peak shear strength of the mudstones decreased with increasing wet-dry cycles regardless of if samples were wet or dry. Dry specimens exhibited strain hardening behavior for dry specimens, whereas when samples were wetted, the shear mode changed to strain softening.

Tests conducted by Botts (1986) on Pierre Shale show a drastic reduction in strength by a single cycle of partial drying followed by rewetting under confinement. Figure 2-10 summarizes the change in stress-strain behaviour as the clay-shale softens from intact rock to a remolded state. Softening reduces both effective friction angle and the cohesion intercept of Pierre Shale.

According to Yoshida (1990), mudstones do not disintegrate simply on immersion under in-situ moisture content. When mudstone is dried beyond a critical value of dryness, slaking begins immediately upon contact with water. Cyclic wetting and drying promotes slaking significantly and the end-product of slaking is a remolded clay or silt with a high-water content.

Literature available on the topic of slaking of mudstone and strength reduction tends to point towards the fact that slaking destroys the structure of the rock and reduces the material to a remolded matrix of constituent particles (clay or silt) devoid of any stress history. Thus, the resulting material is effectively a newly formed, normally consolidated soil. This process is referred to as softening and the strength of a material that has undergone complete strength loss has been termed "fully softened shear strength (FSS)". Fully softened shear strength has been studied extensively in overconsolidated clays and in some mudstones. Overconsolidated clays and mudstones exhibit similar behavior on wetting

and drying, whereby the materials undergo slaking and transform into remoulded normally consolidated clays.

From a geological perspective, mudrocks and overconsolidated clays are similar (Cripps and Taylor 1981). Interparticle bonds are destroyed by progression of weathering due to which the material is returned to a normally consolidated, remolded condition. As a result of softening, strength and deformation modulus are reduced. According to literature compiled by Castellanos (2014) the fully softened shear strength is the lower bound which the strength of mudstones can attain due to weathering .

2.7. Fully Softened Shear Strength

Roscoe et al. (1958) discussed the yielding of soils via critical state soil mechanics, whereby the critical state of a given soil is defined for a given value of effective stress in which the soil deforms under constant shear stress at constant void ratio and constant velocity. Regardless of the original stress history, i.e., if the material is normally or over consolidated, the material will ultimately attain a critical state with continued deformation.

According to Skempton (1970) , sensitive clays with bonding and preferred particle orientation exhibit complex behavior, and the determination of critical state is not an easy matter. In sensitive clays, continued deformation can lead to a residual shear strength, which is shown in by the idealized behavior in Figure 2-17. In normally consolidated clays, a peak strength can be measured before reduction to a residual value. The residual shear strength is a characteristic property of the soil independent of stress history.

Skempton (1970) first defined fully softened shear strength as the drained strength of a clay in its normally consolidated state. Fully softened strength was stated as the practical approximation of the critical state (Skempton 1970).

According to Castellanos and Brandon (2019), the fully softened shear strength as the drained strength of a clay in normally consolidated state. This strength is applicable in first time slope failures in cuts in stiff clays, mudstone slopes and embankments built using high plasticity clays. According to Stark & Fernandez (2020) the fully softened shear strength is the strength of soils that remains following removal of the strengthening effects of overconsolidation, compaction or desiccation by weathering, slaking, free-thaw, deformation etc.

2.8. Measurement of Fully Softened Shear Strength.

Fully softened shear strength should be measured using reconstituted, normally consolidated clay specimens (Skempton 1977). According to Burland (1990), a reconstituted clay is one that has been mixed at a water content greater than the liquid limit. To eliminate the effect of aggregation due to diagenetic bonding present in heavily over consolidated clays, mudstones and shales, materials must be thoroughly disaggregated such that clay particles do not clump together.

Stark and Eid (1997) adopted a process where shales and mudstones were air-dried, ball-milled and passed through No. 200 sieve (0.075 mm). The fines are then hydrated to a liquidity index of 1.5. The fully softened shear strength was then measured using a ring shear device.

According to the US Army Corps of Engineers (USACE), the fully softened strength envelop is non-linear with zero (0) effective cohesion intercept. The nonlinearity of the strength envelope warrants measuring the strength at multiple stress levels (i.e., confining stress or vertical stress). It is recommended that tests conducted at five stress levels are enough to define the strength envelope. At a given confining stress, the fully softened strength is measured by the secant friction angle at the point corresponding to the confining stress.

To disaggregate clay shale samples, a technique called "blenderizing" was developed in the 1960s and 1970s. This procedure was developed for direct shear testing, but the principle remains the same for triaxial testing. A broken / shredded sample of clay shale is immeresed in de-ionized water

for at least 48 h. The resulting slurry should have a water content above 300%, or greater than two times its liquid limit, whichever is greater. A mechanical blender is then used to "blenderize" the slurry for 10 minutes. The slurry is then passed through a No. 40 sieve after mixing it.

According to Wang (2019), drained shear strength parameters determined on remolded specimens and specimens consolidated from slurry are comparable to remolded specimens, which require less preparation time. Remolded in this context means soils which are moisture conditioned close to their liquid limit and manually packed in a mold to create a test specimen. Wang (2019) recommends consolidated undrained triaxial compression tests with porewater pressure measurements on normally consolidated remolded specimens because the drained parameters can be accurately measured determined with porewater pressure measurement.

According to Terzaghi et al. (1996), a random arrangement of particles can be ensured by remolding the specimen at a water content higher than the liquid limit.. The friction angle can then be obtained via drained compression or undrained compression with porewater pressure measurements.

To compare fully softened shear strength between slurry consolidated specimens and specimens remolded close to liquid limit, Green and Wright (1986) conducted undrained triaxial compressions test with porewater measurements. The difference in strength and failure envelop were minimal. In addition, Castellanos (2014) reported that the difference in fully softened strength measured by the triaxial test, and the direct shear test was insignificant

Castellanos (2014) also found no significant difference in the failure envelope regardless of the moulding water content. Castellanos (2014) also observed that there was negligible difference in void ratio at failure for the different preparation methods.

Table 2-1 Comparison between top-down and bottom-up construction methods of waste dump (Modified after Zevgolis , 2018).

Characteristic	**Comparison**
Density	Higher densities are achieved in bottom-up stacking because each layer gets compacted as more materials are spread over previous layers
Homogeneity	Top-down processes result in heterogenous dumps as particle segregation occurs while dumping. Larger particles typically roll to the bottom while fines stay near the crest
Stability	Top-down construction results in "meta-stable" dumps. This is because dump inclination is very close to the angle of repose with loose arrangement of particles. Such dumps are prone to failure whereas bottom-up constructions are more stable.
Settlement	Top-down constructed dumps are prone to significant settlement because particles are loosely packed. Bottom-up dumps are less at risk of settlement because they are usually compacted to higher densities.
Permeability	Top-down constructed dumps usually have a highly permeable zones due to particle segregation (i.e., poor gradation). The presence of coarser particles near the base results in higher permeabilities. Conversely, bottom-up construction results in a structure with more constant permeability overall

Table 2-2 Terms associated with fine grained sedimentary rocks (Modified after Kanji et al., 2020).

Term	Significance
Mudrock	Sedimentary rocks containing at least 50% siliclastic minerals finer than 0.06 mm
Siltstone	Sedimentary rock containing more than 60% silt-sized-particles
Mudstone	Sedimentary rock containing between 50%-60% of silt-sized particles.
Claystone	Sedimentary rock composed of more than 50% clay-sized particles
-stone	Suffix used when the layers are greater than 1cm.
-shale	Suffix used when layers are less than 1 cm

Table 2-3 Description of Jar Slake Index test.

Jar Slake Index	General behavior during test
1	Rapid degradation into flakes/mud
2	Breaks down rapidly forming many chips
3	Slow breakdown forming few chips
4	Breaks rapidly developing several fractures
5	Breaks slowly developing few fractures
6	Little to no change in structure

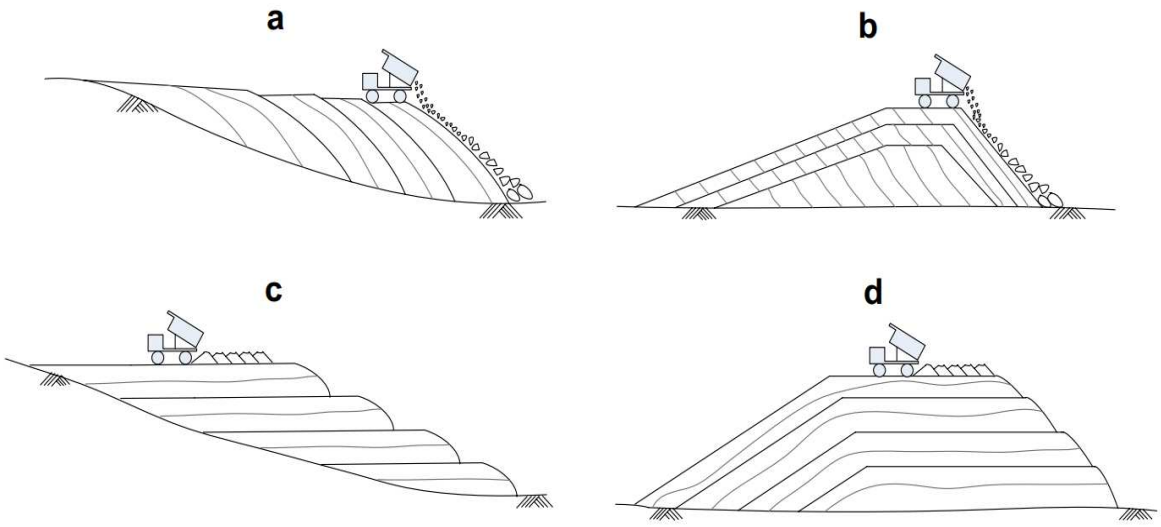

Figure 2-1 a) top-down construction on inclined ground, b) top-down construction on flat ground, c) bottom-up construction on inclined ground d) bottom-up construction on flat ground (Zevgolis, 2018)

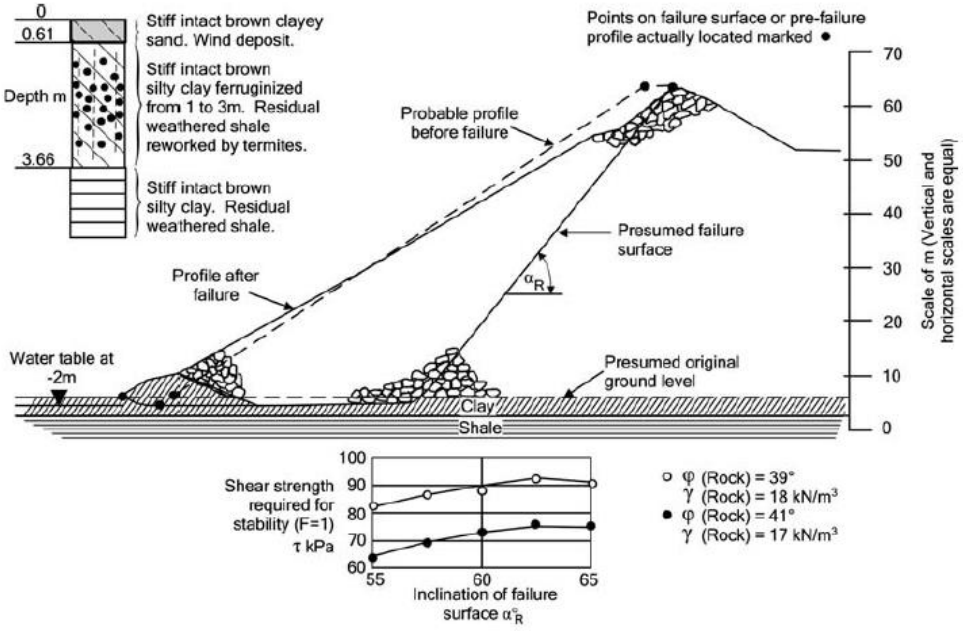

Figure 2-2 Failure of a waste rock dump along a horizontal plane (Blight 2009)

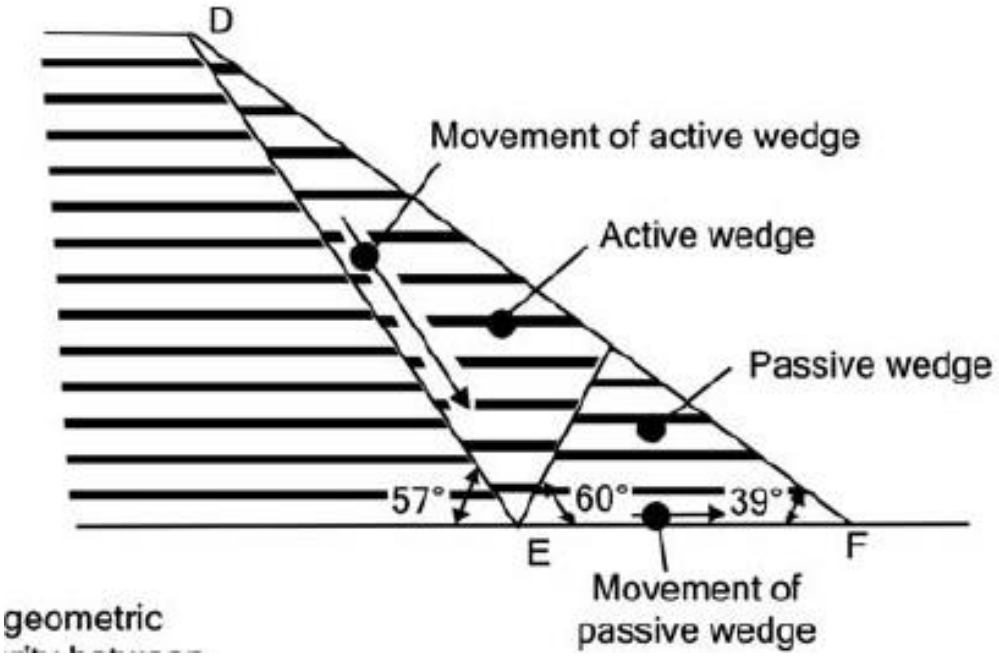

Figure 2-3 Schematic of a "first-time" failure of a waste rock pile (Blight 2009)

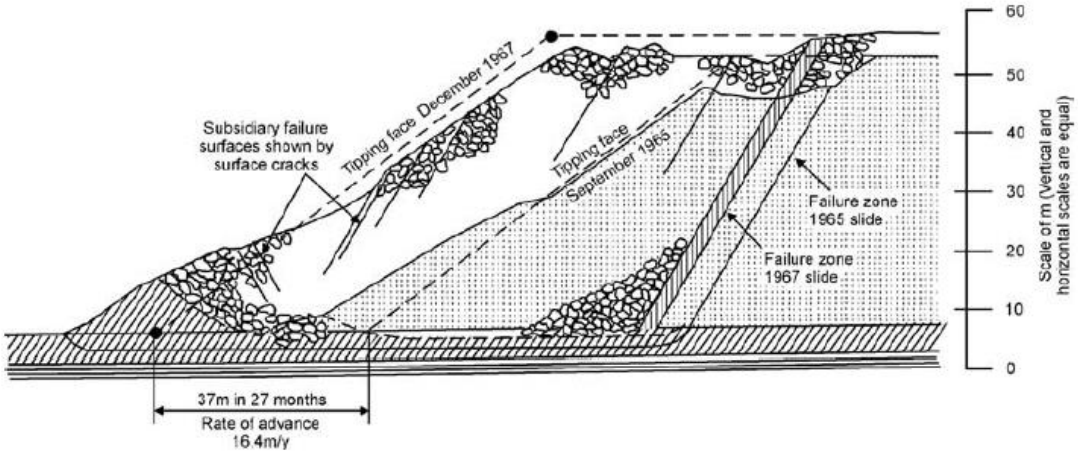

Figure 2-4 A "successive" failure in a waste rock dump (Blight 2009)

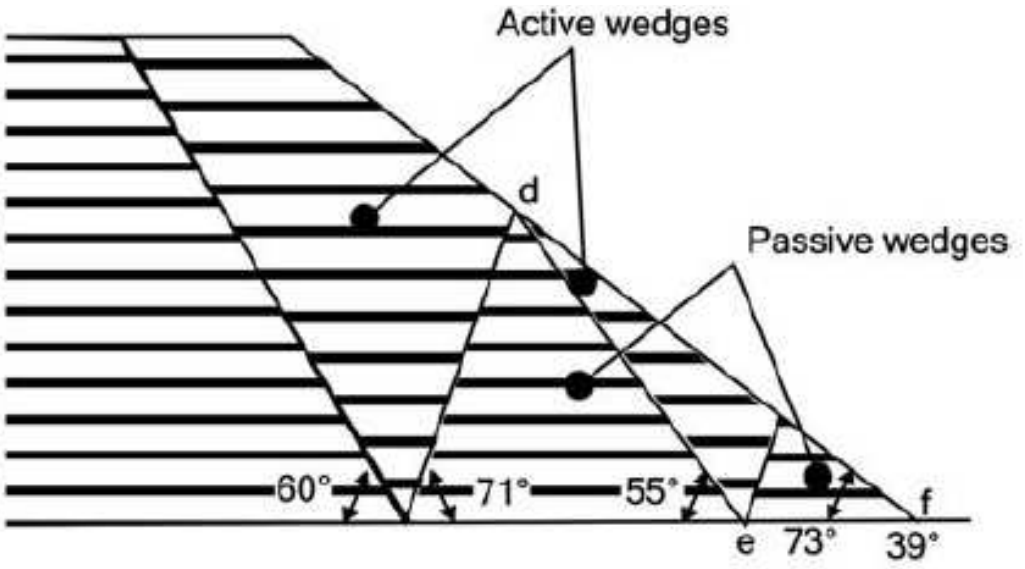

Figure 2-5 Schematic of a "subsequent" failure of a waste rock pile (Blight 2009).

Figure 2-6 Rock exhibiting a jar slake index (Ij) = 1 (Nunt-jaruwong, 2006)

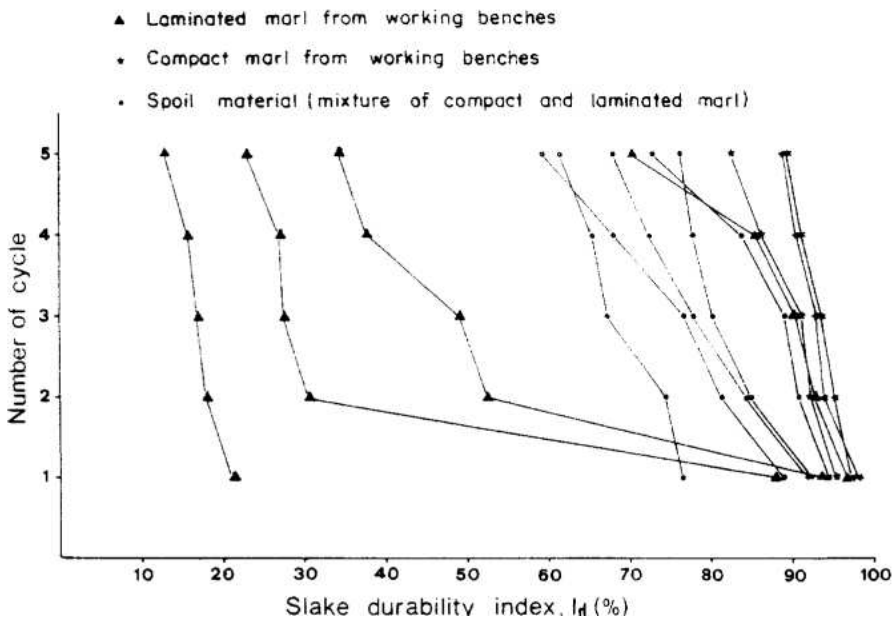

Figure 2-7 Influence of the number of slaking cycles on slake durability of selected spoil and fresh rock materials from the site (Ulusay et al., 1995)

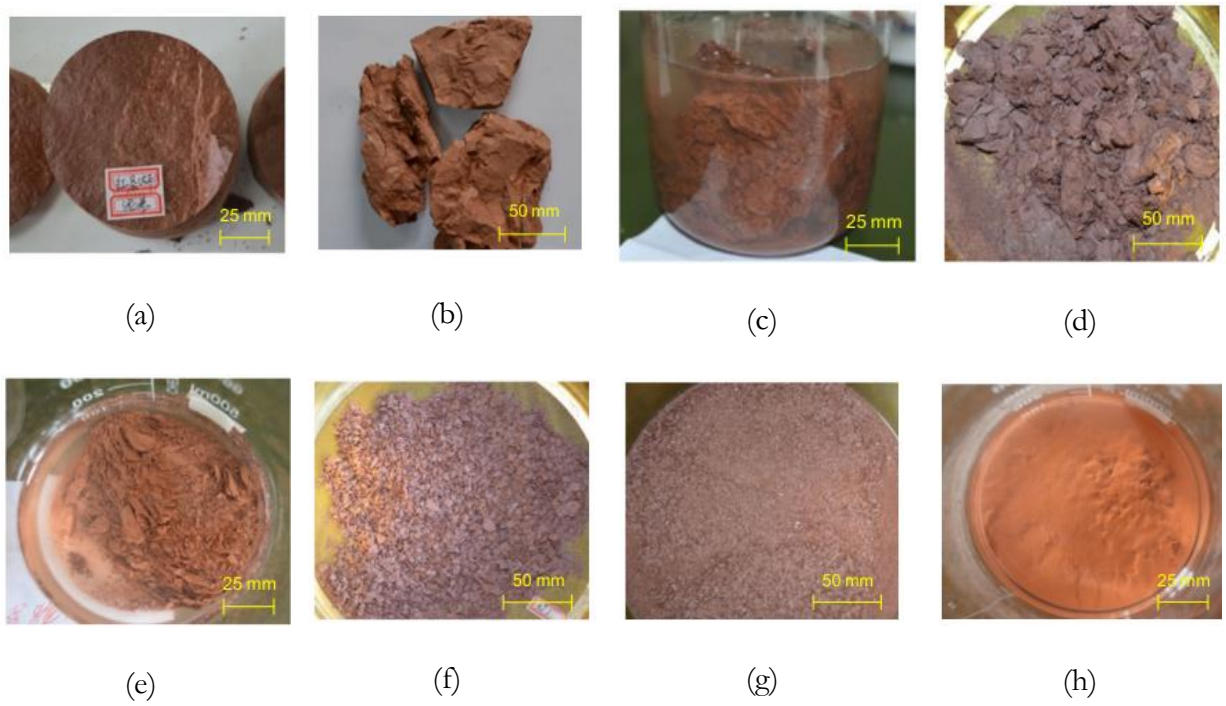

Figure 2-8 Progression of slaking of mudstone with progressive wetting and drying cycles : a) Initial condition b) samples dried c) 1st cycle immersion in water d)1st cycle of drying e) 4th cycle of immersion in water f) 4th cycle of drying g) 8th cycle of immersion and h) 8th cycle of drying(Qi et al., 2015)

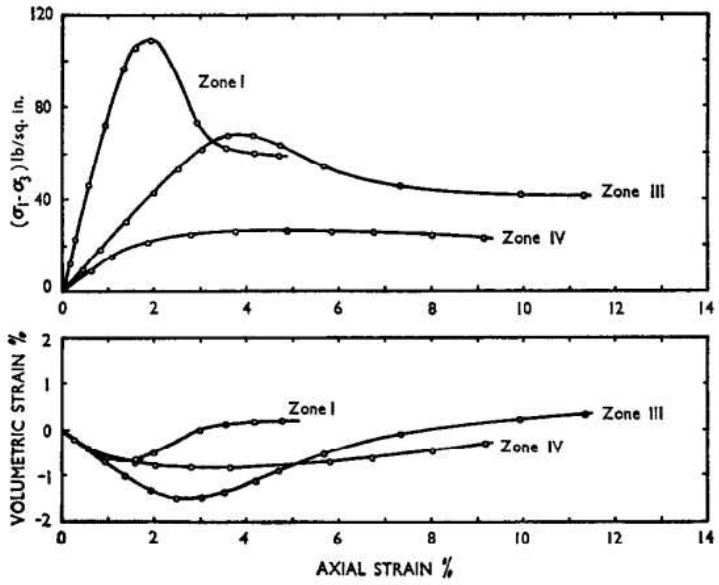

Figure 2-9 Stress-strain relations for different marls in drained triaxial compression tests.(Chandler, 1969)

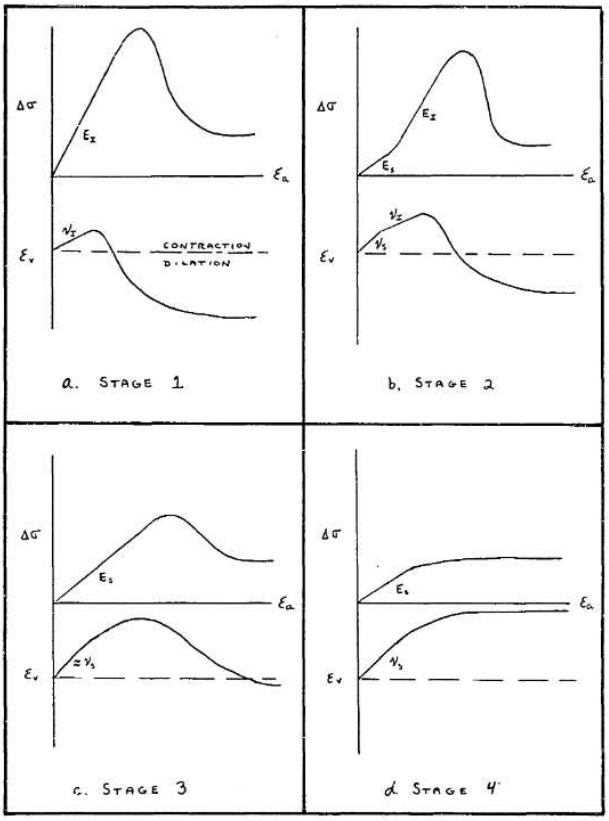

Figure 2-10 Changes in stress-strain behavior of clay shale with progressive softening(Botts, 1986)

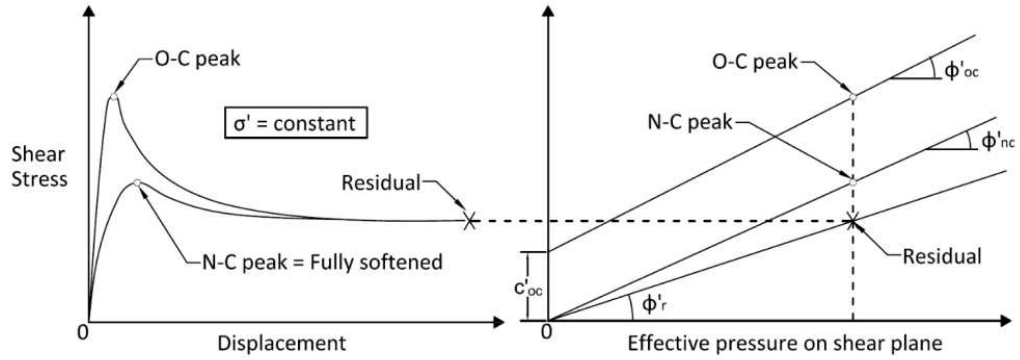

Figure 2-11 Shear Strength of OC and NC Clays (Castellanos, 2014)

Chapter 3 - Site Description: Mae Moh Lignite Mine

3.1. The Mae Moh Lignite Mine

Established in 1954, the Mae Moh Lignite Mine has been in continuous operation under the Electricity Generating Authority of Thailand (EGAT). The primary use of the coal mined is to generate electricity via thermal plants. The total installed capacity of the plants is 2.2 GW. The commercial yield of coal from the mine is estimated to be about 825 million tons. The lignite seams are deposited at depths up to 500 m below the ground surface resulting in a large amount of overburden that must be removed over the life of the mine. An estimated 6,700 million m^3 of overburden is expected to be removed and deposited in waste rock dumps.

3.2. Northwestern Waste Rock Dump

The northwestern waste rock dump has been in constant use since 1992. The location of the waste rock dump is shown in Figure 3-1. The dump has been constructed using the heaped fill and bottom-up construction sequence with a target elevation of 600 m above sea level (approximately 270 m above original ground level). Originally, the ground surface sloped towards the west with vegetation and swamps that were not stripped before dumping commenced. Figure 3-3 shows initial dumping activities. The material that was dumped into water and on existing rice paddies without stripping any vegetation. In 1996, they started dumping the waste in what appeared to be a pool of water.

During a site visit, the surface of the dump was observed to consist of uncompacted clay as shown in Figure 3-2 as opposed to claystone that was extracted to access the coal seam. This observation supports the hypothesis that the claystone waste rock disintegrated upon exposure to the climatic conditions present at the mine and transformed into a soil like material.

3.3. Geology of the site

The Mae Moh basin consists primarily of limestone, sandstone, and argillite shale as shown in Figure 3-5. The coal deposits occur in an oval shaped tertiary basin 16 km long by 6 km wide. The tertiary sedimentary materials are up to 1030 m thick. A stratigraphic section of the site geology is shown in Figure 3-6 that includes strata from three geological ages: quaternary, tertiary, and pre-tertiary. The tertiary rocks containing the lignite seams are termed as the Mae Moh Group. The tertiary rocks are further divided into the Huai Luang formation, Na Khaem formation and the Huai King formation.

3.3.1. Huai Luang Formation

The Huai Luang Formations are also called the Redbeds that consist of red to reddish-brown clays and claystones with some silt and siltstones. The color is due to oxidation during weathering. The maximum thickness of this sequence is 550 m. This layer consists of very low-quality lignite in sparse quantities (about 3-5 m thick seam). Most of the waste that is dumped in the waste dump is from this sequence due to the large depth that must be excavated to reach the productive zone in the Na Khaem formation.

3.3.2. Na Khaem Formation

The Na Khaem formation, also termed as the "Grey beds", consists of grey to greenish claystones and mudstones and include most of the productive coal seams, namely the J, K, Q, R, and S zones. The sediments between the coal sequences that contribute much of the waste from this layer has been divided into three zones: overburden (OB), interburden (IB), and underburden (UB):

Overburden is between 60 m to 100 m thick and consists of grey to greenish-grey, calcareous and pyritic silty claystone. Interburden lies between K and Q lignite zones and consist of semi-consolidated brown to grey claystone with some silts a thin gastropod limestone bed. Finally, Semi-

consolidated claystone and mudstone compose much of the underburden. The R- lignite seam is sandwiched between underburden layers whereas the S-seam is the lower bound of the underburden layer.

3.3.3. Huai King Formation.

The Huai King Formation,composed of clays, silts, sands, gravels, semi-consolidated claystone, and siltston,e starts from the bottom of the S coal zone and continues up until the basement rock. The Triassic Lampang group consisting of limestones, sandstone, shales, and volcanic rock form the basement of the Mae Moh Basin

3.4. Waste Rock

Considering that the coal must be mined from the Na Khaem Formation, the waste generated as a by-product of mining comes mostly from the Redbeds (Huai Luang) and the Grey Beds of the Na Khaem Formation. According to a geotechnical report done in 1985, the term redbeds refer to the red and reddish-brown clays, silts, claystones, and siltstones from the upper sequence. The strength of the material ranges from stiff soil (unconfined compressive strength 300 kPa) to very low rock strength of up to 2.4 MPa. Most of the redbed materials can be classified as stiff fissured clays. They are characterized by a fabric of curved, polished, and slickensided shear surfaces spaced 10 mm to 5 m and dipping between 35° to 45°.

The grey claystones of the Na Khaem formation consists of thinly bedded to massive claystones of uniformly light grey color. These claystone spall rapidly when exposed to air to form lenticular pieces mostly 50 to 200 mm in dimension.

One common characteristic of the claystones present was waste rock at the Mae Moh mine is their tendency to disintegrate by slaking (i.e., repeated wetting and drying cycles). Nidhinandana (2022)

performed jar slaking test and slake progressive test on OB, IB, UB, and Redbed claystones to assess their slaking behavior. The results of the jar slaking test were as follows:

- grey claystones show no significant change upon immersion.
- oven dried samples show higher disintegration; and
- redbed samples completely disintegrated to clay after soaking in water regardless of if the samples were completely immersed.

The progressive slake tests indicated that the Redbeds completely disintegrated into particles having size less than 2 mm in diameter. Among the grey claystones, the UB claystone displayed the greatest slaking tendency. Disintegration occurred rapidly during the initial wet-dry cycles after which the particles approached a constant particle size distribution.

Direct shear tests on the samples before and after slaking indicated that the Redbed claystone was impacted the most by slaking whereby the total stress friction angle reduced to a value of 15.5°. Similarly, total stress friction angles of the grey claystones were also found to have decreased from 35.3° to 22.2° for UB, 36.9° to 22.7° for IB, and 38.1° to 34.16° for OB. However, the tests revealed an increasing cohesion intercept as disintegration increased with wet-dry cycling. This increase in cohesion was attributed to soil suction, which would not play any role in stability as the failure zone was found to be saturated.

3.5. History of Slope Failures at Mae Moh

One of the earliest studies available identifies a major pit slope failure that occurred in 1981 on a portion of the northwestern pit slope. In 1980, a geologist at the site observed an 18-m tall by 20-m long wedge that increased in size following alternating wet and dry cycles. By 1981, the wedge slide along a discontinuity striking NNW and dipping 35° NE, which intersected a vertical joint trending ESE. In August 1981, a circular slope failure took place following the wedge failure that

resulted in a 250-m-long mass movement (Tandicul et al. 1986). As part of the study, strength tests were conducted on grey claystones that indicated intact strength parameters were significantly greater than those in weathered rocks.

A 1985 report states that the waste material when first dumped is granular in nature with an angle of repose of 36°. However, some landslides occurred in October 1984, which demonstrated that the materials break down into clay with an effective friction angle of 22°. The conditions of breakdown and failure were not fully understood at the time of the study. Trenches were cut into a landslide that revealed much of the material was wet and the moisture contents were above the liquid limit. Additionally, rainfall was known to seep into the waste dump generating pore pressure (Nidhinandana, 2022).

3.5.1. 2018 Pells Sullivan Meynink Report

Following a landslide within the waste dump that occurred in 2018, a geotechnical review of the mine was undertaken by Pells Sullivan Meynink Engineering Consultants (Pells Sullivan Meynink Engineering Consolutants, 2018). Their findings are summarized in this section.

In 1990, a geotechnical review of the mine was undertaken where they identified that failure was occurring in the northeastern dump, which was the main dump at that time. The features of that failure are illustrated in Figure 3-7 and included the following observations:

- 45-m-tall low spreader dump;
- Constructed over a 10 m high truck dump;
- Material dumped directly on submerged ground;
- Waste rock deteriorated rapidly into low strength clay; and
- Failure was hypothesized to occurred undrained due to rapid placement of a 45-m-high lift.

Initially, the waste dumps were composed of granular waste rock from Redbeds and Grey beds with a high angle of internal friction. Wetting and drying of the waste rock resulted in breakdown into clay. The breakdown occurred rapidly on the exposed surfaces and slower within the body of the dump. Progressive wet-dry cycling and breakdown of the waste rock resulted in the dump being composed of loosely compacted clay that behaves as a normally consolidated soil with no peak strength.

In the years 2015 and 2016, there were small failures on the NW dump as shown in Figure 3-8. Back analysis of these failures indicated an undrained mode of failure similar to the large failure that occurred in 2018 with similar strength parameters. These mass movements, although smaller in scale, underwent the same failure mechanism as the large slide in 2018.

3.6. The 2018 Landslide

At approximately midnight on 18 March 2018, a landslide with an approximate surface area of 1.54 km^2 with about 70 million m^3 of mass movement occurred in the northwestern waste dump as shown in Figure 3-9. The dump crest had just been raised to an elevation of 465 m above sea level. There were no warning signs before failure and the total time for failure was about 18 h, which was a short time for the scale of failure. Figure 3-10 illustrates the failure showing three distinct features: (i) a main body that stayed intact and moved 35-50 m; (ii) a second area that failed by spreading with mudflow at the toe; and (iii) a third area that failed after the main body moved and showed signs of liquefaction or flow.

Test pits dug adjacent to the failure after the failure occurred identified clay-like material instead of rock fill. The basal layer had stiff clay that could easily be remolded. The material was essentially a newly formed normally consolidated clay. These findings were consistent with the geotechnical reviews done in 1990. Forensic studies conducted after the failure suggested an undrained

failure occurred within a basal layer having and undrained shear strength of approximately 70 kPa (Pells Sullivan Meynink Engineering Consolutants, 2018).

The strength of each type of claystone before and after breakdown was studied by Nidhinandana (2022) via direct shear tests. Additionally, they ran FEM simulation of dumping activities leading to failure. They concluded that slaking of the waste rock could have led to a significant decrease in strength along a basal layer and lead to an undrained failure. Redbed claystone was found to exhibit the most pronounced and rapid reduction in strength due to slaking.

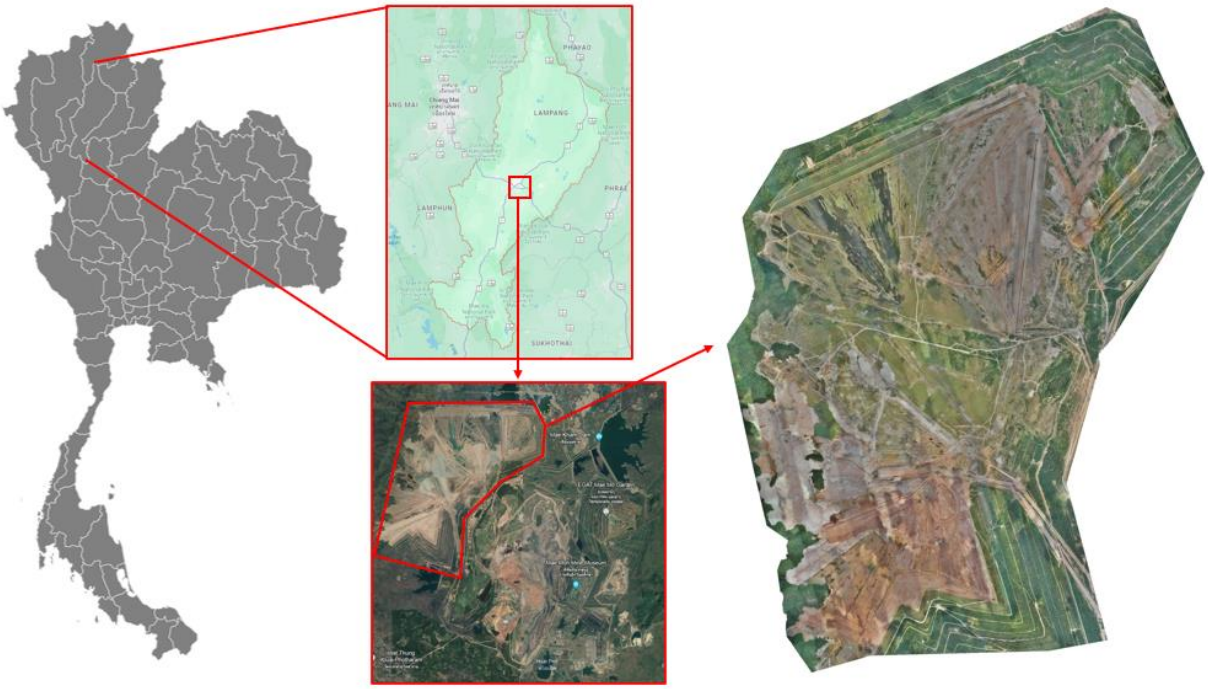

Figure 3-1 Location of the Northwestern Waste Dump within the Mae Moh Lignite Mine, Lampang, Thailand.

Figure 3-2 Surface condition at the top of the waste dump (Picture taken in May 2023).

(a)

(b)

(c)

Figure 3-3 Early dumping activities at the northwestern waste rock dump (Pells Sullivan Meynink Engineering Consultants, 2018).

(a)

(b)

Figure 3-4 (a) Waste rock dumped before spreading and (b) disintegrated rock on the dump.

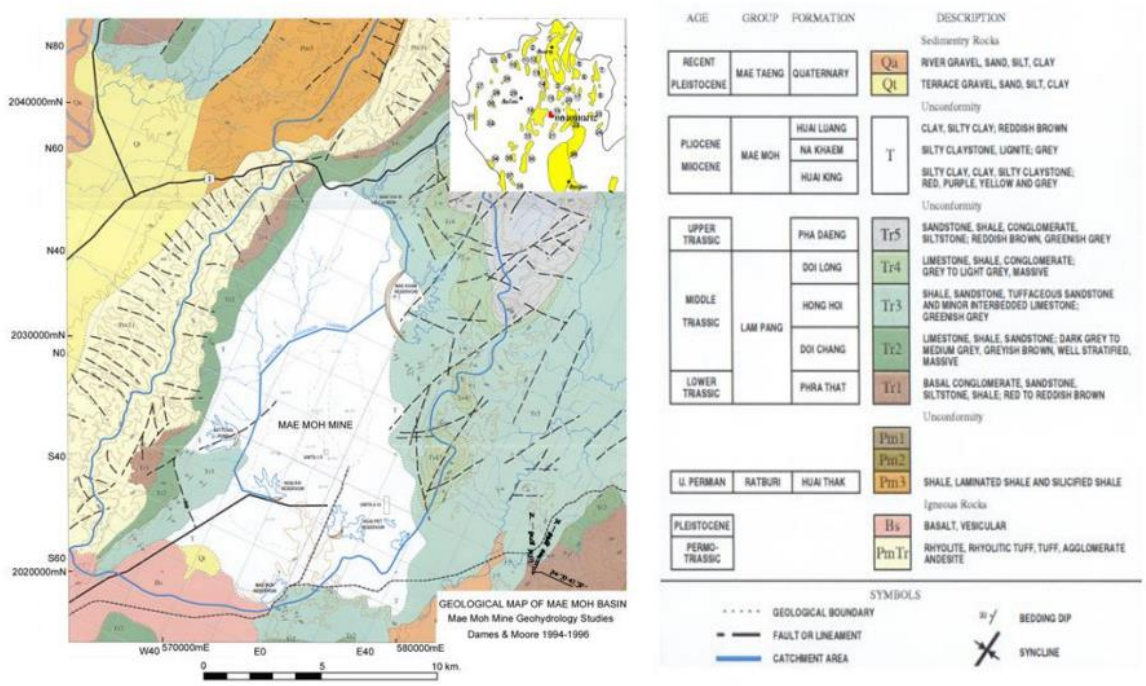

Figure 3-5 Geology of the Mae Moh Basin (Dames & Moore, 1998)

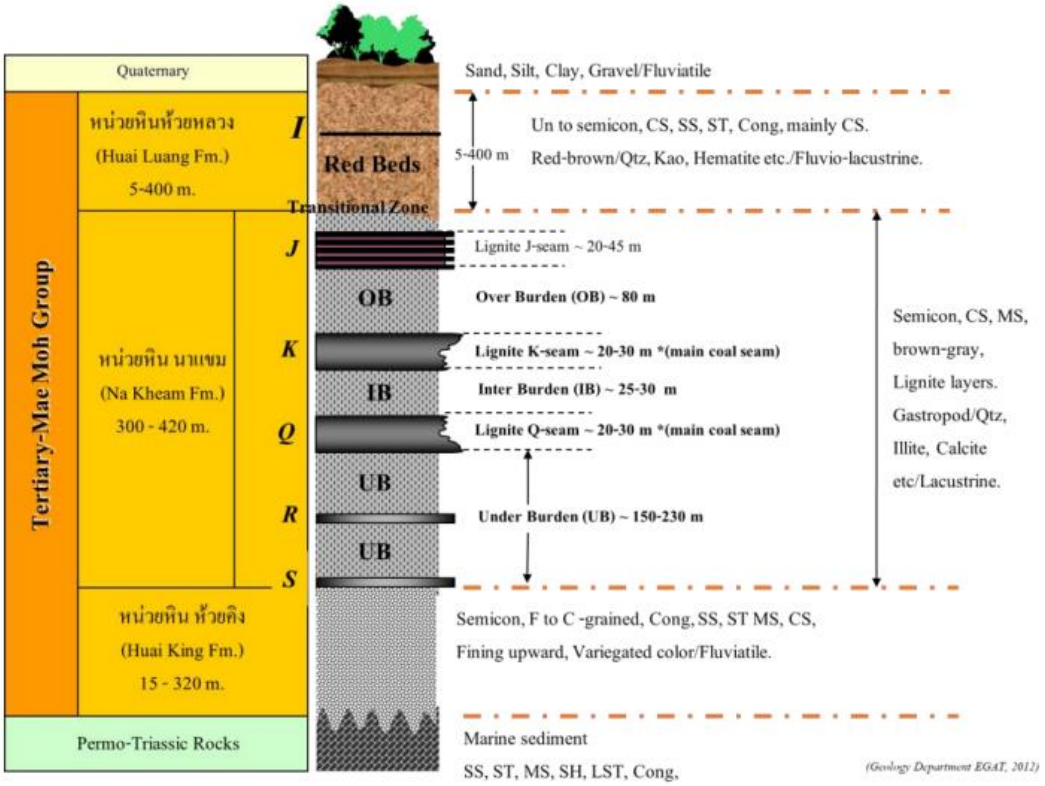

Figure 3-6 Stratigraphy of the Mae Moh Basin

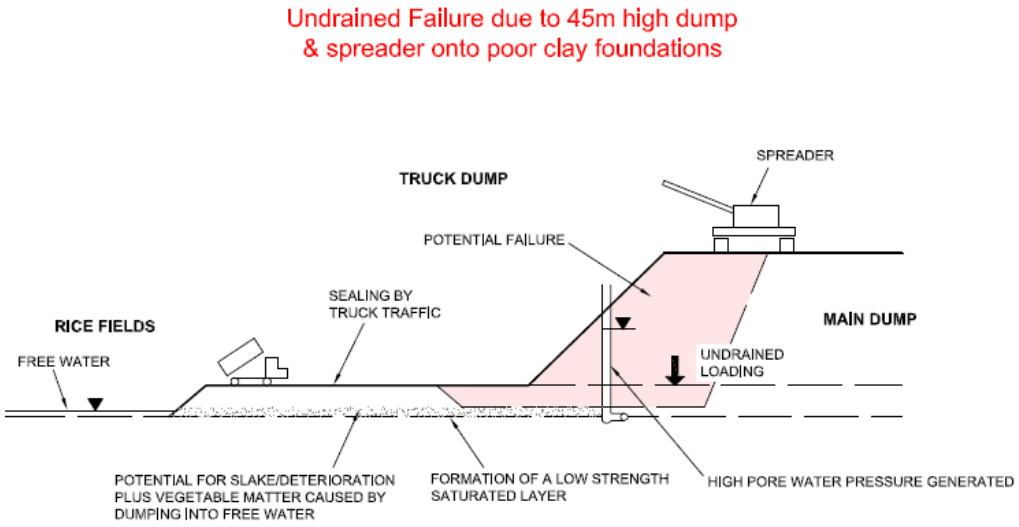

Figure 3-7 Failure mechanism of eastern Dump in 1990 (Pells Sullivan Meynink Engineering Consultants, 2018).

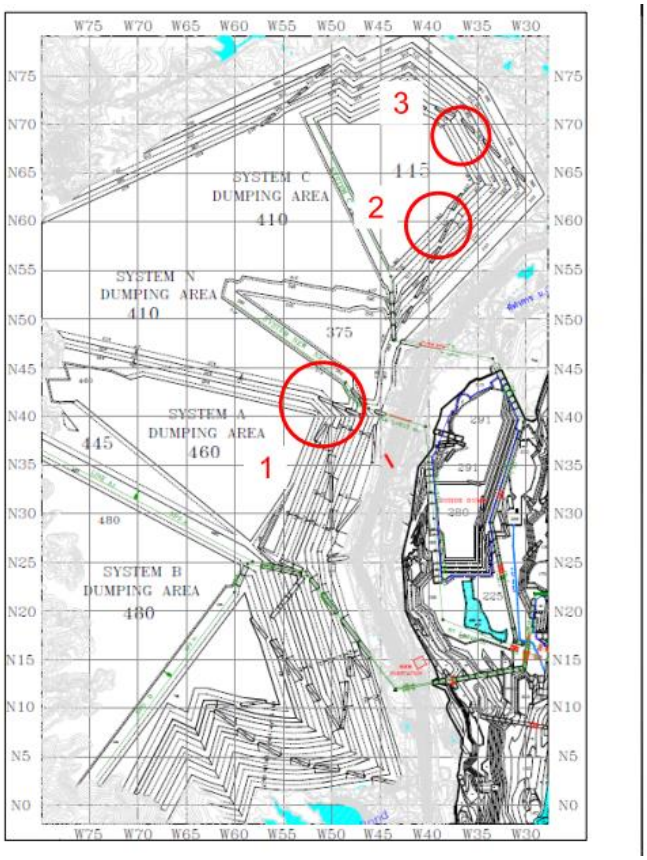

Figure 3-8 Locations of slope failures that occurred in 2015-2016.

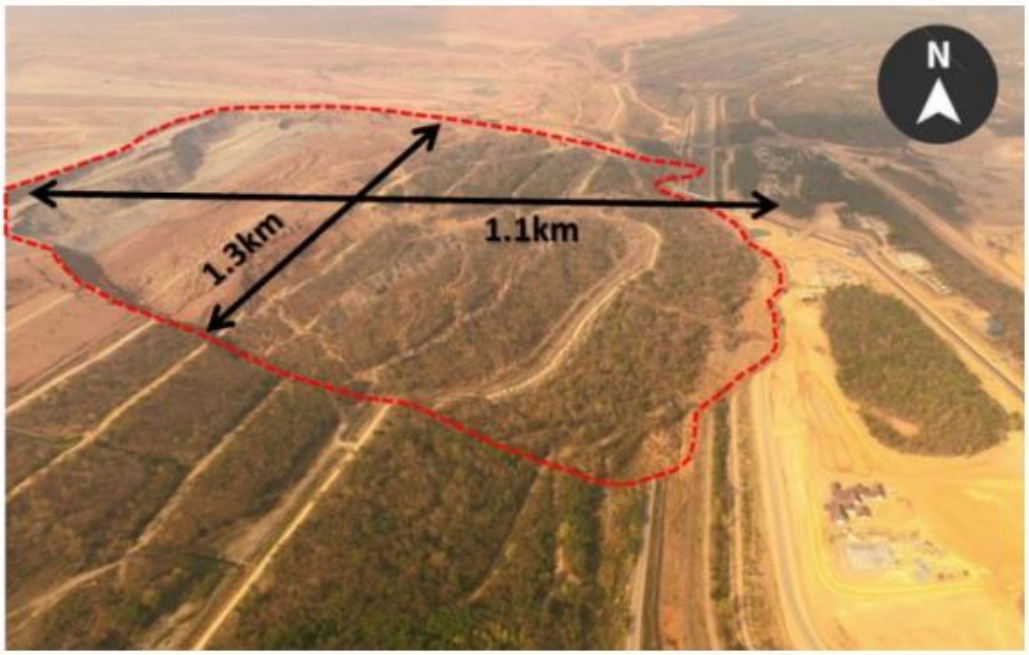

Figure 3-9 Aerial image of the 2018 landslide (Nidhinandana, 2022).

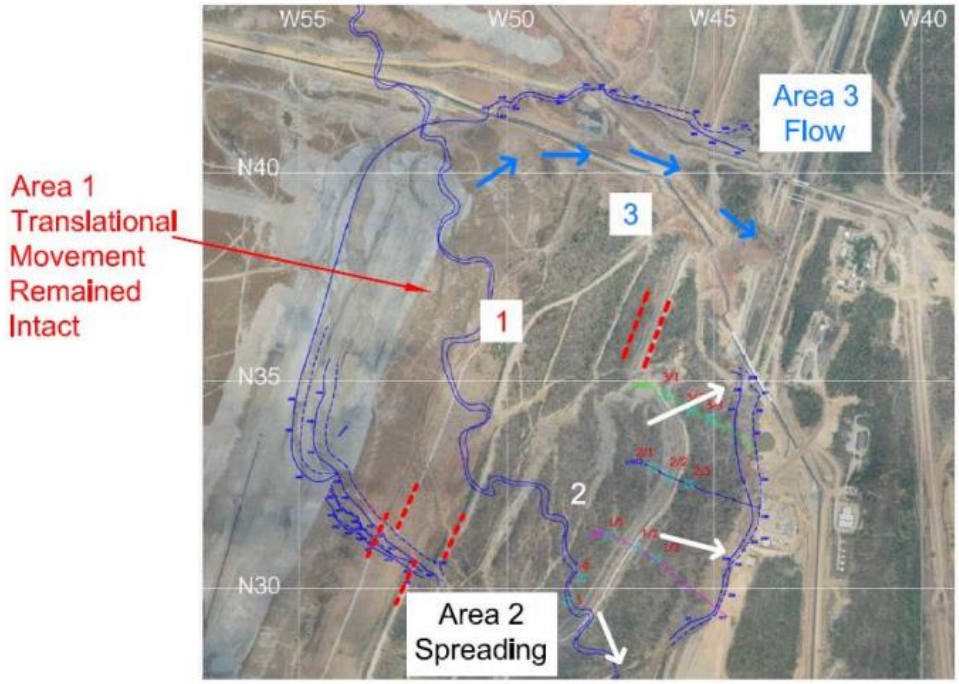

Figure 3-10 Three distinct failure zones observed in 2018 slope failure.

Figure 3-11 Location of the 2018 landslide at the NW dumps (EGAT, 2023)

Chapter 4 - Materials and Methods

4.1. Materials

The claystones of the Redbed formation from the Mae Moh Lignite Mine in Lampang was evaluated in this study. Intact rocks were collected from the run-of-mine waste rock pile at the site. The rocks were packed air-dry and transported to Asian Institute of Technology, Pathum Thani, Thailand, and subsequently shipped to Colorado State University (CSU), Fort Collins, Colorado, USA.

The composite sample of claystone rocks from the Redbed formation was split such that approximate 1/3 of the rocks were maintained in-tact and representative of the form in which they were collected at the mine. The other 2/3 of the rocks were placed in a large tub and inundated with de-ionized waster. The rocks were left to inundate for one week, after which they could be easily broken down and homogenized into a slurry using a rotary drill with mixture attachment. The moisture content of the initial slurry was 135%, which was about three times the liquid limit. After homogenization, the slurry was stored in buckets with lids to prevent desiccation.

To achieve a material with a workable consistency, the slurry was allowed to air dry with occasional mixing to decrease the moisture content close to two times the liquid limit. This was consistent with procedures adopted by Castellanos (2014) to evaluate fully softened strength of clays.

The claystone was characterized via X-Ray diffraction in a commercial laboratory, as well as Atterberg Limits Testing (ASTM D4318) and specific gravity (ASTM D854) at CSU. X-ray diffraction yielded the following mineralogy of the Redbed claystone: 39% illite / mica; 36% quartz; 10% mixed illite / smectite; 9% kaolinite; and 6% other. The Atterberg limit tests yielded a plastic limit of 18 and liquid limit of 45, which agreed with the plasticity measured by Chiang Mai University in 2018. Based on the Unified Soil Classification System, the claystone was classified as Lean Clay (CL). The specific gravity of the clay was 2.72.

4.2. Preparation of Triaxial Specimens

4.2.1. Remolded Specimen

Remolded Redbed claystone specimens were consolidated from slurry in a slurry consolidation frame similar to the one described in Jehring and Bareither (2016). Figure 4-2 shows a schematic of the slurry consolidation frame. The setup includes a load frame through which a vertical load can be transmitted to the surface of a slurry specimen prepared directly on the baseplate of a triaxial cell. The slurry specimen was supported laterally via a cylindrical mold and drainage was allowed on both ends via porous stones. Dead weights were applied to generate stress, and vertical deformation was monitored via a displacement transducer.

Photographs of the specimen setup and consolidation procedure are shown in Fig. 4.2. A 3D printed split-mold was fabricated with an inner diameter equal to the required specimen diameter for triaxial testing (38 mm). The initial specimen setup was similar to what would be for a conventional triaxial specimen prepared in a split-mold. A latex membrane with O-rings around the base was placed around the base pedestal that had a porous stone and filter paper in place. A soluble paper mold was placed around the outside of the membrane to assist in maintaining a vertical specimen following loading and removal of the split-mold. This paper mold would hold the sample in place while assembling the triaxial cell and dissolve in less than 5 min when filling the cell with water and applying an initial cell pressure (triaxial testing described subsequently).

Slurry was placed in the mold to a target initial height that would yield a consolidated specimen with a height-diameter ratio between 2.0 and 2.5, as per ASTM D4767. After the slurry was filled into the mold, a filter paper, porous stone, and top platen were placed on top of the specimen. Subsequently, the cell was positioned in the load frame as shown in Figure 4-1c and subjected to the following loads:

- 12 kPa (load plate and rod);
- 28 kPa (load plate, rod and 2 kg dead weight); and
- 38 kPa (load plate, rod, and 3 kg dead weight).

Each load was applied until the end of primary consolidation, which was monitored and confirmed via vertical displacement measurements. In general, primary consolidation required 3-4 d to complete for the 1st and 3rd load, and 2 d for the 2nd load. In total, slurry consolidation required approximately 8-10 d before a specimen was ready to be unloaded and moved to the triaxial testing stage. Upon deconstructing the split-mold, the specimen height was measured with a caliper.

4.2.2. Intact Specimen

Intact Redbed claystone specimens were cut directly from rocks collected from the mine. Berre (2011) recommended that rock specimen containing swelling clay minerals should be machined without water to avoid modification / disintegration of the rock upon contact with water. Thus, the rock specimen for triaxial testing were hand trimmed using a hack saw to form cuboids of the required diameter. The cuboidal specimens were then ground down to a cylindrical shape using a sanding block.

4.3. Consolidated Undrained Triaxial Compression Testing

Consolidated undrained (CU) triaxial compressions tests were conducted in accordance with ASTM D4767 on remolded specimens while ad hoc procedures were adopted for intact specimens. Remolded specimens were reconstituted from slurry and assumed to be fully saturated from the start of preparation in the consolidation frame. Following consolidation, drainage lines were connected to the top platen, the triaxial cell was assembled, and then filled with tap water. A low initial confining stress (≈ 10 kPa) was applied during which all drainage lines were flushed with de-aired water and initial readings of cell pressure and back pressure burettes were established. Subsequently, specimens

were consolidated isotopically to a target effective confining stress during which the burette levels were monitored to track primary consolidation. Saturation prior to testing was verified by a B-check; all remolded specimens returned B values > 0.95.

The strain rate of compression loading was 0.25%/h, which was determined slow enough for pore pressure equalization across the entire specimen based on consolidation behavior of the slurry claystone. The specimen height after isotropic consolidation was computed from the height measured after slurry consolidation and vertical deformation of the specimen measured via the load piston. All tests were carried out to a target axial 25%.

During shear testing, measurements of axial load (in Newtons), porewater pressure (in kPa), cell pressure (in kPa), and axial displacement (in mm) were recorded. A load cell (Artech Industries, Inc., 8900 ± 0.4 N) was used to measure the axial load. A Linear Variable Differential Transformer (Novotechnik, 50 ± 0.003 mm) was used to measure axial displacement. Pressure transducers (ELE International, Ltd., 700 ± 0.07 kPa ; GeoTac, 1378 ± 0.07 kPa) were used to monitor pressure cell and pore pressures respectively). Pore water pressures were measured at the base of the specimen. A data acquisition system was used to collect all the data.

At the end of shearing, all drainage lines were closed, the cell pressure was reduced, and the cell was disassembled. The specimen was frozen to preserve the moisture content such that void ratio was determined via end-of-test freezing (Reid et al., 2021). After freezing, the o-rings, membrane, porous stones and filter paper were removed, and the mass of the frozen specimen was recorded. The specimen was then oven dried to calculate the moisture content and subsequently void ratio based on the measured specific gravity and assumed saturation of 100% .

Intact Redbed claystone specimens were back-pressure saturated in the triaxial cell at the target consolidation stress. The specimens were saturated applying a back pressure of 500 kPa for a duration of 3 to 4 weeks. B-value of approximately 0.86 was achieved for intact specimens. Chiu and Johnston

(1980) remarked that the B-value for mudstones are generally lower than unity due to skeleton rigidity. Thus, the lower B-value was accepted and the specimen assumed sufficiently saturated to monitor pore pressure during undrained loading.

Chiu et al. (1983) suggested that a strain rate for CU tests on mudstones of 0.12%/h . This was considered slow enough that the behavior would be unaffected by strain rate. Other researchers (e.g., Zhang and Rothfuchs 2004; Giger et al., 2018) have recommended similar slow rates on mudstones, and thus a strain rate of 0.12%/h as suggested by Chiu et al. (1983) was used in this study. The tests were terminated at 20% strain.

A noticeable challenge in conducting the tests on the in-tact claystone specimens was that there was minor leaking at the contact of the load rod and linear bearing, perhaps attributed to the long duration under constant cell pressure prior to loading. During shearing, there was some fluid loss from the cell, which combined with the slow loading rate, required premature termination of the tests. Only one of the tests on in-tact claystone proceeded to completion at 20% strain.

4.4. One-Dimensional Consolidation

4.4.1. Remolded Specimen

A total of four one-dimensional consolidation tests were performed on remolded slurry specimens of the Redbed claystones. Two tests were performed using an automated load frame and two tests were performed using conventional oedometers with dead weights.

Consolidation test specimens prepared for the automated load frame were pre-loaded from slurry external to the load frame to create a workable specimen for testing. The automated load frame was not sufficiently sensitive to apply very low stress to a slurry, and thus, slurry samples were consolidated using dead weights to a target vertical effective stress of 25 kPa. Upon completion of

primary consolidation at 25 kPa, the slurry consolidated sample was extruded, and carved fit into a 63.5-mm diameter by 25.4-mm tall consolidation ring. The two specimens prepared in this manner had moisture contents between 43% and 45% when transferred into the automated load frame. The specimens in the automated load frame were subjected to loadings of 5 kPa to 2000 kPa, doubling the previous load after a consolidation period of 24 h, and unloaded to 500 kPa.

Slurry Redbed claystone specimens were prepared directly into the consolidation cell to initial specimen dimensions of 70 mm diameter and approximately 20 mm tall. The actual heights computed from the volume of specimen in the consolidation ring were 17.52 mm and 17.70 mm. A low-weight top-platen was fabricated from PVC such that the initial vertical stress applied via the porous stone plus load platen was less than 1 kPa. The slurry specimens were loaded from 1 kPa to 2000 kPa doubling the previous load after a consolidation period of 24 h, which was then followed by unloading in a similar manner to 128 kPa.

Compression of the top platen and consolidation cell was measured in the absence of any specimen and discounted from the total deformation recorded by the linear potentiometer during testing to accurately compute the vertical deformation. The final void ratio of the specimen was determined via weight-volume calculations on the end-of-test specimen and void ratios for all loading and unloading points were corrected relative to the final state. Individual results are presented in Appendix B.

4.4.2. Intact sample

The intact Redbed claystone specimens used for consolidation testing were carved using a hacksaw and sanding block to obtain a circular specimen with height = 19.5 mm and diameter = 63.5 mm. This specimen was saturated by immersing in deaired water for about one week after which vacuum was applied for 24 h. The specimens were contained between two porous PVC plates with

filter paper to maintain and intact specimens following saturation. Subsequently, the specimens were transferred to a floating ring consolidation cell and loaded in a conventional oedometer.

4.5. Critical State Soil Mechanics

4.5.1. Modified Cam Clay Theory (Burland, 1965)

The Modified Cam Clay model is a soil yield model based on critical state. The soil is assumed to be isotropic with irrecoverable shear strains. Burland (1965) modified the yield surface in the original Cam Clay model from a log spiral to an ellipse. The model captures many of the behaviors of normally consolidated and lightly over consolidated clays and is popular in numerical modelling.

The yield locus is given by the formula in Eq. 1:

$$p' = \frac{p'_o M^2}{M^2+\eta^2} \tag{1}$$

where p'_o is the pre-shear consolidation stress, p' is the mean normal stress (Cambridge Notation), M is the slope of the critical state line in the q-p' plot, and η is the stress ratio (q/p'). The incremental shear and volumetric strains are computed via Eqs. 2 and 3:

$$d\varepsilon_s = \frac{\lambda-\kappa}{1+e}\left(\frac{2\eta}{M^2-\eta^2}\right)\left(\frac{2\eta d\eta}{M^2+\eta^2}+\frac{dp'}{p'}\right) \tag{2}$$

$$d\varepsilon_v = \frac{1}{1+e}\left(\frac{2\eta(\lambda-\kappa)d\eta}{M^2+\eta^2}+\lambda\frac{dp'}{p'}\right) \tag{3}$$

where λ is the slope of the isotropic consolidation line in e-ln p' plot, K is the slope of the isotropic swelling line in e-ln p' plot, e is void ratio, $d\eta$ is the incremental stress ratio (dq/dp'), and dp' is the incremental mean effective stress (Cambridge Notation). There are no volumetric strains in an undrained test and the total strain can be calculated using only the equation for shear strain. The stress paths for an undrained test are obtained by the state boundary surface described by Eq. 4.

$$\frac{p'}{p'_o} = \left(\frac{M^2}{M^2+\eta^2}\right)^{\left(1-\frac{\lambda}{\kappa}\right)} \tag{4}$$

Wroth (1984) derived an expression for undrained shear strength ratio (S_u/σ'_v) and Skempton's A-parameter at failure (A_f) of isotropically consolidated normally consolidated clays under triaxial compression. These two parameters can be computed via Eqs. 5 and 6, respectively:

$$\frac{S_u}{\sigma'_v} = \frac{M}{2}\left(\frac{1}{r}\right)^{\Lambda} \tag{5}$$

$$A_f = \frac{1}{M}\left\{\left(\frac{1}{r}\right)^{-\Lambda} + \frac{M}{3} - 1\right\} \tag{6}$$

where r is the spacing ratio that equals 2 for Modified Cam Clay model and $\Lambda = (\lambda - k) / \lambda$.

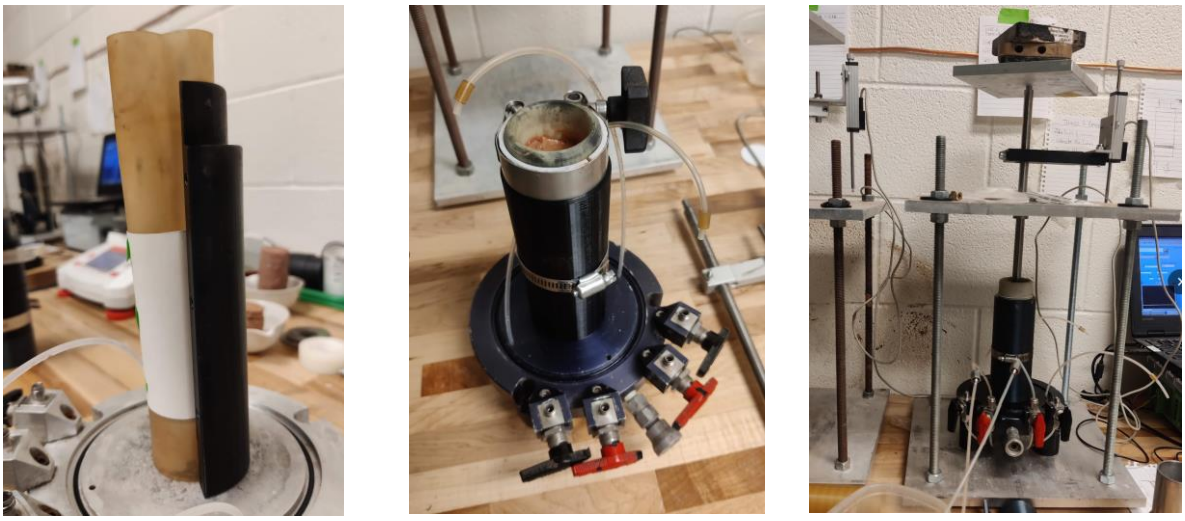

(a) (b) (c)

Figure 4-1 Specimen preparation steps : (a) setup of split mold with membrane and paper mold, (b) split mold with slurry filled in, and (c) application of dead load to slurry.

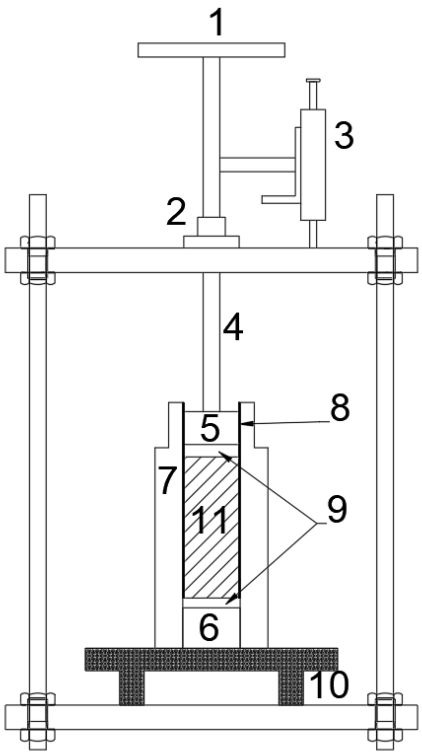

1. Loading Plate
2. Linear Bearing
3. LVDT
4. Loading Rod
5. Top Platten
6. Bottom Platten
7. Split Mold
8. Membrane + Paper Mold
9. Porous stones
10. Base of Triaxial Cell
11. Claystone Slurry

Figure 4-2 Schematic of slurry consolidation load frame.

Chapter 5 - Results and Discussions

Results of the consolidated undrained triaxial compression tests conducted on remolded Redbed claystone are summarized in Table 5-1. The summary includes the following test results: target effective consolidation stress; failure criteria; axial strain at failure; mean and deviator stresses (Cambridge Notation) at failure; principal effective stresses at failure; porewater pressure at failure; void ratio at failure; M parameter; the effective stress friction angle based on failure criteria; undrained shear strength; and undrained shear strength ratio. The data from triaxial tests have been used to evaluate the strength of the Redbed claystone in a remolded state for effective confining stresses ranging from 60 kPa to 400 kPa. Results of individual triaxial test results are compiled in Appendix A.

A compilation of the three triaxial tests on intact specimens is in

Table 5-2. Two tests were conducted at an effective stress of 100 kPa and a third test was conducted at 200 kPa. The objectives of the triaxial tests on the intact Redbed claystone were to (i) provide a comparison of shear behavior with the remolded specimens and (ii) estimate shear strength for comparable levels of effective confining stresses.

A summary of the one-dimensional consolidation tests conducted on remolded Redbed claystone is presented in Table 5-3. The data compilation includes initial and final water contents, void ratios, compression and swelling index and their corresponding λ and K values. The two tests coded Re-x were conducted on samples first consolidated to 25 kPa vertical effective stress from a slurry and then extruded and trimmed. These two tests exhibited recompression and virgin compression during loading and swell during unloading. The two consolidation specimens prepared directly as from slurry show only virgin compression during loading and swell during unloading.

5.1. Slaking Behavior of Redbed Claystone

Photographs of the rock fragments of the Redbed claystone collected from the mine prior to and post inundation with deionized water are shown in Figure 5-1. The Redbed claystone completely disintegrated into constituent clay particles when left inundated and unconfined. The disaggregated rocks in Figure 5-1b were subsequently mixed to create the slurry used in this study. Slaking of the Redbed claystone, however, was not observed for the intact triaxial and consolidation tests specimens that were saturated under confinement. Photographs of intact triaxial and consolidation test specimens after testing are shown in Figure 5-2. All of the intact Redbed claystone specimens tests in triaxial compression and 1-D consolidation remained intact throughout the duration of test. Furthermore, a clear failure plane developed within the intact Redbed claystone specimens, as shown in Figure 5-2a.

5.2. Shear Behavior of Redbed Claystone

5.2.1. Shear Behavior of Remolded Redbed Claystone

Figure 5-3 shows the relationships of deviator stress and excess pore pressure versus axial strain in undrained triaxial compression for all remolded Redbed claystone. Peak deviator stress for all remolded specimens was attained between 7% and 11% axial strain. In addition, all remolded test specimens generated positive excess pore pressure that was representative of contractive tendencies during shear deformation. After reaching the peak deviator stress, all specimens displayed slight strain-softening behavior as evident by decreasing deviator stress. A very slight continued increase in positive excess pore pressure can also be observed after the specimens reached their peak stress. This behavior may be reflective of end effects from the non-oversized and non-lubricated end-platens. Regardless of the slight strain-softening behavior, all remolded test specimens essentially reach a critical state at failure as they continue to shear under constant stress, void ratio, and velocity. The stress-strain

behavior for specimen Re-100 was not consistent with that of the other tests. For this reason, a duplicate test (Re-100-2) was run at 100 kPa effective confining stress and showed behavior consistent with the other tests. This difference in behavior is more pronounced when viewed in the normalized deviator strain versus strain plot discussed subsequently.

Effective undrained stress paths of deviator stress versus mean effective stress expressed in Cambridge notation for all remolded Redbed claystone triaxial tests are presented in Figure 5-4. All stress paths show expected behavior of a contractive material that generates positive pore pressure during undrained shear. Furthermore, all effective stress paths terminate at defined points representative of failure or show modest movement down that the failure line (K_f-line). For example, after reaching a peak stress, stress paths for Re-200 and Re-300 advance down along the K_f-line with decreasing deviator and mean effective stress that is reflective of the slight softening behavior. An approximate K_f-line is sketched in Figure 5-4 that captures the failure points from the triaxial tests.

The plot of Skempton's A-parameter is shown in Figure 5-5. The A values for specimens Re-60 and Re-100 are lower than the other specimens and indicating these specimen developed lower excess pore pressure relative to the strength of the specimens. At failure, their values are about 0.7 which is within the range of A at failure for contractive materials (Bishop, 1962). The A parameters for the other test specimens overlap quite well and shown a rapid increase to $A \approx 1.0$ that corresponds to with strains representative of failure (i.e., ≈ 7% to 11% axial strain). The subsequent increase in A following failure reflects the slight decrease in deviator stress with near constant excess pore pressure (Figure 5-3).

Comparison of the behavior of the remolded Redbed triaxial test specimens at varying confining stresses was conducted by evaluating the normalized behavior. The following stress normalizations were computed and presented graphically: Figure 5-6 = deviator stress normalized to initial effective confining stress versus axial strain; Figure 5-7 = principal stress ratio versus axial strain;

and Figure 5-8 = normalized undrained effective stress paths, which includes deviator stress versus p' with both parameters normalized to the pre-shear mean effective consolidation stress.

All remolded triaxial specimens show similar behavior when evaluating the normalized deviator stress (Figure 5-6), except for specimen Re-100. This test specimen experienced disturbance prior to shearing due to a leaking membrane, which required draining and disassembling the triaxial cell, replacing the membrane, and reconsolidating the specimen. Thus, a second test at 100 kPa was run, which yielded data that conformed much better to the other tests. Another observation from Figure 5-6 is that the triaxial tests at lower confining stresses showed some noise (i.e., localized spikes) in the data that were attributed to measurements in the lower range of the load cell. Although there was some noise, the data trends align well with the other sets of data. The noise can also be observed in the stress ratio plot (Figure 5-8), which further confirms that shear behavior of specimens Re-60 and Re-100 slightly deviated from the other four specimens: i.e., Re-100-2, Re-200, Re-300, and Re-400. The similarity in shear behavior for these four specimens provides confidence that the undrained shear behavior was adequately captured for a stress range of 100 kPa to 400 kPa effective confining stress.

The normalized stress paths in Figure 5-8 show two distinct groups: (i) stress paths at higher confining stresses (200-400 kPa) overlap well ending up at a single critical state point; and (ii) stress paths for Re-60 terminates at a slightly lower point and Re-100 terminated at a slightly higher final point. The stress path for Re-100-2 exhibits some noise but terminates at an end-state that is coincident with the higher stress tests; further supporting the similarity in shear behavior for the four tests Re-100-2, Re-200, Re-300, and Re-400. Stress paths for Re-60 and Re-100 show a stiffer initial response with a near vertical rise that is reflective of lower generation of excess porewater pressure.

The critical state lines and isotropic consolidation lines were plotted in e-ln p' space for all triaxial compression tests (Figure 5-9). Assuming critical state was attained at peak deviator stress, the

critical state line was plotted using the mean effective stress at peak deviator stress. Table 5-4 lists the values of mean effective stress at maximum deviator stress and void ratio. The slope of the isotropic consolidation line and critical state line (both λ) were 0.168 and 0.193.

However, the shear behavior of Re-60 and Re-100 did not conform to the shear behavior of specimens Re-100-2, Re-200, Re-300, and Re-400, which were more similar. Re-60 developed less excess porewater pressure and ended up at a failure line that was lower. Conversely, Re-100 developed lower excess porewater pressure and higher deviator stress in addition to ending up at a failure line a little higher than Re-100-2, Re-200, Re-300, and Re-400. For these reasons, the tests Re-60 and Re-100 were excluded from the critical state analysis. When these two data points are excluded, the slope of the critical state line is 0.171 (Figure 5-10), which is much closer the slope of the isotropic consolidation line thus reaffirming the consistent undrained behavior of Re-100-2, Re-200, Re-300, and Re-400.

5.2.2. Shear Behavior of Intact Redbed Claystone

Figure 5-11 shows the relationships of deviator stress and excess pore water pressure versus axial strain for intact Redbed claystone specimens. Additionally, effective stress paths and relationships of Skempton's A parameter versus axial stress are shown in Figure 5-12 and Figure 5-13 respectively for the triaxial tests on the intact Redbed claystone specimens. Specimens In-100 and In-100-2 (effective confining stress 100 kPa) exhibited a ductile stress-strain response in which the deviator stress attained a peak value and remained constant for the duration of the test. In contrast, In-200 (effective confining stress 200 kPa) displayed brittle failure i.e., rapid drop in strength post peak deviator stress. All three test specimens attained peak strength at an axial strain of approximately 5%.

Excess pore pressure for the CU compression tests was negative for all intact specimens. The two specimens sheared under a confining stress 100 kPa displayed vastly different negative excess

porewater pressure, whereby specimen In-100-2 generated nearly double the excess pore pressure measured for In-100. The differences in behavior may be attributed to a couple factors. On the one hand, there may have been anisotropy in the rock fabric that was not captured due to the random carving of block samples from the collected claystone. On the other hand, Re-100 experienced some leakage from the cell during that test that resulted in early termination of the test. Regardless of the factor influencing the test, the two specimens sheared under a confining stress of 100 kPa exhibit similar shear behavior until an axial strain of 4%, which can be taken as representative shear behavior.

The test specimen In-200 also developed negative porewater pressures similar to both tests at 100 kPa until an axial strain of 4%. The unique brittle behavior of In-200 is captured by a minimum excess pore pressure at 5.7% axial stress following by an increasing trend, which is somewhat reflective of the behavior of In-100. The comparison of shear behavior is further evaluated via Skempton's A parameter in Figure 5-12, whereby In-100 and In-200 show similar normalized behavior, and In-100-2 deviates from the other two specimens. The A parameter for In-100 and In-200 show a slight increase followed by a drop indicating development of negative excess porewater pressure. This drop in A-parameter continues until it reaches a minimum at around a strain of 5% when it starts increasing again. The strain at which excess pore pressure starts increasing seems to coincide with that of maximum deviator stress. This behavior is not observed in In-100-2 where the excess pore pressure continuously decreases as shear progresses.

The undrained stress paths for all the specimens are characteristic of dilative materials, i.e., increasing mean effective stress as deviator stress increases. However, the stress paths for In-100 and In-100-2 do not coincide with each other. From failure envelope drawn for the two tests based, the M values are 1.58 and 1.18 respectively for In-100 and In-100-2 respectively. In-200 however, showed similar behavior to In-100 with a M value of 1.66. The plots of normalized undrained stress path paint a similar picture where the plots for In-100 and In-200 overlap up to the peak, but the stress path In-

100-2 follows a different path from the two ending up at difference failure line. This variation in behavior could be attributed to anisotropy in the rock fabric.

5.2.3. Shear Behavior Comparison

The differences in shear behavior between intact and remolded Redbed claystone are shown in Figure 5-14 to Figure 5-17, which include normalized deviator stress versus strain, normalized effective stress paths, normalized excess porewater pressure versus strain, and Skempton's A-parameter versus strain.

The comparison was developed for CU triaxial tests on specimens consolidated to confining effective stresses of 100 kPa and 200 kPa. Furthermore, only the specimen Re-100-2 was included for the comparison because this specimen exhibited shear behavior that was more consistent with the remolded specimens tested at 200, 300, and 400 kPa.

The strength of Redbed claystone reduced dramatically in a remolded state as compared to an intact state. At the same confining stress levels, the peak deviator stress developed in the intact claystone is an order of magnitude greater than in the remolded claystone. The intact material is also stiffer as observed by attaining a peak stress between 4-6%, whereas the remolded material attained peak stress at around 10% strain. All the remolded specimens displayed ductile behavior with a near constant deviator stress maintained with increasing strain once the peak stress was reached. Although In-200 shows brittle failure (Figure 5-13), all the intact specimens exhibit similar normalized deviator stress behavior to an axial strain of approximately 5%.

The claystones transitions from a dilative to contractive behavior as the claystone softens evident by the plots of normalized excess porewater pressure versus strain and the normalized undrained stress paths. All the remolded specimens generated positive excess porewater pressure whereas the intact specimens generated negative excess porewater pressure. The undrained stress paths for the remolded claystone are characteristic of a contractive normally consolidated soil whereas

the undrained stress paths for the intact claystone are typical of dilative material. The failure lines of the intact material have a steeper slope than that of the remolded claystone, which correspond to higher strength parameters. The contrast in the behaviors of intact and remolded claystone shows that stronger intact rock is reduced to a remolded state that is essentially a normally consolidated clay with all effects of stress history, induration and diagenesis lost due to wetting and drying.

5.3. Shear Strength of Redbed Claystone

The following failure criteria were chosen to evaluate and compare shear strength parameters: (a) maximum deviator stress, (b) maximum stress obliquity ($\sigma'3/\sigma'1$), and (c) axial stress = 25% (i.e., end of test conditions). The stress-strain behavior of Bangkok clay was evaluated at maximum deviator stress criteria and the maximum stress obliquity criteria by Kim (1991). The third criterion is chosen on the assumption that at such large strains, the critical state would be achieved.

Table 5-1 and Table 5-2 summarizes the results of CU triaxial test on remolded and intact Redbed claystone specimens respectively. It includes the stress and strength parameters determined at the three failure criteria. In particular, the summary tables include effective stress friction angles and undrained shear strength ratios computed for each of the three criteria which represent the drained and undrained strength parameters from the test specimens.

Peak deviator stress was achieved at axial strains of 7-10%, whereas maximum stress obliquity was achieved at axial strains of 12-15%. However, there is negligible change in the value of M between these two criteria. The average values of M from all tests were 0.82 for maximum deviator stress and 0.83 for maximum stress obliquity. At large strains, there is a drop in the value of M to 0.79. The similarity in M is also reflected in the similarity in effective friction angles computed for each criteria.

The average effective stress friction angles were 21.1° for maximum deviator stress, 21.4° for maximum stress obliquity, and 20.4° end-of-test conditions at maximum axial strain achieved.

As stated in section 5.2.1, Re-60 and Re-100 exhibited behavior that were inconsistent with the other specimens. This is reflected in the strength parameters computed for these specimens; for Re-60 M-value (slope of the failure line) is lesser than the averages, ranging from 0.65 to 0.69. Specimen Re-100 had an M-value higher than that of the other specimens (0.92-0.95).

Although the remolded Redbed claystone tends to exhibit a slight peak, the softening is not very pronounced such that the remolded claystone may be treated as a nonlinear elasto-plastic material reaching a critical state at peak deviator stress. Although there is a drop in strength at large strain, if the soil has progressed to such large strains, failure would have already occurred for practical purposes.

There was practically no difference in undrained shear strength ratio evaluated at the maximum deviator stress criteria (0.285) or the maximum obliquity criteria (0.282. At large strains, the undrained strength ratio decreased to 0.255.

The average A parameter (of all specimens) at failure evaluated for maximum deviator stress and maximum stress obliquity were 0.88 and 0.91, respectively. The A-parameter (of all specimens) evaluated at end of test averages to 1.02. These values agree well with established literature (Bishop 1962).

The strength of intact claystone was evaluated based on only the peak deviator stress criterion owing to the face that behavior of the intact claystone post peak was inconsistent, as discussed previously. The slopes of the failure line were M= 1.56 for In-100, M = 1.18 for In-100-2, and M = 1.61 for In-200 at peak deviator stress. This variation in measured strength could be attributed to anisotropy within the rock fabric, the effect of which McLamore & Gray (1967) noted is more prominent at lower confining stresses. Ajalloeian & Lashkaripour (2000) also reported similar behavior in mudrocks where the uniaxial compressive strength of silt shales and mudshales decreased up to

60% depending on the orientation of discontinuities. According by Ademović & Kurtović (2021), mechanical properties of Miljevina stone were found to be affected by anisotropy on the micro-scale

The undrained shear strength ratios of the intact claystone were 3.35 for In-100, 3.33 for In-100-2, and 2.91 for In-200. The range of stresses that these tests were conducted was very low, and the failure envelop of intact rocks are curved in nature with the strength parameters decreasing at higher confining stresses (Hoek & Brown, 1980). To fully define the strength envelope and strength parameters of intact claystone, tests at a larger range of confining stresses are required.

As noted in section 5.2.3, the strength of remolded claystone is drastically lower than that of intact claystone as evident by the slope of the failure lines in p'-q space and the undrained shear strength ratio. This comparison in strength parameter further supports the hypothesis that there is significant effect of diagenesis in the intact specimen which is not present in the remolded claystones.

5.4. Consolidation Behavior of Redbed Claystone

5.4.1. Consolidation Behavior of Remolded Redbed Claystone

The results from 1-D consolidation tests on all remolded and intact Redbed claystone specimens are shown in Figure 5-18. The consolidation tests on remolded claystone were conducted on two types of specimens: (i) starting from slurry and (ii) pre-consolidated to a vertical effective stress of 25 kPa. Initial water content of the slurry specimens was 80%, corresponding to a void ratio of 2.18 and liquidity index of 1.78. The preloaded specimens had a starting moisture content of 45%, which was close to the liquid limit, and void ratio of 1.22.

The specimens consolidated from slurry follow a single compression to the final applied stress of 2000 kPa and then single swell curve, which is consistent with behavior described by Burland (1990). The compression index was computed for the compression line between vertical effective stress of

100 kPa and 1000 kPa, and swell index was computed as the slope at an overconsolidation ratio of 10; the compression index was 0.360 and swell index was 0.087. The respective λ and K were 0.156 and 0.038, respectively. The compression and swell indices for the preloaded remolded claystone tests were computed similarly and yielded 0.382 for compression and 0.075 for swell. The λ and K corresponding to the compression and swell indices were 0.166 and 0.033, respectively.

These values of λ from one-dimensional consolidation test are comparable to the λ obtained from the isotropic consolidation line and the critical state line obtained from the critical state line discussed in section 5.2.1 which provides further confidence in the data from the triaxial tests as well as validates the consolidation tests.

The specimens that were pre-consolidated and those prepared from slurry were obtained from two different buckets with slightly different initial water content, which likely contributes to the curves not exactly overlapping with each other. However, the compression and recompression behavior are quite consistent between all four consolidation specimens. It should be noted that during testing of one of the remolded samples (Re-1), the automatic load frame apparatus had a technical glitch and did not maintain a constant load of 2000 kPa thus leading to deviation in final void ratio for that stage.

5.4.2. Consolidation Behavior of Intact Redbed Claystone

Figure 5-17 presents the results from consolidation tests on both the intact Redbed claystone specimens and the remolded consolidation. The final vertical stress for the intact specimen was 1560 kPa, which was slightly lower than the tests conducted on the remolded specimen. The data indicates compression and recompression stages for the intact with indices 0.060 and 0.026 respectively.

The initial void ratio of the intact specimen prior to consolidation was 0.443 whereas the void ratio of slurry specimen at a consolidation load of 2000 kPa was ≈ 0.489. This could indicate that the pore fabric of intact rock is influenced by diagenesis which creates a much stiffer skeleton that exhibited minor compression which is most likely all recompression and the preconsolidation stress

was not exceeded. Similar observations were observed by Favero et al. (2016) on Opalinous Shale where void ratio of remolded shale was higher than that of the intact shale, which indicated the influence of diagenesis in shaping the pore fabric of the shale at stress range up to 100 MPa.

5.4.3. Consolidation Behavior Comparison

The compression and swelling indices of the intact claystones were considerably lower than that for the remolded and slurry Redbed claystone at similar stress levels, which support the high observed stiffness of the intact material. The consolidation tests confirm the fact that once broken down, the Redbed claystone does not retain any stress history or diagenetic bonding and behaves as a normally consolidated soil evidenced by the absence of preconsolidation pressure in the compression curves of slurry specimen.

5.5. Modified Cam Clay Parameterization and Simulation

The strength parameter (M) was obtained from triaxial test results of the four specimens Re-100-2, Re-200, Re-300 and Re-400. The specimens Re-60 and Re-100 were not used in the analysis because their behaviors deviated from that of the other four specimen as discussed previously. The consolidation and swelling parameters were adopted based on the one-dimensional consolidation test on both remolded and slurry specimens. Thus, the following parameters were adopted for the modeling procedure: $M = 0.81$, which is the average from all failure criteria; $\lambda = 0.162$ and $K = 0.036$, which are averages from the four 1-D consolidation tests.

Comparison between the expected shear behavior under undrained conditions as predicted by the Modified Cam Clay model and experimental results were made for the following: (a) normalized deviator stress versus axial strain; (b) normalized excess porewater pressure versus axial strain; and (c) normalized effective stress paths. These plots are presented from Figure 5-19 to Figure 5-21.

Shear strength and shear behavior are effectively captured by the Modified Cam Clay model for the specimens tested at effective confining(consolidation) stresses of 100 kPa or higher. However, the model does exhibit a slightly stiffer initial response as observed by the steeper initial curve in q/p' versus strain (Figure 5-20). At larger strains, the critical state predicted by the MCC model is attained as evident by the overlap of experimental and predicted stress strain. However, porewater pressures generated in undrained shear are overestimated by the MCC model. This is illustrated Figure 5-20 where the predicted normalized excess porewater pressure is higher than the experimental data.

The initial portion of the stress path for the tests at higher stresses (200-400 kPa) is predicted well by the Modified Cam Clay model. Experimental data diverges from predicted behavior at a q/p' value of 0.4. The notable deviation between the experimental data and model predictions is that the real samples exhibit higher strength. However, once the stress paths reach the failure line, they tend to converge towards the critical state predicted by the model.

The model deviated from observed behavior in two aspects : a) it failed to predict the peak deviator stress, and b) it overpredicted the excess porewater pressure generated.

Failure to predict a peak deviator stress is a well-documented limitation of many critical state models as noted by Yu (1998) .

Deviation in experimental data versus predicted results of excess porewater pressure can be observed by Skempton's A parameter at failure listed in Table 5-5. The summary in Table 5-5 includes the average A parameter at failure and undrained shear strength ratio at failure for test specimens Re-100-2, Re-200, Re-300 and Re-400 and predicted with the Modified Cam Clay model. The predicted A parameter is greater than experimental data by about 20% for the maximum deviator strain and maximum stress obliquity criteria. A parameter at large strain is comparable to the predicted value. MCC also slightly underpredicts the undrained shear strength.

Nevertheless, many aspects of stress-strain behavior and strength characteristics of the slaked Redbed claystone were represented well by the Modified Cam Clay. This comparison supports the use of the undrained shear behavior of the remolded specimens and fully softened strength as captured in the Modified Cam Clay for future evaluations of stress-deformation within the waste rock piles and Mae Moh Mine.

5.6. Practical Implications

The study was conducted to evaluate the shear and consolidation behavior of Redbed claystone in a remolded state. There is information present in past forensic reports and literature that suggests the base of the waste rock piles at Mae Moh Mine are composed primarily of Redbed claystone that is most likely broken down into clay via slaking. The presence of this lower strength layer at the base of the waste rock pile has been hypothesized to be the primary cause of landslides.

One of the significant results from this study was the validation of the Modified Cam Clay model as a viable material model for the remolded Redbed claystone. Back calculated strength parameters from numerical models of the landslide can be compared to the parameters obtained in this study in order to verify the hypothesis that slaked Redbed claystone is indeed present at the basal layer of the waste dump and its breakdown is impacting the stability of the waste dumps. The information from this study can also be useful for future operation of the mine as the waste dumps are still actively being used.

Table 5-1 Summary of consolidated undrained triaxial compression tests on remolded Redbed claystone.

Sample no.	Target σ' (kPa)	Actual σ' (kPa)	Failure Criteria	ε at failure (%)	$\Delta\sigma_f$ (kPa)	$\sigma'3_f$ (kPa)	$\sigma'1_f$ (kPa)	U_{ef} (kPa)	p'_f (kPa)	M	Su (kPa)	Su/p'c	Φ' (°)	Af
Re-60	60	64	Maximum Δσ	7.07	35.57	41.12	76.69	23.13	52.9	0.67	17.78	0.29	17.57	0.65
			Maximum σ'3/σ'1	12.24	35.52	39.5	75.02	24.31	51.3	0.69	17.76	0.28	18.07	0.68
			ε at end of test	12.49	33.06	39.52	72.58	24.38	50.5	0.65	16.53	0.26	17.15	0.74
Re-100	100	122	Maximum Δσ	8.71	89.22	63.89	153.1	57.76	93.6	0.95	44.61	0.37	24.28	0.65
			Maximum σ'3/σ'1	8.71	89.22	63.89	153.1	57.76	93.6	0.95	44.09	0.37	24.28	0.65
			ε at end of test	22.91	79.32	59.42	138.7	57.76	93.6	0.92	39.66	0.32	23.60	0.72
Re-100- 2	100	125	Maximum Δσ	9.67	69.28	63.11	132.3	62.7	86.2	0.80	34.64	0.28	20.76	0.91
			Maximum σ'3/σ'1	15.78	66.59	60.2	126.7	65.22	82.4	0.81	33.30	0.27	20.86	0.98
			ε at end of test	24.38	56.69	59.14	115.8	67.21	78.04	0.73	28.35	0.23	18.90	1.19
Re-200	200	224	Maximum Δσ	9.90	118.07	103.55	221.6	119.74	142.9	0.83	59.04	0.26	21.29	1.01
			Maximum σ'3/σ'1	12.80	117.92	101.27	219.1	121.8	140.5	0.84	58.96	0.26	21.59	1.03
			ε at end of test	25.76	104.17	95.74	199.9	127.1	130.4	0.80	52.09	0.23	20.63	1.22
Re-300	300	313	Maximum Δσ	9.74	164.10	142.99	307.1	168.64	197.70	0.83	82.05	0.26	21.38	1.03
			Maximum σ'3/σ'1	14.04	160.99	136.66	297.65	173.85	190.32	0.85	80.50	0.26	21.76	1.08
			ε at end of test	24.14	145.09	130.59	275.67	177.51	178.95	0.81	72.54	0.23	20.92	1.22
Re-400	400	421	Maximum Δσ	11.62	222.58	195.15	417.73	224.85	269.34	0.83	111.29	0.27	21.29	1.01
			Maximum σ'3/σ'1	15.01	222.36	190.56	412.92	229.94	264.68	0.84	111.18	0.27	21.62	1.03
			ε at end of test	18.98	216.72	193.29	410.02	224.85	265.53	0.82	108.36	0.26	21.05	1.04

Table 5-2 Summary of consolidated undrained triaxial compression test results on intact Redbed claystone.

Sample no.	Target σ' (kPa)	Actual σ' (kPa)	Failure Criteria	ε at failure (%)	$\Delta\sigma_f$ (kPa)	σ'_{3f} (kPa)	σ'_{1f} (kPa)	u_{ef} (kPa)	p'_f (kPa)	M	S_u (kPa)	S_u/p'_c	A_f
In-100	100	106	Maximum Δσ	6.92	705.26	218.31	923.57	-122.73	453.39	1.56	352.63	3.33	-0.17
In-100-2	100	107	Maximum Δσ	6.20	719.39	368.67	1088.06	-264.26	608.46	1.18	359.69	3.35	-0.37
In-200	200	228	Maximum Δσ	4.92	1327.82	382.83	1710.65	-161.46	825.44	1.61	663.91	2.91	-0.12

Table 5-3 Summary of results of 1-D consolidation test on remolded and slurry Redbed claystone

Sample		Initial void Ratio	Final Void Ratio	Initial water Content (%)	Final Water Content (%)	Compression Index	Swelling Index	λ	K
Slurry	Slurry 1	2.217	0.607	81	22	0.3636	0.081	0.158	0.035
	Slurry 2	2.183	0.603	80	22	0.3554	0.095	0.154	0.041
Remolded	Re -1	1.255	0.467	46	17	0.384	0.067	0.167	0.029
	Re -2	1.31	0.459	48	16	0.38	0.083	0.167	0.036

Table 5-4 Void ratios of normally consolidated Redbed claystones before and after shear

Specimen	Mean effective stress, p' (kPa)		Void Ratio (e)
	Prior to shear	At maximum deviator Stress	
Re-60	64	53.0	0.95
Re-100	122	93.6	0.84
Re-100 -2	125	86.2	0.83
Re-200	224	142.9	0.74
Re-300	313	197.7	0.68
Re-400	421	269.3	0.64

Table 5-5 Comparison of Skempton's A parameter at failure (A_f) and the undrained shear strength ration (S_u/σ'_v) between experimental results and modified cam clay model prediction.

	Criteria	M	Af	Su/p'c
Average values from experiment	Maximum $\Delta\sigma$	0.82	0.99	0.29
	Maximum σ'_3/σ'_1	0.83	1.03	0.28
	ε at end of test	0.79	1.17	0.26
CSSM MCC Prediction.	Maximum $\Delta\sigma$	0.82	1.21	0.24
	Maximum σ'_3/σ'_1	0.83	1.20	0.24
	ε at end of test	0.79	1.20	0.23

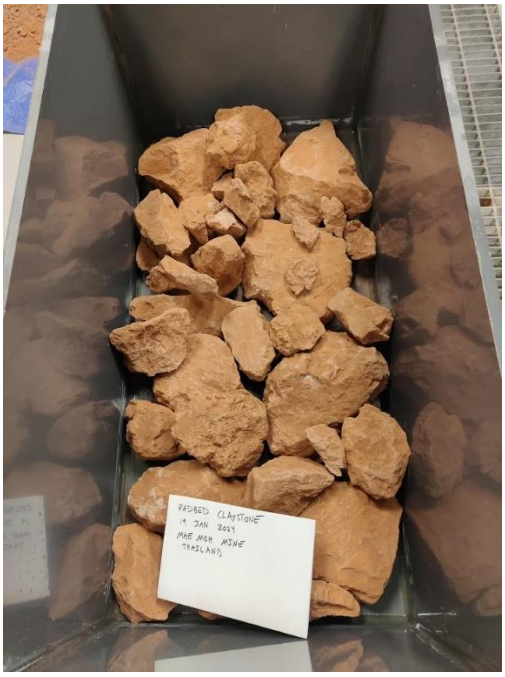

(a)

(b)

Figure 5-1 (a) Intact claystone before inundation with water and (b) after inundation with water.

(a)

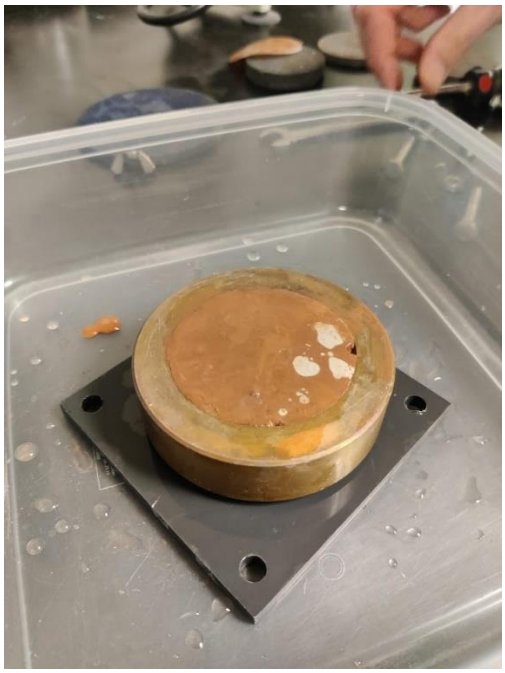

(b)

Figure 5-2 Photographs showing no breakdown of the Redbed claystone upon saturation as a result of confinement for the (a) at end of triaxial test and (b) consolidation ring specimen prior to testing.

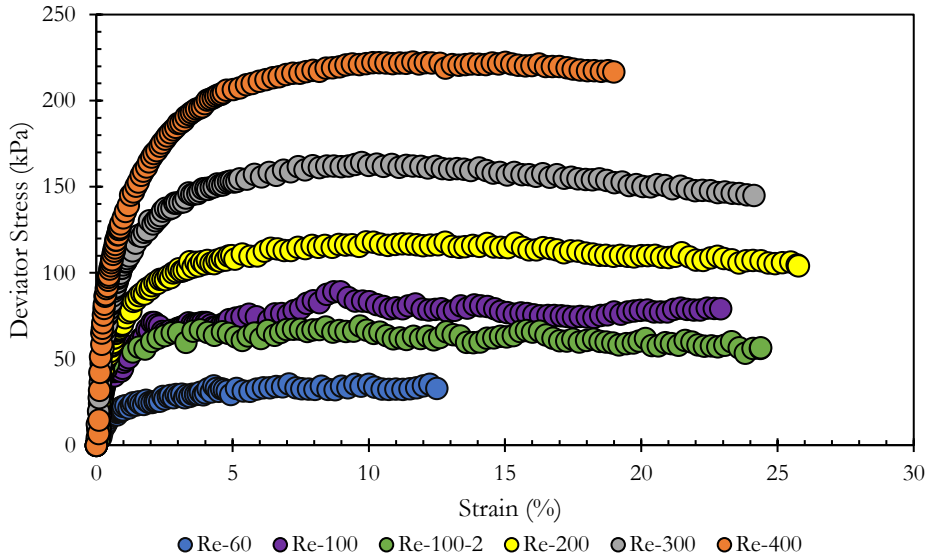

(a)

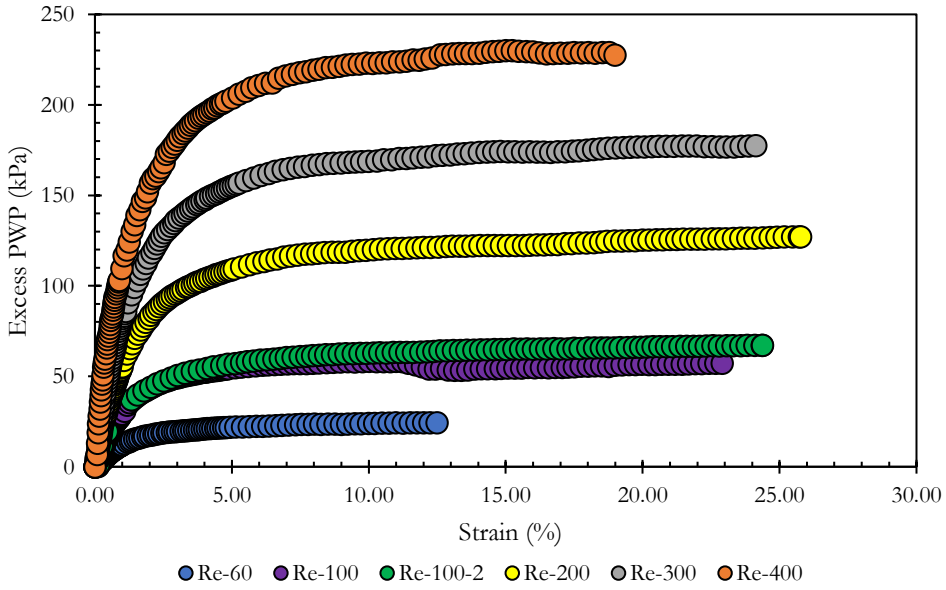

(b)

Figure 5-3 Plots of (a) deviator stress versus axial strain and (b) excess porewater pressure versus axial strain plot for normally consolidated remolded Redbed claystone under undrained triaxial compression

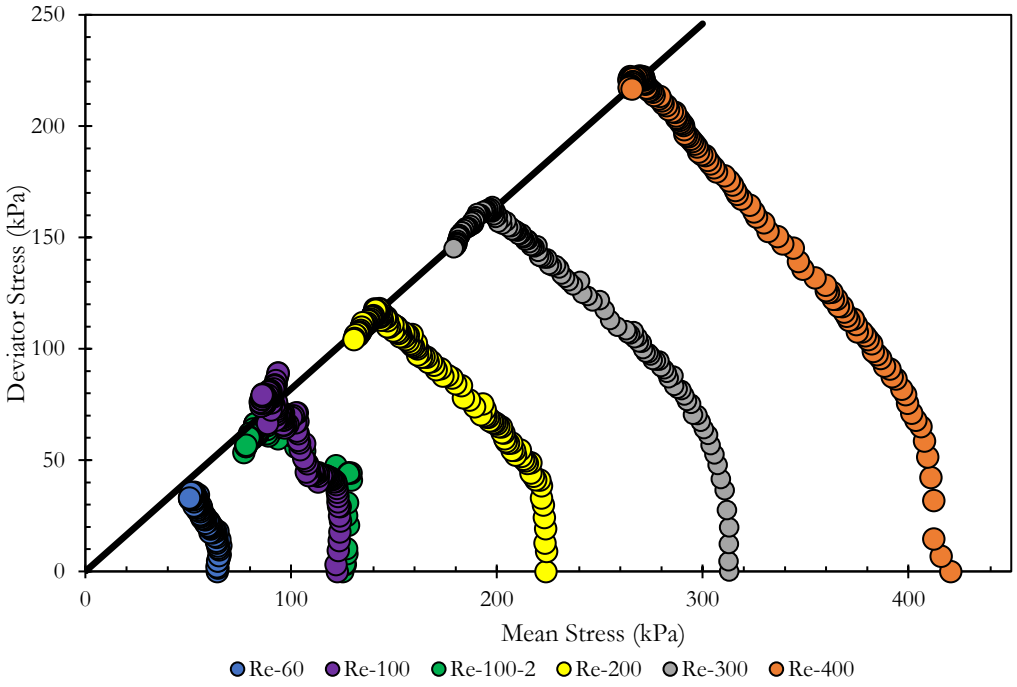

Figure 5-4 Undrained Effective stress paths in Cambridge notation for normally consolidated remolded Redbed claystone.

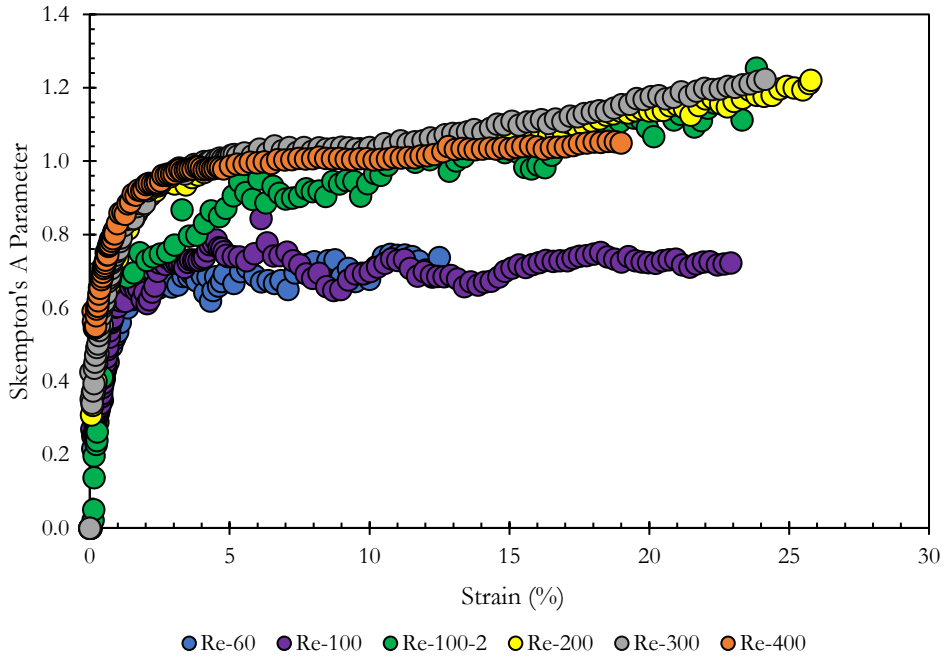

Figure 5-5 Skempton's A parameter versus axial strain plot for normally consolidated remolded Redbed claystone under undrained triaxial compression.

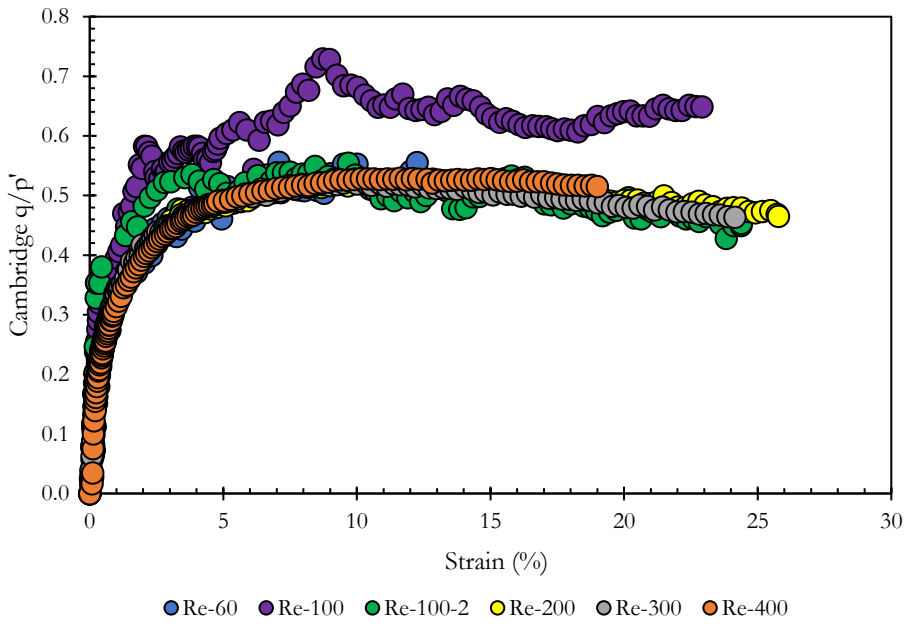

Figure 5-6 Normalized deviator stress versus axial strain for normally consolidated remolded Redbed claystone under undrained triaxial compression.

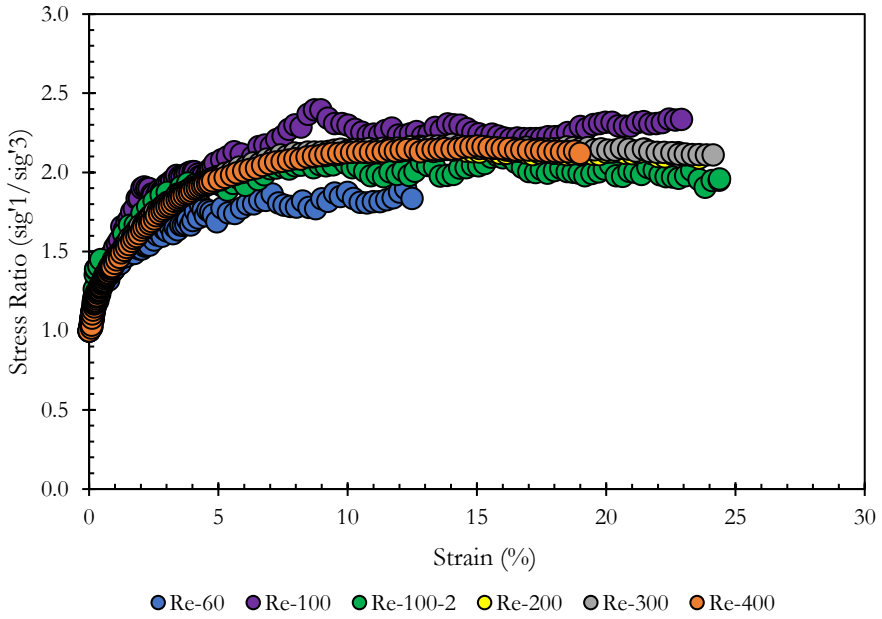

Figure 5-7 Principal stress ratio versus axial strain for normally consolidated remolded Redbed claystone under undrained triaxial compression

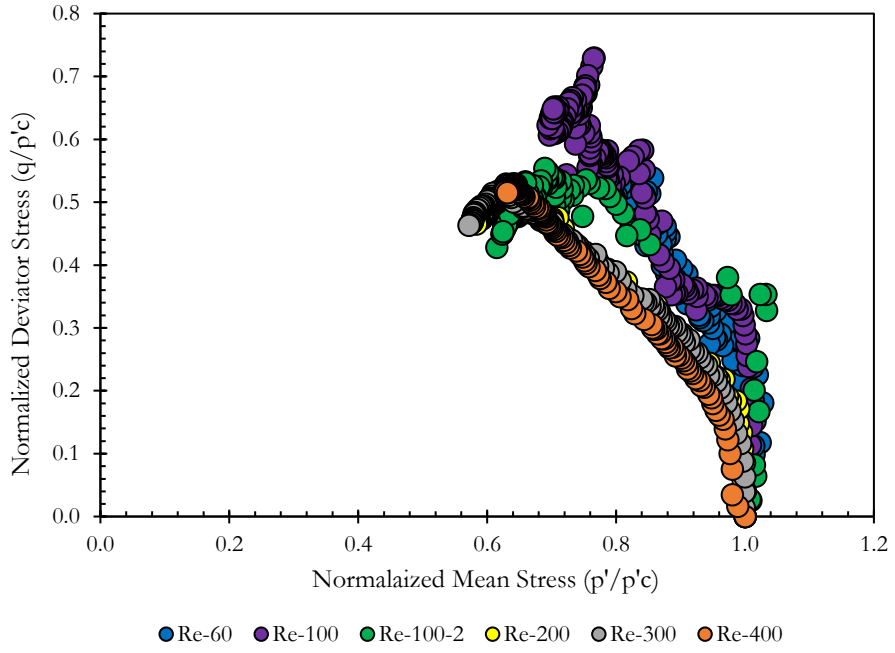

Figure 5-8 Normalized effective stress paths in Cambridge notation for normally consolidated remolded Redbed claystone.

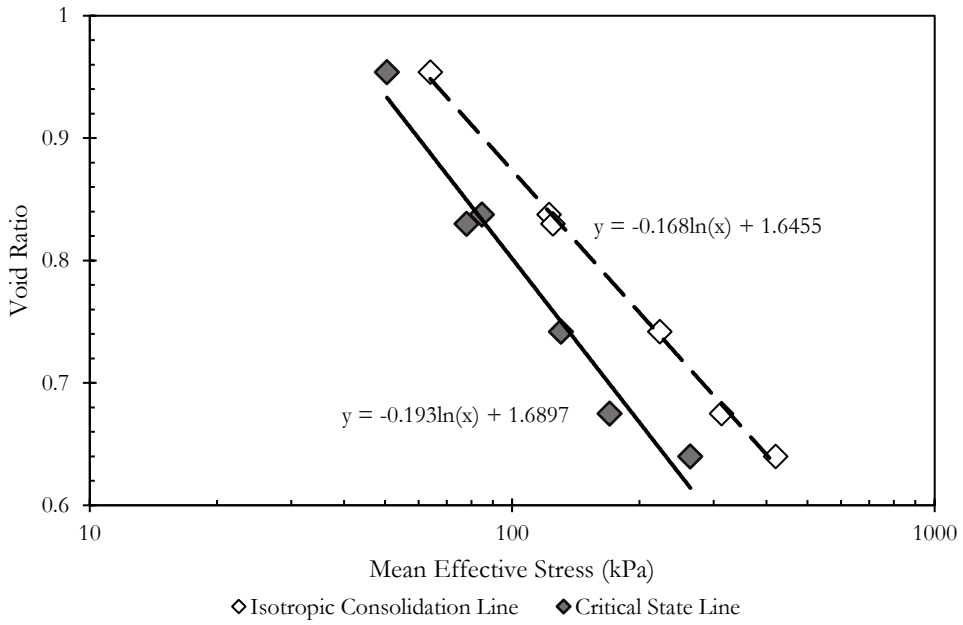

Figure 5-9 Plots of isotropic consolidation line and critical state line obtained by determining void ratio and mean effective stress prior and after shearing.

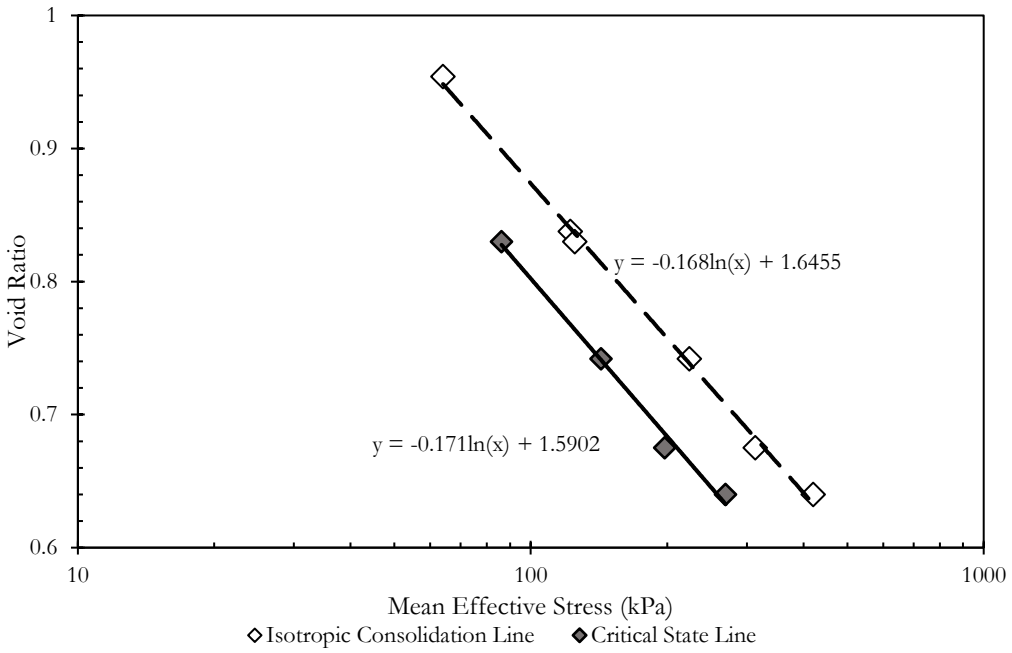

Figure 5-10 Plots of isotropic consolidation line and critical state line discarding the result for Re-60 and Re-100.

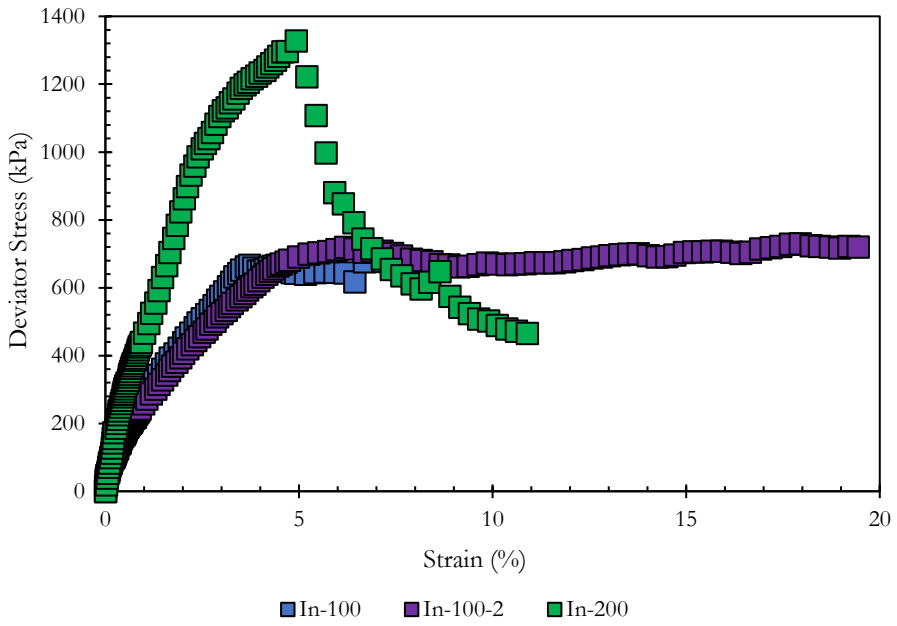

(a)

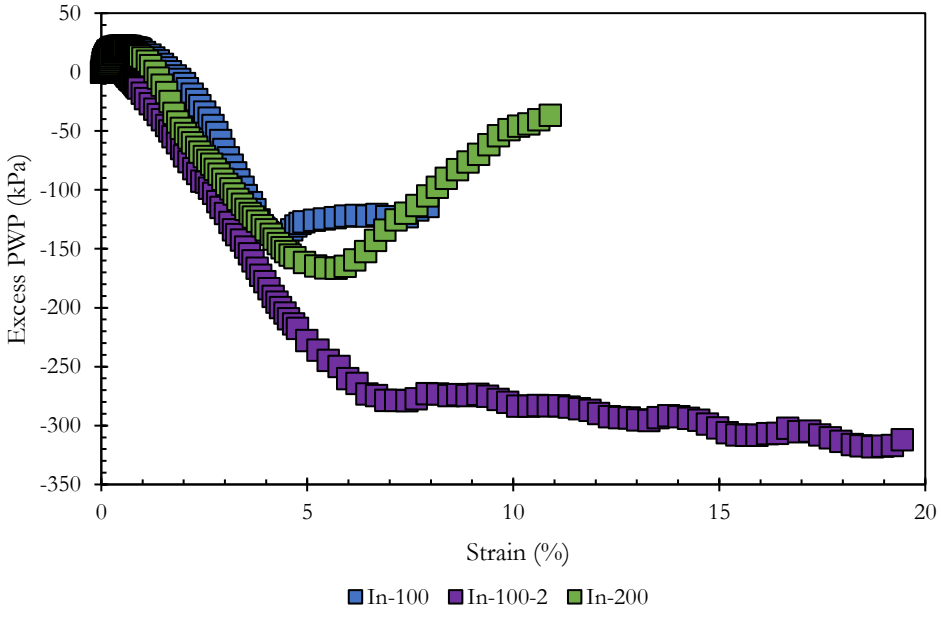

(b)

Figure 5-11 Plots of (a) deviator stress versus axial strain and (b) excess porewater pressure versus axial strain for intact Redbed claystone under undrained triaxial compression.

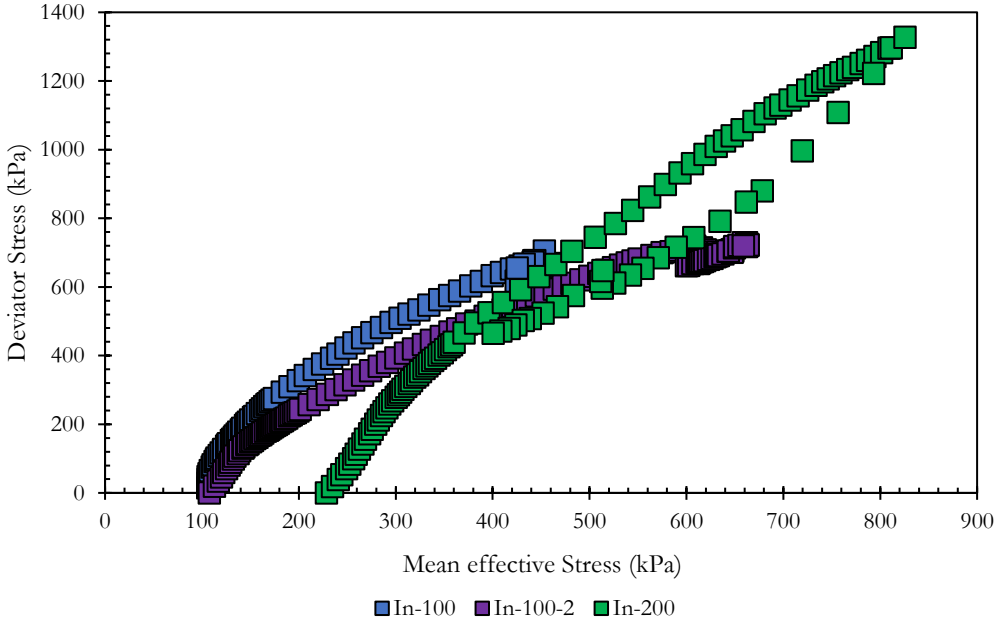

Figure 5-12 Undrained effective stress paths in Cambridge notation for intact Redbed claystone under undrained triaxial compression.

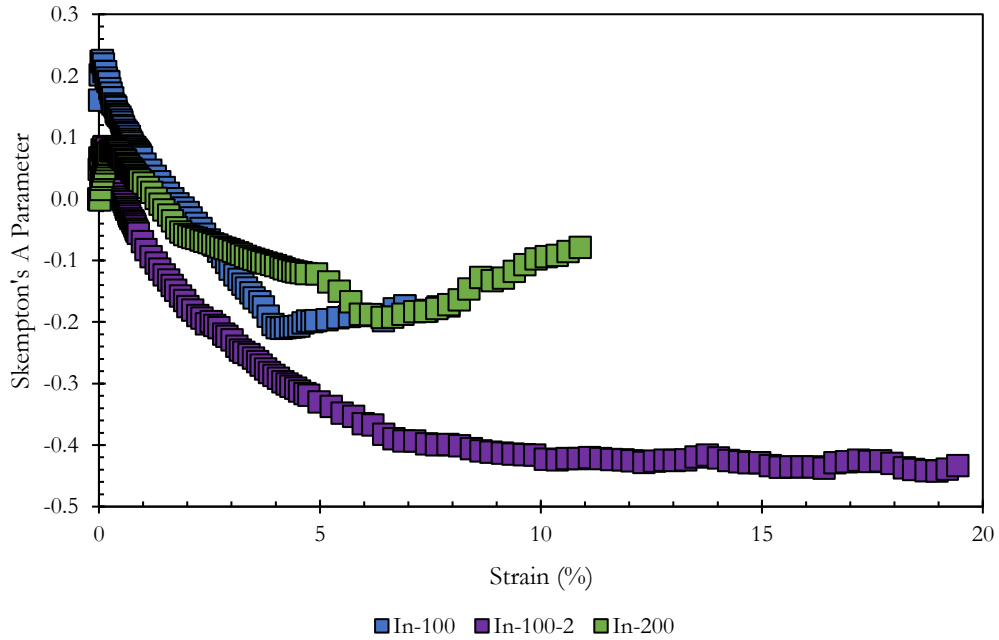

Figure 5-13 Skempton's A parameter versus axial strain plot for intact Redbed claystone under undrained triaxial compression.

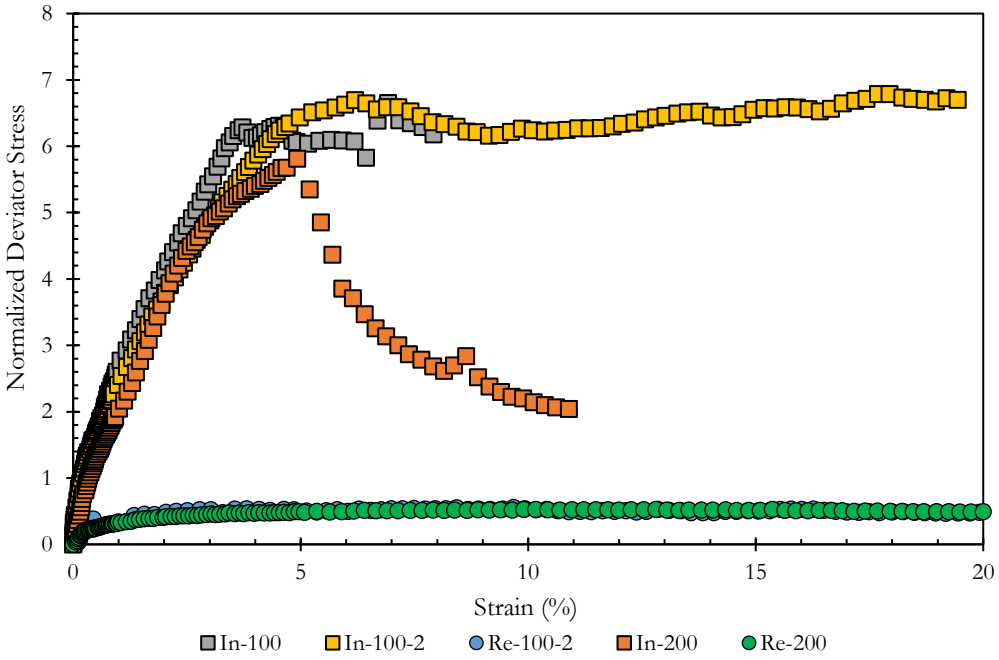

Figure 5-14 Comparison of normalized deviator stress versus strain between intact and remolded claystone.

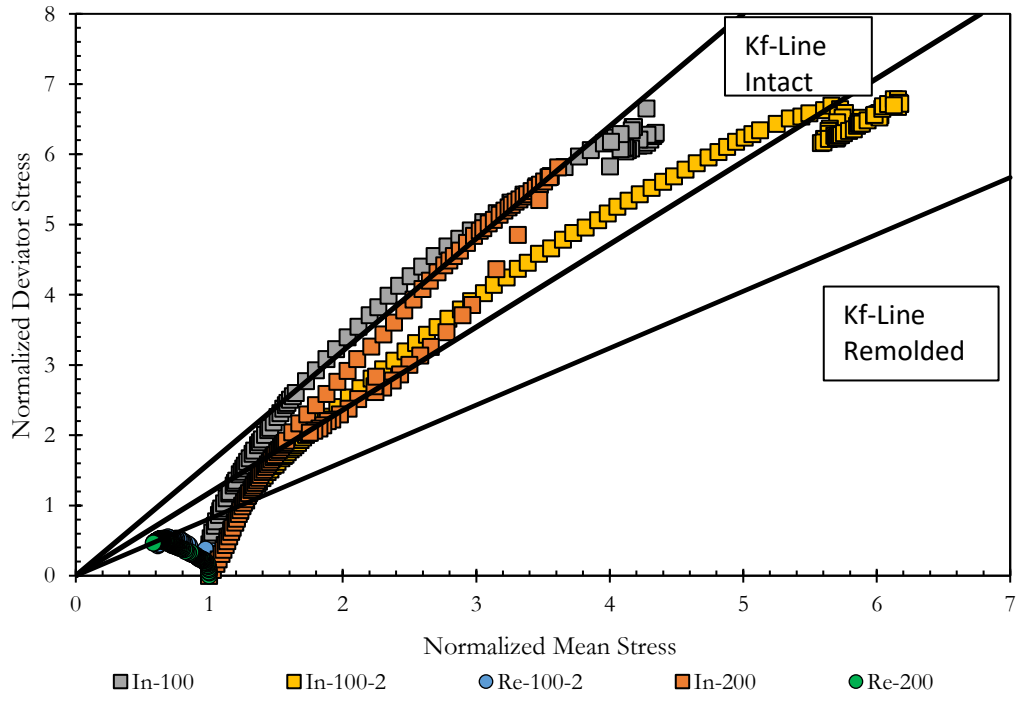

Figure 5-15 Comparison of normalized undrained effective stress paths of intact and remolded claystone.

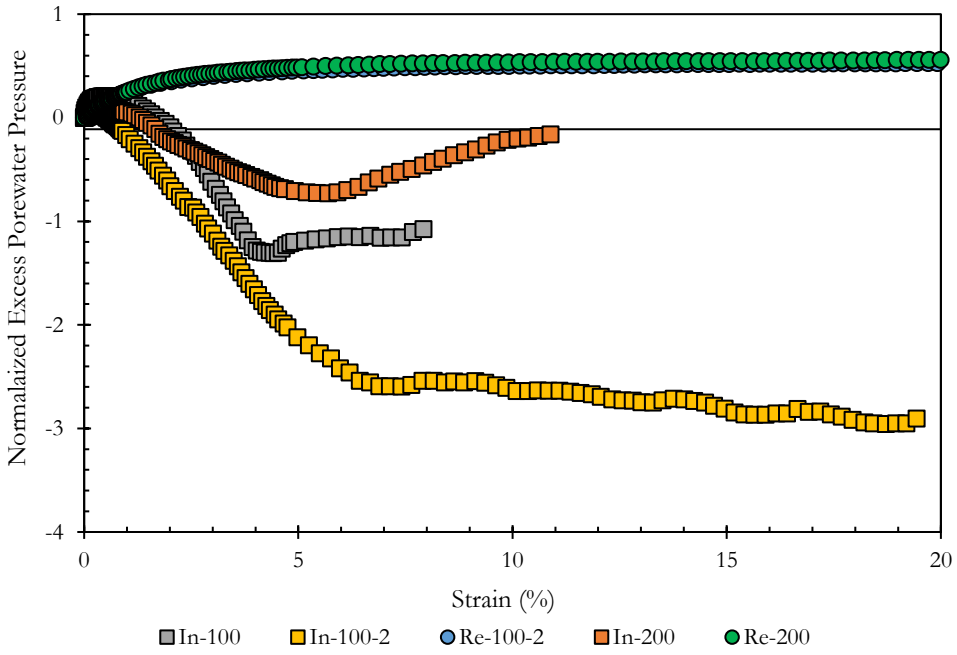

Figure 5-16 Comparison of normalized excess porewater pressure versus strain between intact and remolded claystone.

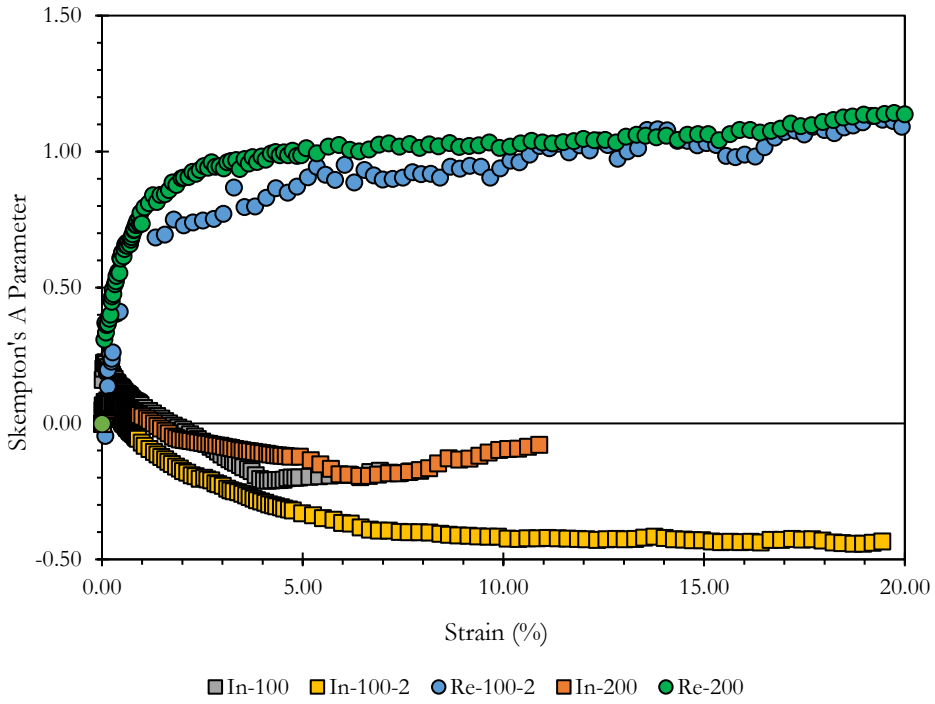

Figure 5-17 Comparison of Skempton's A parameter versus strain between intact and remolded claystone.

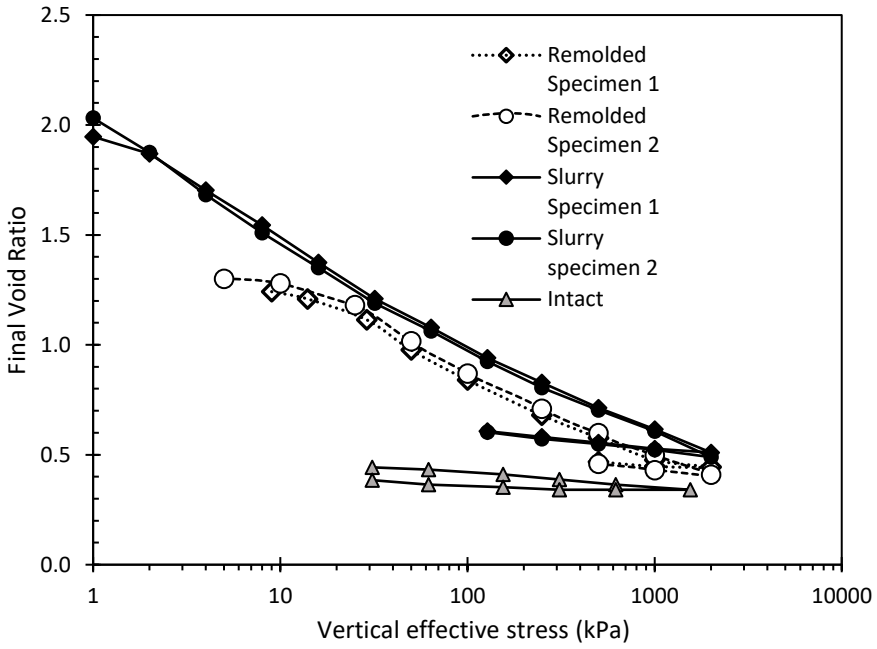

Figure 5-18 Void ratio versus vertical effective stress for all one-dimensional consolidation tests on remolded and intact Redbed claystone.

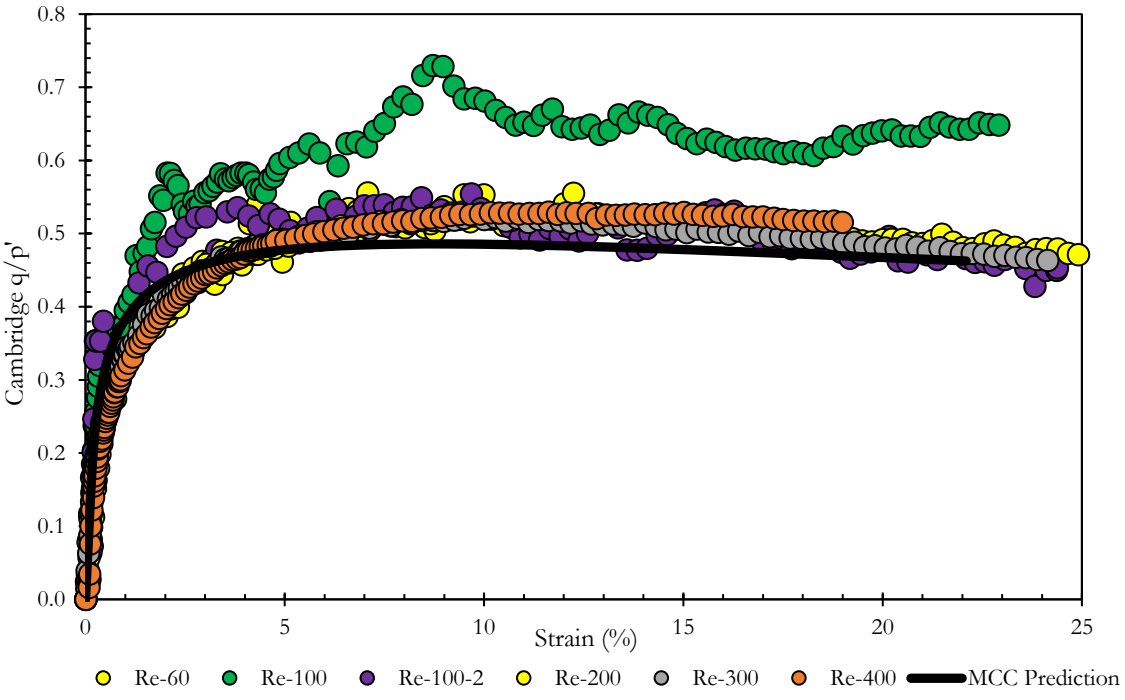

Figure 5-19 Comparison of normalized deviator stress versus axial strain predicted by modified Cam Clay model against experimental data for remolded Redbed claystone.

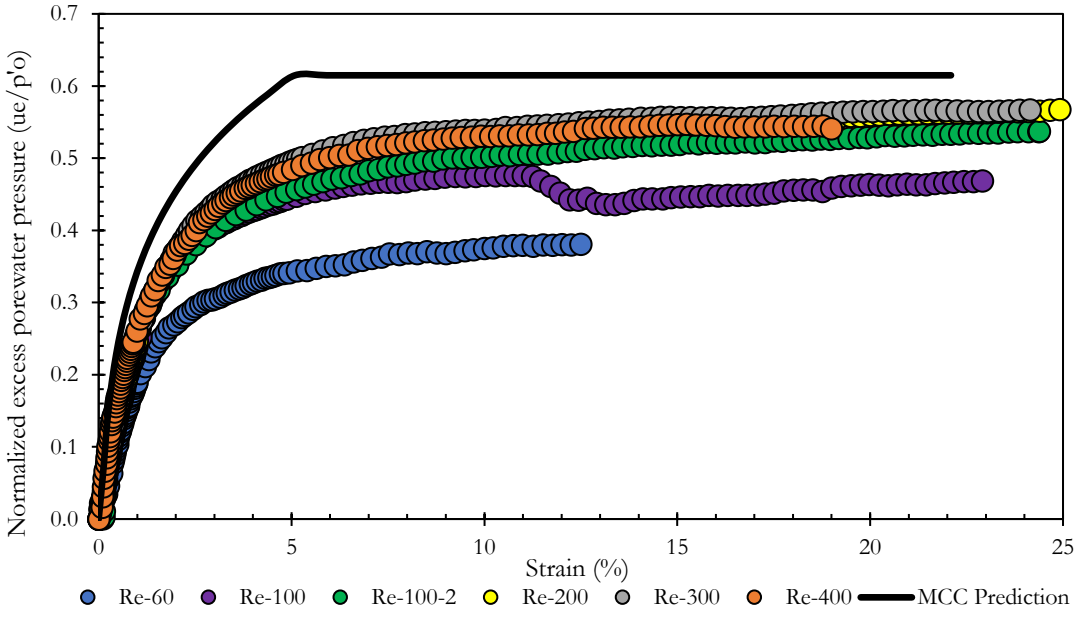

Figure 5-20 Comparison of excess porewater pressure predicted by modified Cam Clay model (normalized with respect to pre-shear isotropic consolidation pressure) versus axial strain for normally consolidated remolded Redbed claystone.

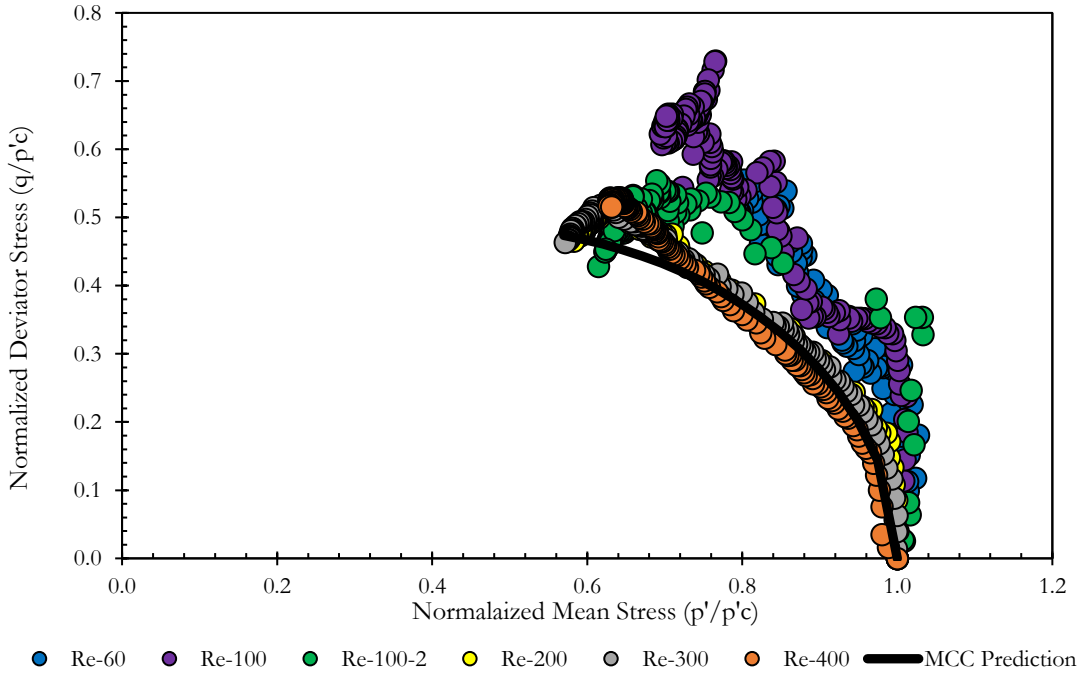

Figure 5-21 Comparison of effective stress path predicted by modified cam clay model (normalized with respect to pre-shear isotropic consolidation pressure) versus experimental data for normally consolidated remolded Redbed claystone.

Chapter 6 - Conclusions and Recommendations

6.1. Conclusions

The strength and consolidation characteristics of remolded and intact Redbed claystone were evaluated in this study. The motivation for the study was the recurrence of landslides occurring in the northwestern waste rock dump at the Mae Moh Lignite Mine, Lampang, Thailand. The following conclusions can be drawn from this study:

6.2. Strength Characteristics

- The slope of the failure line of the intact claystone ranged from 1.16 to 1.61 for three test specimens. The range suggests the rock fabric could be anisotropic at the micro scale.
- The effective stress friction angle of the remolded claystone obtained from isotropically consolidated undrained triaxial compression tests ranged between 20° and 21°.
- The undrained shear strength ratio of the remolded Redbed claystone ranged from 0.255 to 0.285.
- The undrained shear behavior of the intact Redbed claystones was represented by a tendency to dilate, whereas the remolded specimens exhibited a tendency to contract in undrained shear.
- The remolded specimens reached a critical state at around 7% to 11% axial strain, and the behavior of specimens consolidated to effective confining stresses ranging from 100 kPa to 400 kPa all exhibited similar shear behavior.

6.3. Consolidation Characteristics

- The compression (C_c*) and swelling index (C_s*) obtained from slurry consolidation were 0.156 and 0.038, respectively, which compared well to the compression index (Cc) and swelling index (Cs) obtained by 1-D consolidation test on remolded samples.
- The average values of λ and K for the remolded Redbed claystone were 0.165 and 0.036, respectively.

6.4. Applicability of Modified Cam Clay theory to model fully softened strength

- Using the critical state parameters obtained for the remolded Redbed triaxial and consolidation tests (M = 0.81, λ = 0.162, and K = 0.036), the MCC model effectively predicted the deviator stress-axial strain response of the remolded claystone.
- The model effectively captured the critical state, whereby the stress paths of all specimens approached a unique stress ratio at large strain.
- Excess porewater pressures were overestimated by the model as reflected by the predicted A-parameter whereas strength predictions are slightly conservative as undrained shear strength ratios were underestimated.
- The non-linear elastic-plastic stress-strain response along with the predicted stress path imply the Modified Cam Clay model is a viable tool to model the behavior of remolded (i.e., fully softened) Redbed claystone.
- The fully softened strength and shear behavior of the Redbed claystone can be modelled with reasonable accuracy using the Modified Cam Clay theory.

6.5. Recommendations for future work

- The slaking and breakdown of intact rock should be studied under confining stresses representative of the dump height.
- Additional strength tests at confining stresses levels that represent the higher overburden on site should be conducted to observe behavior at higher stresses.
- Slaking behavior of rockfill with particle gradation and density representative of field conditions (confining stresses, field void ratio) should be established.
- K_o-consolidated triaxial tests in both compression and extension should be conducted to study stress-strain behaviors that more accurately represent K_0 conditions in the field.
- The effect of mixing the other types of claystones with Redbed should be studied.
- Strength and consolidation tests on in situ undisturbed samples from the basal layers of the waste dump are recommended to compare their characteristics to remolded laboratory specimens.

REFERENCES

Ademović, N., & Kurtović, A. (2021). Influence of planes of anisotropy on physical and mechanical properties of freshwater limestone (Mudstone). *Construction and Building Materials*, *268*, 121174. https://doi.org/10.1016/j.conbuildmat.2020.121174

Aird, P. (2019). Deepwater Geology & Geoscience. In *Deepwater Drilling* (pp. 17–68). Elsevier. https://doi.org/10.1016/B978-0-08-102282-5.00002-8

Ajalloeian, R., & Lashkaripour, G. R. (2000). Strength anisotropies in mudrocks. *Bulletin of Engineering Geology and the Environment*, *59*(3), 195–199. https://doi.org/10.1007/s100640000055

Alonso, E. E., & Pinyol, N. M. (2015). Slope stability in slightly fissured claystones and marls. *Landslides*, *12*(4), 643–656. https://doi.org/10.1007/s10346-014-0526-5

Bell, F. G., Entwisle, D. C., & Culshaw, M. G. (1997). A geotechnical survey of some British Coal Measures mudstones, with particular emphasis on durability. *Engineering Geology*, *46*(2), 115–129. https://doi.org/10.1016/S0013-7952(96)00106-8

Berre, T. (2011). Triaxial Testing of Soft Rocks. *Geotechnical Testing Journal*, *34*(1), 61–75. https://doi.org/10.1520/GTJ102879

Bishop, A. W. (Alan W. (1962). *The measurement of soil properties in the triaxial test* (2nd ed.). Arnold.

Botts, M. E. (1986). *The Effects of Slaking on The Engineering Behaviour of Clay Shales*. University of Colorado.

Burland, J. B. (1965). The Yielding and Dilation of Clay. *Géotechnique*, *15*(2), 211–214. https://doi.org/10.1680/geot.1965.15.2.211

Burland, J. B. (1990). On the compressibility and shear strength of natural clays. *Géotechnique*, *40*(3), 329–378. https://doi.org/10.1680/geot.1990.40.3.329

Castellanos, B. A. (2014). *Use and Measurement of Fully Softened Shear Strength* [Doctoral Dissertation]. Virginia Polytechnic Institute and State University.

Castellanos, B. A., & Brandon, T. L. (2019, November 17). *Fully Softened Shear Strength: Application, Measurement, and Correlations*. XVI Pan American Conference on Soil Mechanics and Geotechnical Engineering, Cancun, Mexico.

Chandler, R. J. (1969). The Effect of Weathering on the Shear Strength Properties of Keuper Marl. *Géotechnique*, *19*(3), 321–334. https://doi.org/10.1680/geot.1969.19.3.321

Chiu, H. K., Johnston, I. W., & Donald, I. B. (1983). Appropriate Techniques for Triaxial Testing of Saturated Soft Rock. *International Journal of Rock Mechanics and Mining Sciences & Geomechanics Abstracts*, *20*(3), 107–120. https://doi.org/10.1016/0148-9062(83)91301-3

Cripps, J. C. (1987). ENGINEERING CHARACTERISTICS OF BRITISH OVER-CONSOLIDATED CLAYS AND MUDROCKS, II. MESOZOIC DEPOSITS. *Engineering Geology*, *23*.

Cripps, J. C., & Taylor, R. K. (1981). The engineering properties of mudrocks. *Quarterly Journal of Engineering Geology*, *14*(4), 325–346. https://doi.org/10.1144/GSL.QJEG.1981.014.04.10

Czerewko, M. A., & Cripps, J. C. (2001). Assessing the durability of mudrocks using the modified jar slake index test. *Quarterly Journal of Engineering Geology and Hydrogeology*, *34*(2), 153–163. https://doi.org/10.1144/qjegh.34.2.153

D18 Committee. (n.d.-a). *Test Method for Consolidated Undrained Triaxial Compression Test for Cohesive Soils*. ASTM International. https://doi.org/10.1520/D4767-11R20

D18 Committee. (n.d.-b). *Test Methods for Liquid Limit, Plastic Limit, and Plasticity Index of Soils*. ASTM International. https://doi.org/10.1520/D4318-17E01

D18 Committee. (n.d.-c). *Test Methods for Specific Gravity of Soil Solids by Water Pycnometer*. ASTM International. https://doi.org/10.1520/D0854-23

Erguler, Z. A., & Shakoor, A. (2009). Quantification of Fragment Size Distribution of Clay-Bearing Rocks after Slake Durability Testing. *Environmental and Engineering Geoscience*, *15*(2), 81–89. https://doi.org/10.2113/gseegeosci.15.2.81

Favero, V., Ferrari, A., & Laloui, L. (2016). On the hydro-mechanical behaviour of remoulded and natural Opalinus Clay shale. *Engineering Geology*, *208*, 128–135. https://doi.org/10.1016/j.enggeo.2016.04.030

Ferrari, A., Rosone, M., Ziccarelli, M., & Giger, S. B. (2020). The shear strength of Opalinus Clay shale in the remoulded state. *Geomechanics for Energy and the Environment*, *21*, 100142. https://doi.org/10.1016/j.gete.2019.100142

Franklin, J. A., & Chandra, R. (1972). THE SLAKE-DURABILITY TEST. *International Journal of Rock Mechanics and Mining Sciences & Geomechanics Abstracts*, *9*(3), 325–328. https://doi.org/10.1016/0148-9062(72)90001-0

Gautam, T. P., & Shakoor, A. (2013). Slaking behavior of clay-bearing rocks during a one-year exposure to natural climatic conditions. *Engineering Geology*, *166*, 17–25. https://doi.org/10.1016/j.enggeo.2013.08.003

Giger, S. B., Ewy, R. T., Favero, V., Stankovic, R., & Keller, L. M. (2018). Consolidated-undrained triaxial testing of Opalinus Clay: Results and method validation. *Geomechanics for Energy and the Environment*, *14*, 16–28. https://doi.org/10.1016/j.gete.2018.01.003

Green, R., & Wright, S. G. (1986). *Factors Affecting the Long Term Strength of Compacted Beaumont Clay* (FHWA/TX-87/39+436-1; p. 222). University of Texas at Austin,.

H K Chiu, & Johnston, I. W. (1980). The Effects of Drainage Conditions and Confining Pressures on the Strength of Melbourne Mudstone. *Proceedings of the 3rd ANZ Conference on Geomechanics*. The Third Australia-New Zealand Conference on Geomechanics, Wellington.

Haldar, S. K., & Tišljar, J. (2014). Sedimentary Rocks. In *Introduction to Mineralogy and Petrology* (pp. 121–212). Elsevier. https://doi.org/10.1016/B978-0-12-408133-8.00005-5

Hoek, E., & Brown, E. T. (1980). Empirical Strength Criterion for Rock Masses. *Journal of the Geotechnical Engineering Division*, *106*(9), 1013–1035. https://doi.org/10.1061/AJGEB6.0001029

Jehring, M. M. (2014). *EFFECT OF TAILINGS COMPOSITION ON THE SHEAR STRENGTH BEHAVIOR OF MINE WASTE ROCK AND TAILINGS MIXTURES* [Masters]. Colorado State University.

Kanji, M., He, M., & Ribeiro E Sousa, L. (Eds.). (2020). *Soft Rock Mechanics and Engineering*. Springer International Publishing. https://doi.org/10.1007/978-3-030-29477-9

Kim, S. R. (1991). *Stress-Strain Behaviour and Strength Characteristics of Lightly Overconsolidated Clays* [Doctoral Dissertation]. Asian Institute of Technology.

McLamore, R., & Gray, K. E. (1967). The Mechanical Behavior of Anisotropic Sedimentary Rocks. *Journal of Engineering for Industry*, *89*(1), 62–73. https://doi.org/10.1115/1.3610013

Nahazanan, H., Clarke, S., Asadi, A., Md.Yusoff, Z., & Huat, B. K. (2013). Effect of inundation on shear strength characteristics of mudstone backfill. *Engineering Geology*, *158*, 48–56. https://doi.org/10.1016/j.enggeo.2013.03.003

Nakano, R. (1967). On Weathering and Change of Properties of Tertiary Mudstone Related to Landslide. *Soils and Foundations*, *7*(1), 1–14. https://doi.org/10.3208/sandf1960.7.1

Nidhinandana, P. (2022). *EVALUATION OF SLOPE FAILURE DUE TO THE REDUCTION OF SHEAR STRENGTH FROM THE SLAKING EFFECT AT THE MAE MOH MINE IN THAILAND*. Asian Institute of Technology.

Nunt-jaruwong, S. (2006). *Engineering geology of the Patonga Claystone, Central Coast, New South Wales, with particular reference to slaking behaviour* [UNSW Sydney]. https://doi.org/10.26190/UNSWORKS/16938

Pells Sullivan Meynink Engineering Consolutants. (2018). *Geotechnical Report of Mae Moh Mine*.

Pineda, J. A., Alonso, E. E., & Romero, E. (2014). Environmental degradation of claystones. *Géotechnique*, *64*(1), 64–82. https://doi.org/10.1680/geot.13.P.056

Potter, P. E., Maynard, J. B., & Depetris, P. J. (2005). *Mud and mudstones: Introduction and overview*. Springer.

Primus, J. M. (2024). *Shear and Consolidation Behaviour of Slurry Deposited, Desiccated Tailings and Compacted Filtered Tailings* [Masters]. Colorado State University.

Qi, J., Sui, W., Liu, Y., & Zhang, D. (2015). Slaking Process and Mechanisms Under Static Wetting and Drying Cycles Slaking Tests in a Red Strata Mudstone. *Geotechnical and Geological Engineering*, *33*(4), 959–972. https://doi.org/10.1007/s10706-015-9878-4

Reid, D., Fourie, A., Ayala, J. L., Dickinson, S., Ochoa-Cornejo, F., Fanni, R., Garfias, J., Da Fonseca, A. V., Ghafghazi, M., Ovalle, C., Riemer, M., Rismanchian, A., Olivera, R., & Suazo, G. (2021). Results of a critical state line testing round robin programme. *Géotechnique*, *71*(7), 616–630. https://doi.org/10.1680/jgeot.19.P.373

Roscoe, K. H., Schofield, A. N., & Wroth, C. P. (1958). On The Yielding of Soils. *Géotechnique*, *8*(1), 22–53. https://doi.org/10.1680/geot.1958.8.1.22

Seedsman, R. (1986). The behaviour of clay shales in water. *Canadian Geotechnical Journal*, *23*(1), 18–22. https://doi.org/10.1139/t86-003

Sharma, K., Kiyota, T., & Kyokawa, H. (2017). Effect of slaking on direct shear behaviour of crushed mudstones. *Soils and Foundations*, *57*(2), 288–300. https://doi.org/10.1016/j.sandf.2017.03.006

Shen, P., Tang, H., Wang, D., Su, X., & Huang, L. (2020). Weakening of mudstone fragments due to disintegration: An experimental investigation. *Bulletin of Engineering Geology and the Environment*, *79*(10), 5477–5497. https://doi.org/10.1007/s10064-020-01874-z

Skempton, A. W. (1970). First-Time Slides in Over-Consolidated Clays. *Géotechnique*, *20*(3), 320–324. https://doi.org/10.1680/geot.1970.20.3.320

Skempton, A. W. (1977). *Slope Stability of Cuttings in Brown London Clay*. 261–270. https://doi.org/10.1680/sposm.02050

Stark, T. D., & Fernandez, R. (2020). Fully Softened Shear Strength Measurement and Correlations. *Geotechnical Testing Journal*, *43*(5), 1201–1215. https://doi.org/10.1520/GTJ20190124

Stephens, I., & Branch, A. (2013). *Testing Procedure for Estimating Fully Softened Shear Strengths of Soils Using Reconstituted Material*. U. S. Army Corps of Engineers. https://apps.dtic.mil/sti/pdfs/ADA586283.pdf

Tandicul, W., Muangnoicharoen, N., & Gumperayarnnont, N. (1986). The slope stability problem at Mae Moh Lignite Mine, Lampang Province, Northern Thailand. *Bulletin of the Geological Society of Malaysia*, *19*, 613–625. https://doi.org/10.7186/bgsm19198645

Taylor, R. K., & Spears, D. A. (1970). The breakdown of British Coal Measure rocks. *International Journal of Rock Mechanics and Mining Sciences & Geomechanics Abstracts*, *7*(5), 481–501. https://doi.org/10.1016/0148-9062(70)90002-1

Terzaghi, K., Peck, R. B., Mesri, G., & Peck, R. B. (1996). *Soil mechanics in engineering practice* (3. ed). Wiley.

Ulusay, R., Arlkan, F., & Yoleri, M. F. (1995). *Engineering geological characterization of coal mine waste material and an evaluation in the context of back-analysis of spoil pile instabilities in a strip mine, SW Turkey*.

Wang, C. (2019). *Meaning, measurement, and field application of fully softened shear strength of stiff clays and clay shales* [Doctoral Dissertation, University of Illinois at Urbana-Champaign]. https://cdnsciencepub.com/doi/10.1139/cgj-2020-0663

Wei, T., Chen, G., Wu, L., & Liu, F. (2022). Rapid reduction in the shear resistance and permeability of the weak layer in the evolution of water-rock weathering. *Engineering Geology*, *299*, 106545. https://doi.org/10.1016/j.enggeo.2022.106545

Wroth, C. P. (1984). The interpretation of in situ soil tests. *Géotechnique*, *34*(4), 449–489.

Yoshida, N. (1990). *Time-Dependent Instability in Fissured Overconsolidated Clays and Mudstones*. The University of Alberta.

Yu, H. S. (1998). CASM: A unified state parameter model for clay and sand. *International Journal for Numerical and Analytical Methods in Geomechanics*, *22*(8), 621–653. https://doi.org/10.1002/(SICI)1096-9853(199808)22:8<621::AID-NAG937>3.0.CO;2-8

Zevgolis, I. E. (2018). Geotechnical characterization of mining rock waste dumps in central Evia, Greece. *Environmental Earth Sciences*, *77*(16), 566. https://doi.org/10.1007/s12665-018-7743-5

Zhang, C., & Rothfuchs, T. (2004). Experimental study of the hydro-mechanical behaviour of the Callovo-Oxfordian argillite. *Applied Clay Science*, *26*(1–4), 325–336. https://doi.org/10.1016/j.clay.2003.12.025

APPENDIX A: RESULTS FROM CIU TRIAXIAL TEST

Specimen Re 60

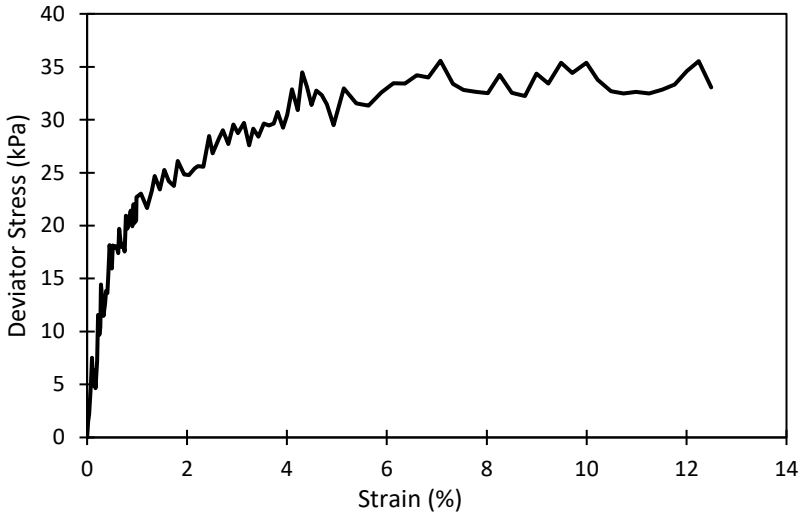

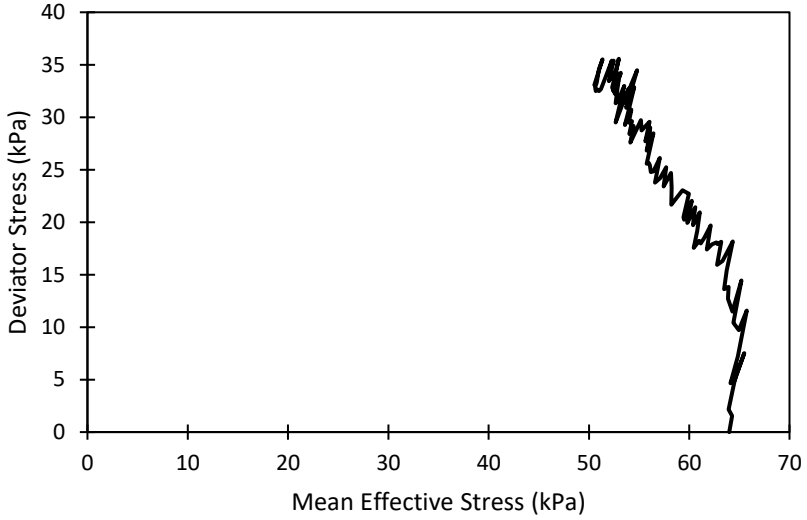

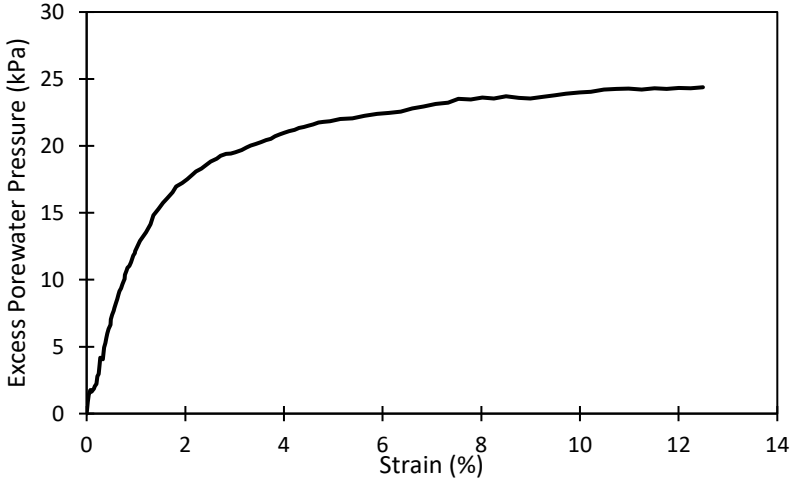

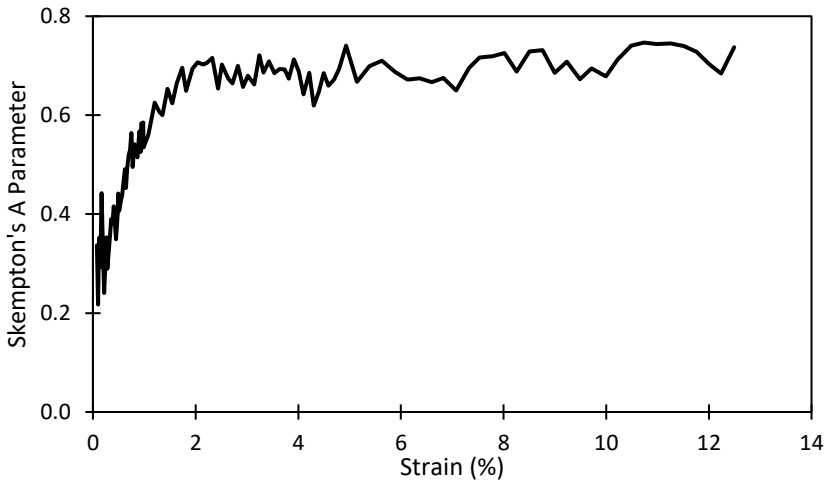

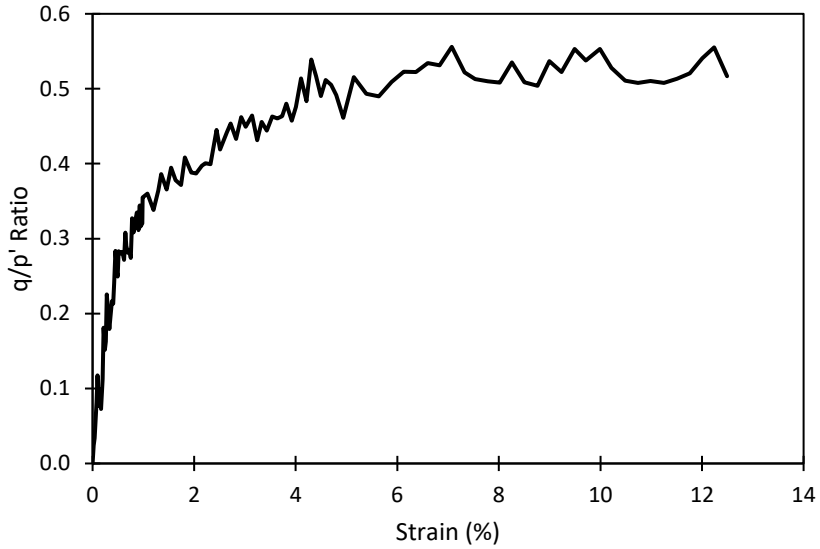

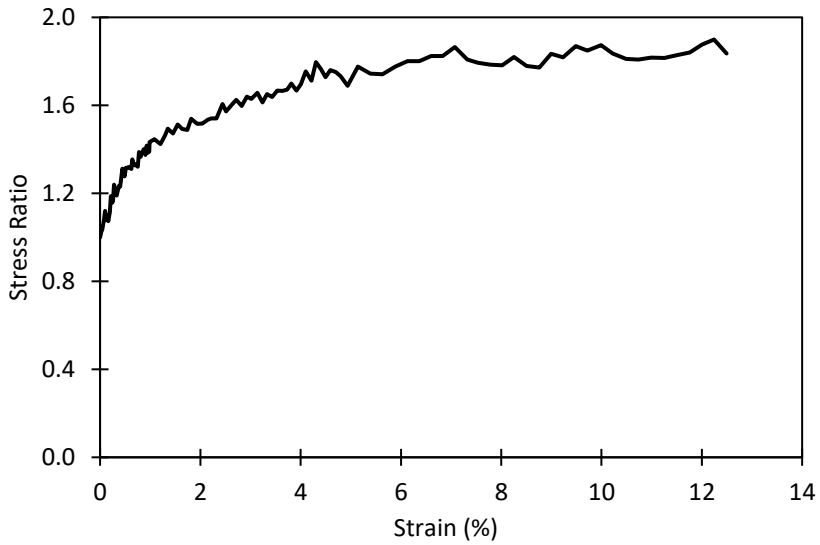

Sample no.	Target σ' (kPa)	Actual σ' (kPa)	Failure Criteria	ε at failure (%)	$\Delta\sigma_f$ (kPa)	$\sigma'3_f$ (kPa)	$\sigma'1_f$ (kPa)	U_{ef} (kPa)	p'_f (kPa)	M	Su (kPa)	Su/p'c	phi' (°)	Af
ReRb 60	60	64	Maximum Δσ	7.07	35.57	41.12	76.69	23.13	52.9	0.67	17.78	0.278	17.57	0.65
			Maximum σ'3/σ'1	12.24	35.52	39.5	75.02	24.31	51.3	0.69	17.76	0.278	18.07	0.68
			ε at end of test	12.49	33.06	39.52	72.58	24.38	50.5	0.65	16.53	0.258	17.15	0.74

Specimen Re 100

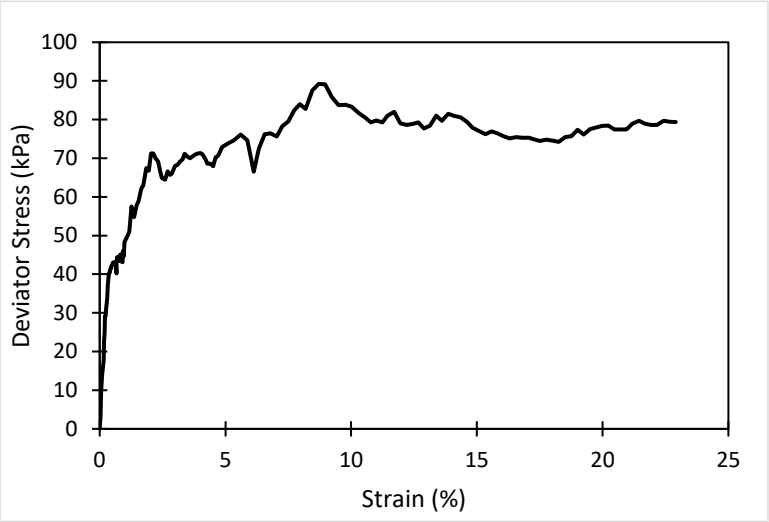

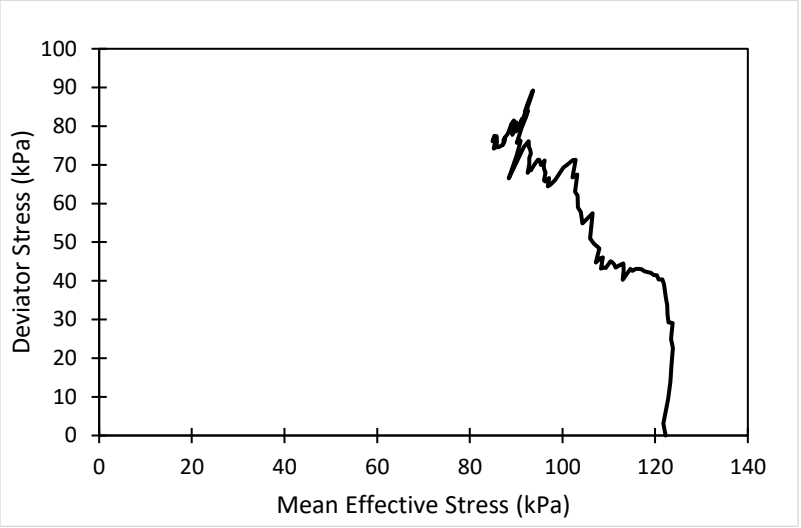

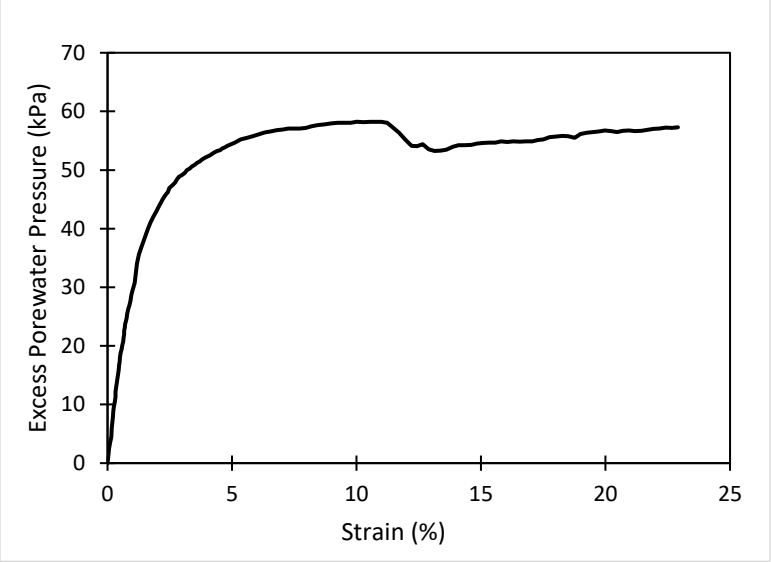

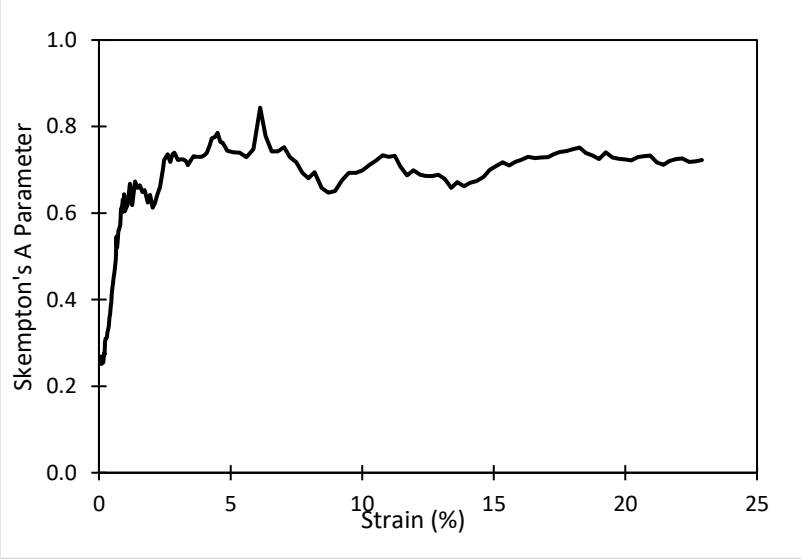

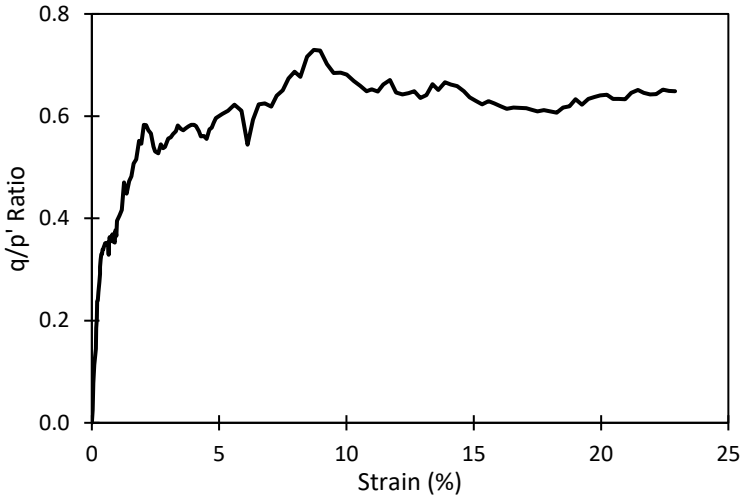

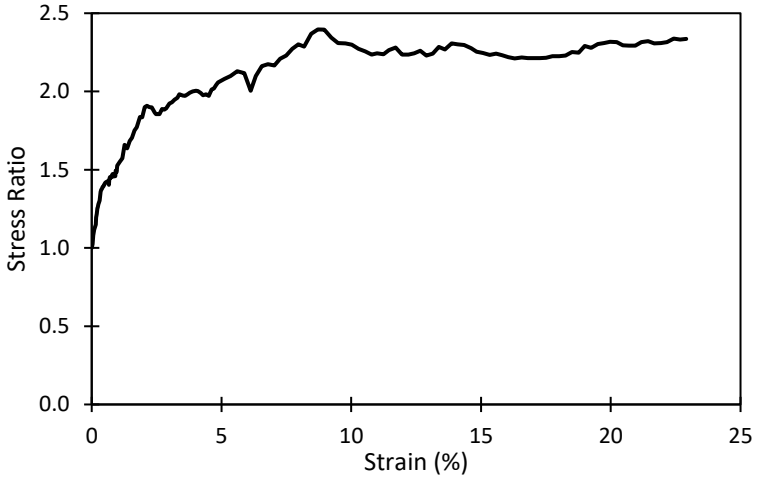

Sample no.	Target σ' (kPa)	Actual σ' (kPa)	Failure Criteria	ε at failure (%)	$\Delta\sigma_f$ (kPa)	$\sigma'3_f$ (kPa)	$\sigma'1_f$ (kPa)	U_{ef} (kPa)	p'_f (kPa)	M	Su (kPa)	Su/p'c	phi' (°)	Af
ReRb 100	100	122	Maximum Δσ	8.71	89.22	63.89	153.1	57.76	93.6	0.95	44.61	0.365	24.28	0.65
			Maximum σ'3/σ'1	8.71	89.22	63.89	153.1	57.76	93.6	0.95	44.09	0.365	24.28	0.65
			ε at end of test	22.91	79.32	59.42	138.7	57.76	93.6	0.92	39.66	0.324	23.60	0.72

Re 100-2

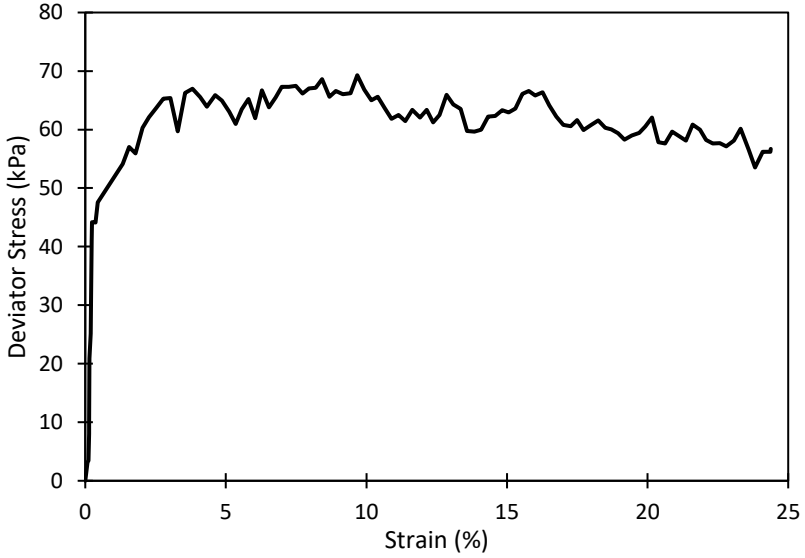
Deviator Stress (kPa)
Strain (%)
0
10
20
30
40
50
60
70
80
0
5
10
15
20
25

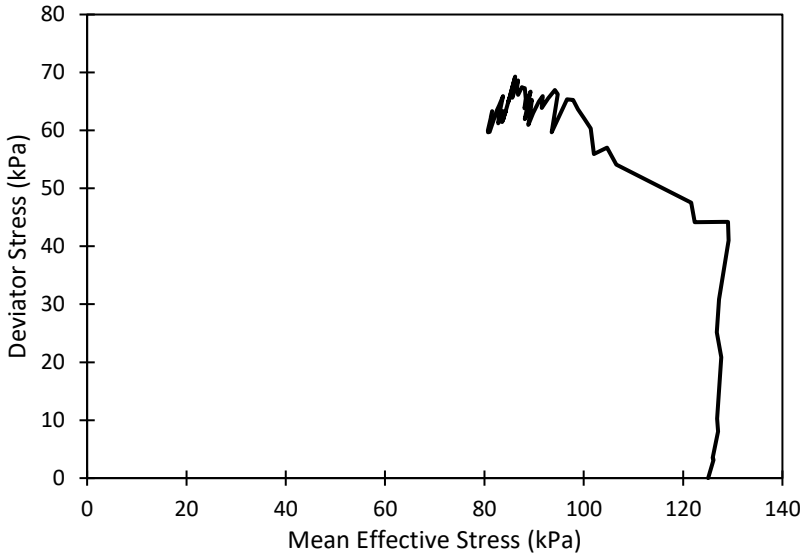
Deviator Stress (kPa)
Mean Effective Stress (kPa)
0
10
20
30
40
50
60
70
80
0
20
40
60
80
100
120
140

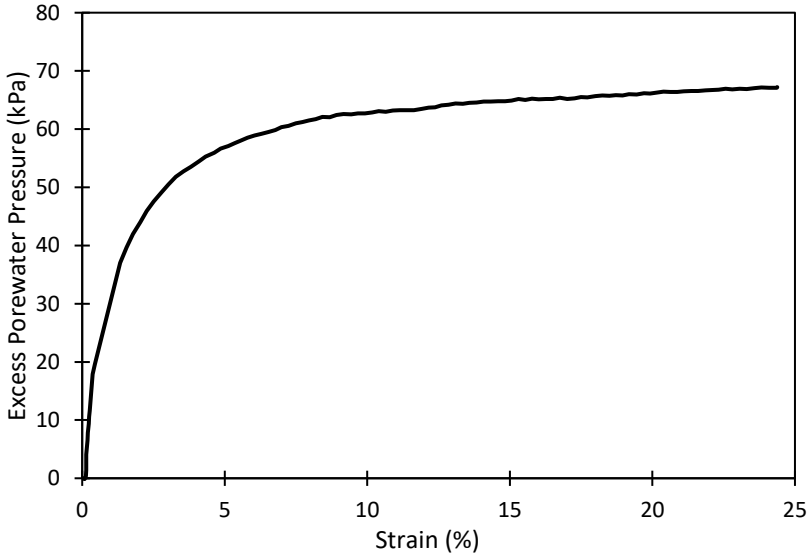
Excess Porewater Pressure (kPa)
Strain (%)
0
10
20
30
40
50
60
70
80
0
5
10
15
20
25

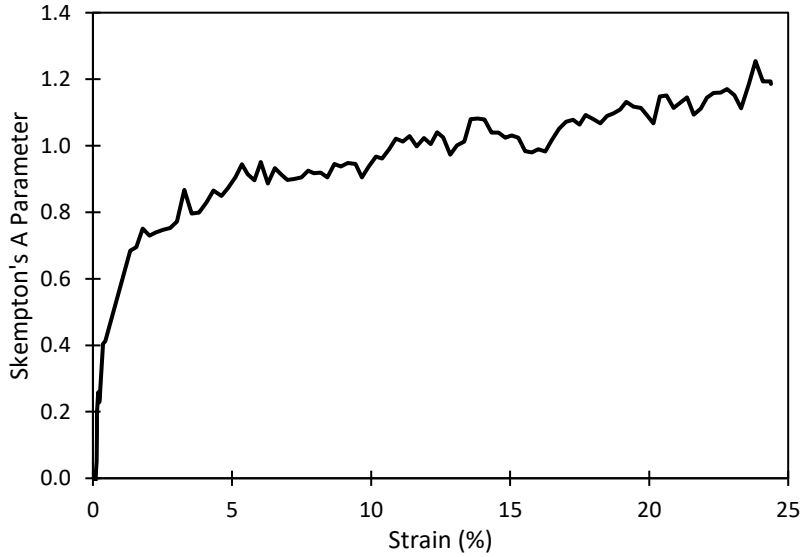
Skempton's A Parameter
Strain (%)
0.0
0.2
0.4
0.6
0.8
1.0
1.2
1.4
0
5
10
15
20
25

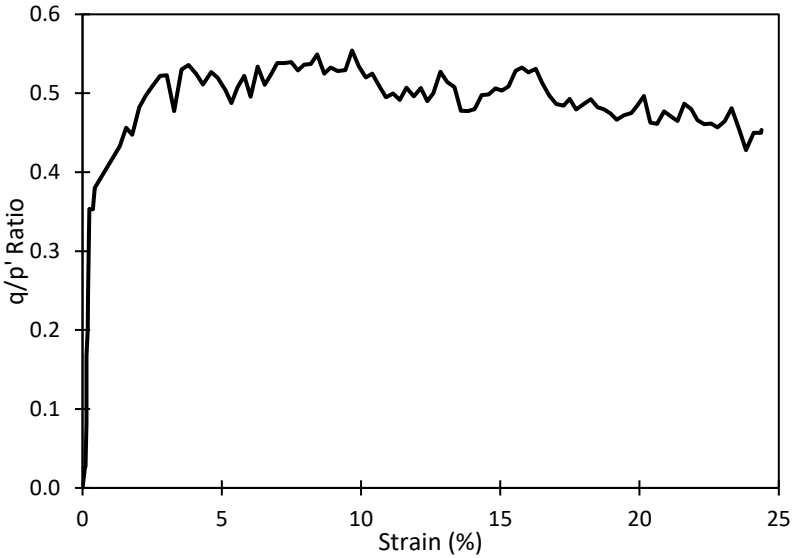

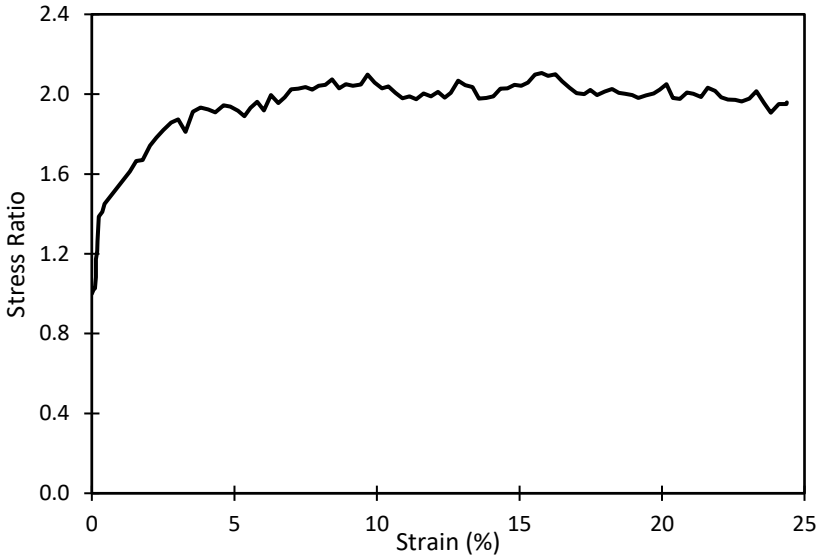

Sample no.	Target σ' (kPa)	Actual σ' (kPa)	Failure Criteria	ε at failure (%)	$\Delta\sigma_f$ (kPa)	$\sigma'3_f$ (kPa)	$\sigma'1_f$ (kPa)	U_{ef} (kPa)	p'_f (kPa)	M	Su (kPa)	Su/p'c	phi' (°)	Af
ReRb 100- 2	100	125	Maximum $\Delta\sigma$	9.67	69.28	63.11	132.3	62.7	86.2	0.80	34.64	0.277	20.76	0.91
			Maximum σ'3/σ'1	15.78	66.59	60.2	126.7	65.22	82.4	0.81	33.30	0.266	20.86	0.98
			ε at end of test	24.38	56.69	59.14	115.8	67.21	78.04	0.73	28.35	0.227	18.90	1.19

Re 200

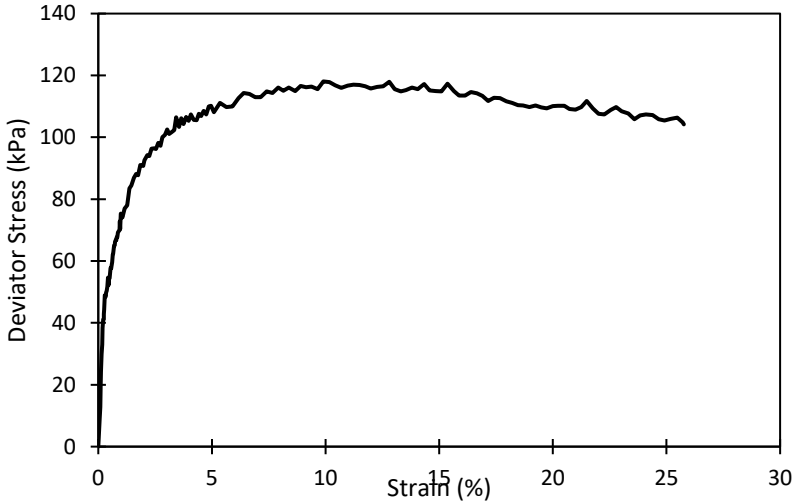
Deviator Stress (kPa)
Strain (%)
0
20
40
60
80
100
120
140
0
5
10
15
20
25
30

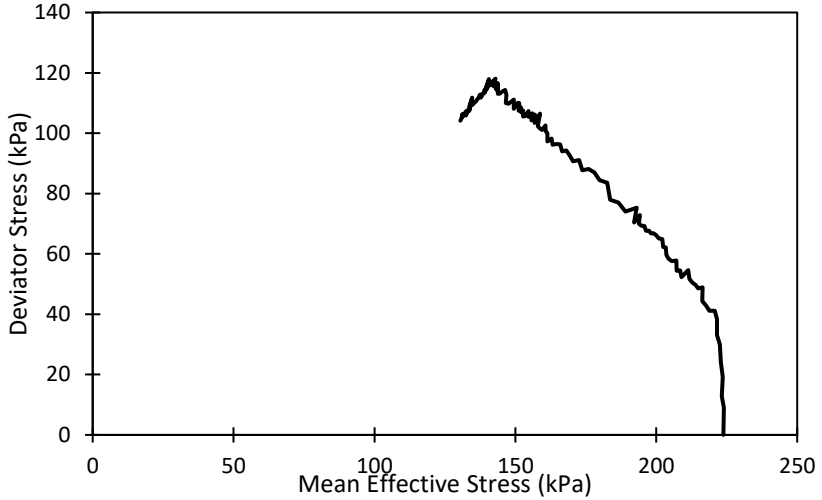
Deviator Stress (kPa)
Mean Effective Stress (kPa)
0
20
40
60
80
100
120
140
0
50
100
150
200
250

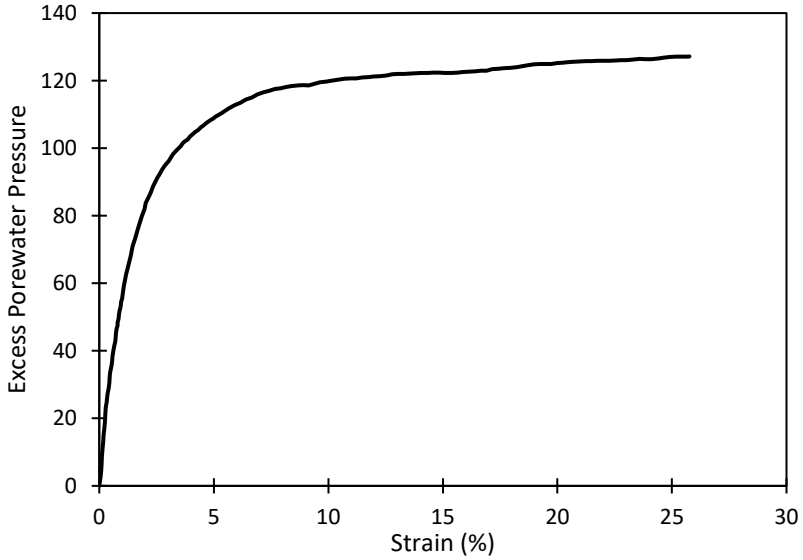
Excess Porewater Pressure
Strain (%)
0
20
40
60
80
100
120
140
0
5
10
15
20
25
30

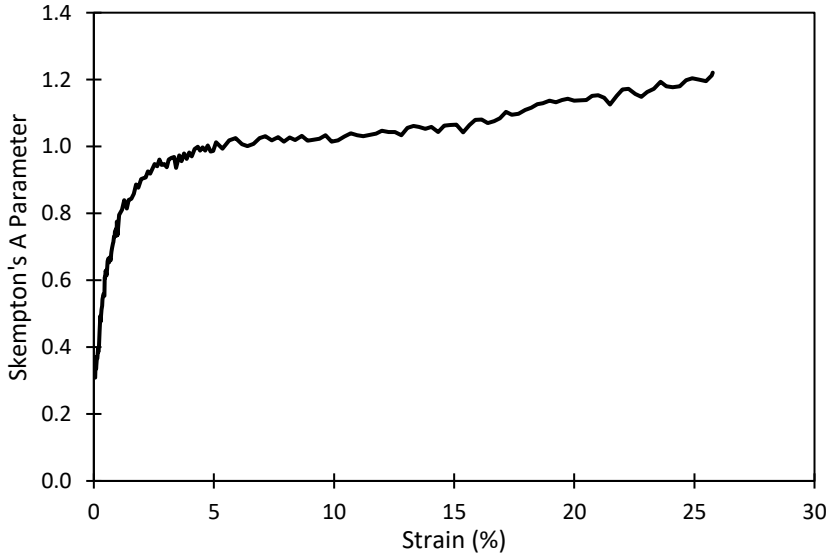
Skempton's A Parameter
Strain (%)
0.0
0.2
0.4
0.6
0.8
1.0
1.2
1.4
0
5
10
15
20
25
30

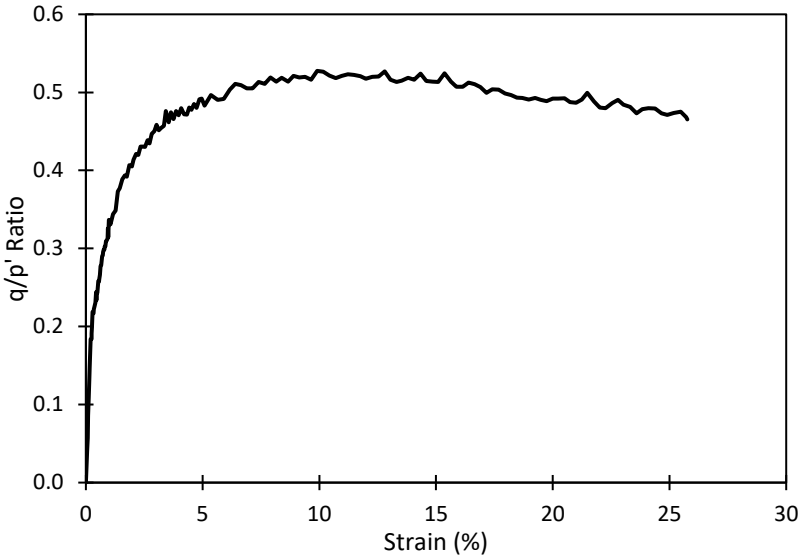

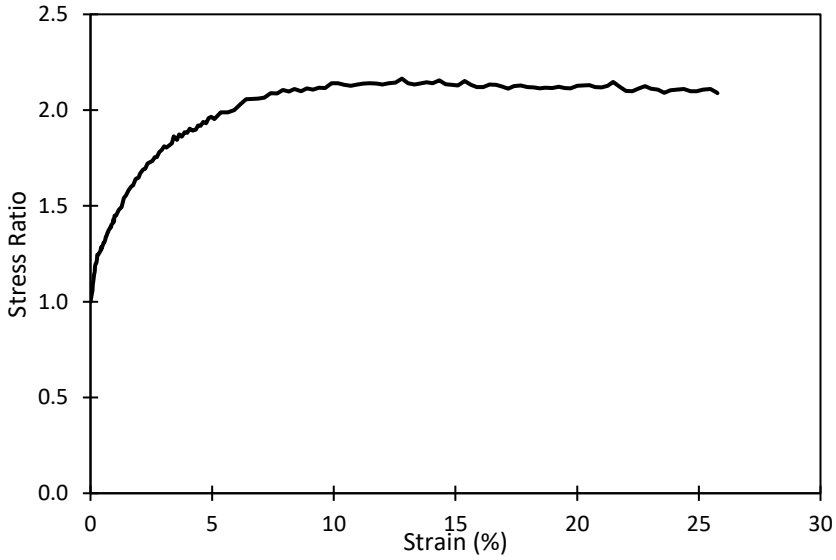

Sample no.	Target σ' (kPa)	Actual σ' (kPa)	Failure Criteria	ε at failure (%)	$\Delta\sigma_f$ (kPa)	$\sigma'3_f$ (kPa)	$\sigma'1_f$ (kPa)	U_{ef} (kPa)	p'_f (kPa)	M	Su (kPa)	Su/p'c	phi' (°)	Af
ReRb 200	200	224	Maximum Δσ	9.90	118.07	103.55	221.6	119.74	142.9	0.83	59.04	0.264	21.29	1.01
			Maximum σ'3/σ'1	12.80	117.92	101.27	219.1	121.8	140.5	0.84	58.96	0.263	21.59	1.03
			ε at end of test	25.76	104.17	95.74	199.9	127.1	130.4	0.80	52.09	0.233	20.63	1.22

Re 300

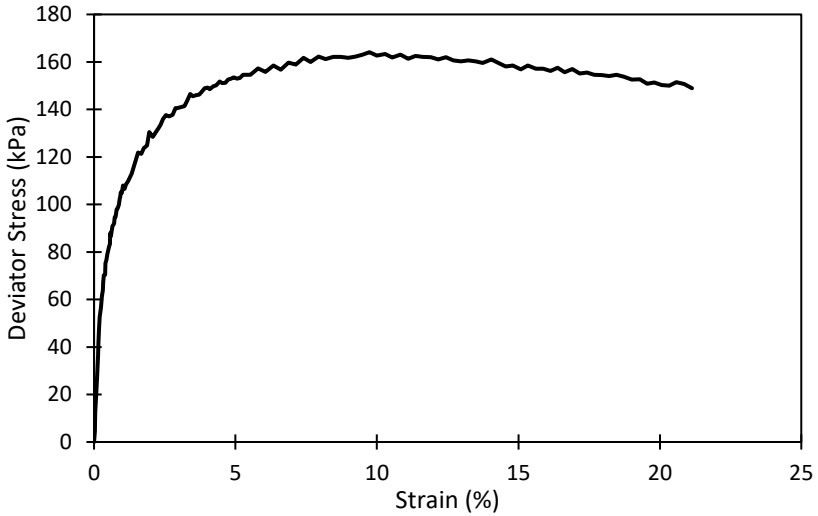
Deviator Stress (kPa)
Strain (%)
0
20
40
60
80
100
120
140
160
180
0
5
10
15
20
25

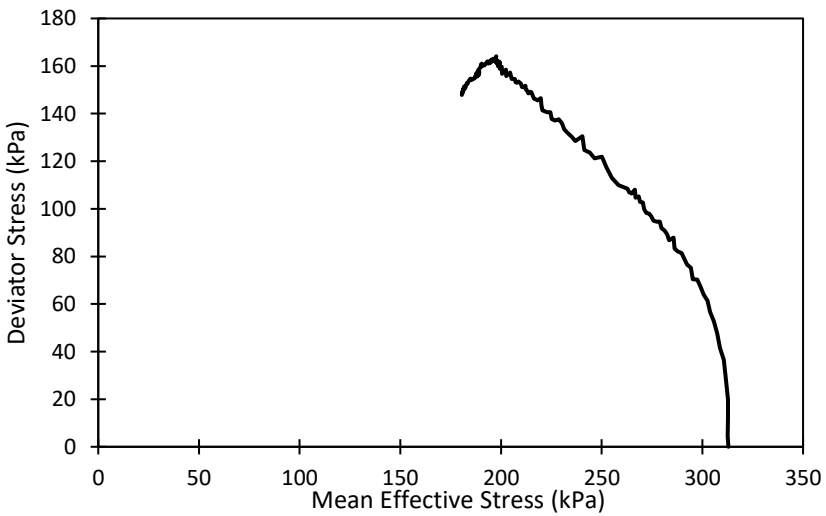
Deviator Stress (kPa)
Mean Effective Stress (kPa)
0
20
40
60
80
100
120
140
160
180
0
50
100
150
200
250
300
350

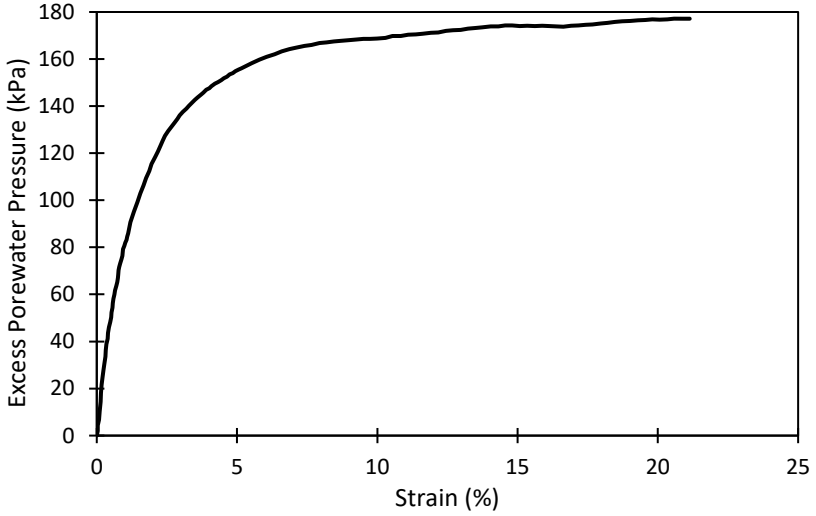
Excess Porewater Pressure (kPa)
Strain (%)
0
20
40
60
80
100
120
140
160
180
0
5
10
15
20
25

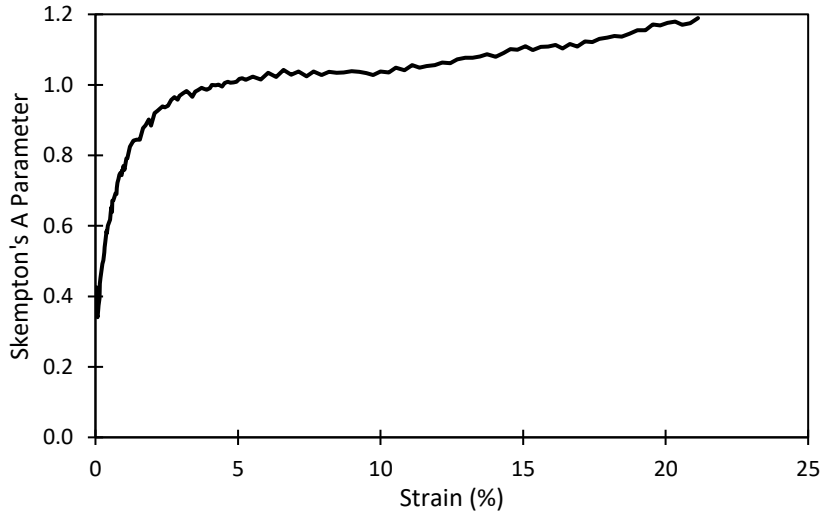
Skempton's A Parameter
Strain (%)
0.0
0.2
0.4
0.6
0.8
1.0
1.2
0
5
10
15
20
25

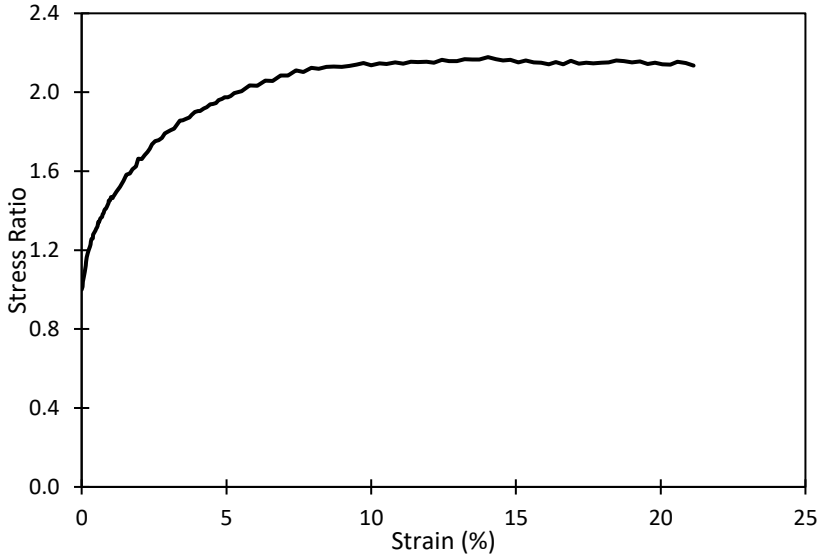

Sample no.	Target σ' (kPa)	Actual σ' (kPa)	Failure Criteria	ε at failure (%)	$\Delta\sigma_f$ (kPa)	$\sigma'3_f$ (kPa)	$\sigma'1_f$ (kPa)	U_{ef} (kPa)	p'_f (kPa)	M	Su (kPa)	Su/p'c	phi' (°)	Af
ReRb 300	300	313	Maximum Δσ	9.74	164.10	142.99	307.1	168.64	197.70	0.83	82.05	0.262	21.59	1.03
			Maximum σ'3/σ'1	14.04	160.99	136.66	297.65	173.85	190.32	0.85	80.50	0.257	20.63	1.08
			ε at end of test	24.14	145.09	130.59	275.67	177.51	178.95	0.81	72.54	0.232	20.63	1.22

Re 400

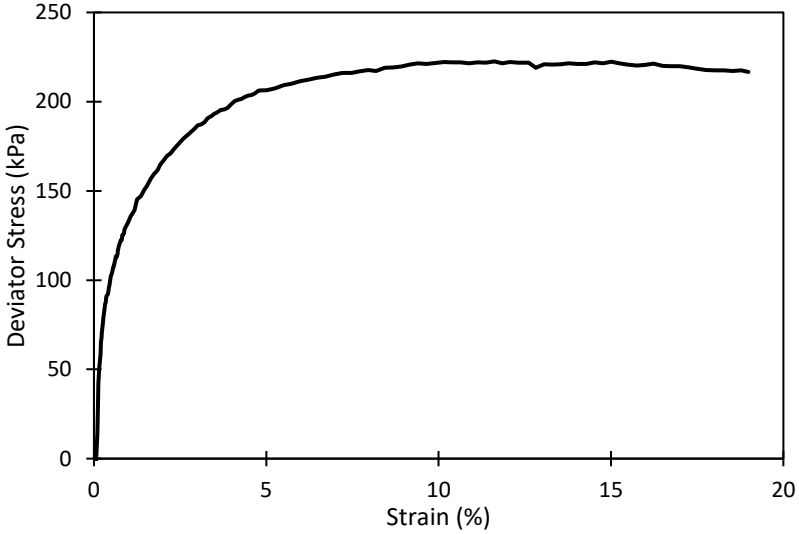
Deviator Stress (kPa)
Strain (%)
0
50
100
150
200
250
0
5
10
15
20

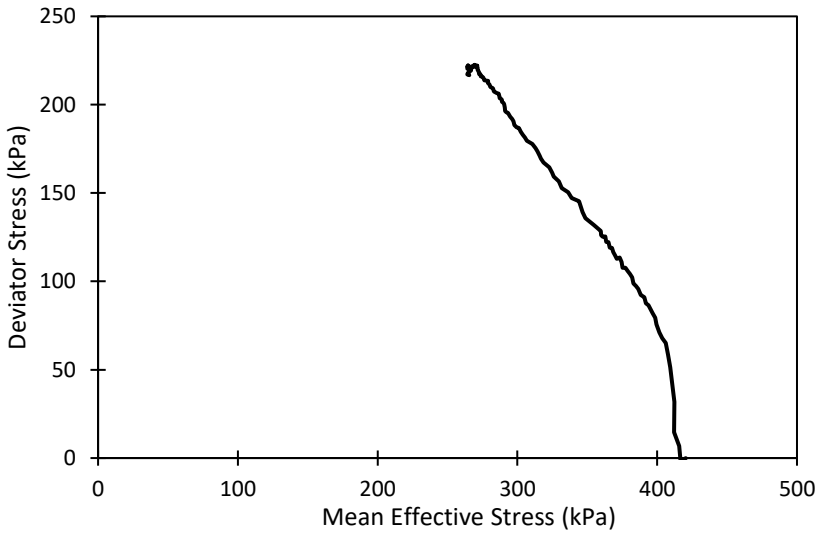
Deviator Stress (kPa)
Mean Effective Stress (kPa)
0
50
100
150
200
250
0
100
200
300
400
500

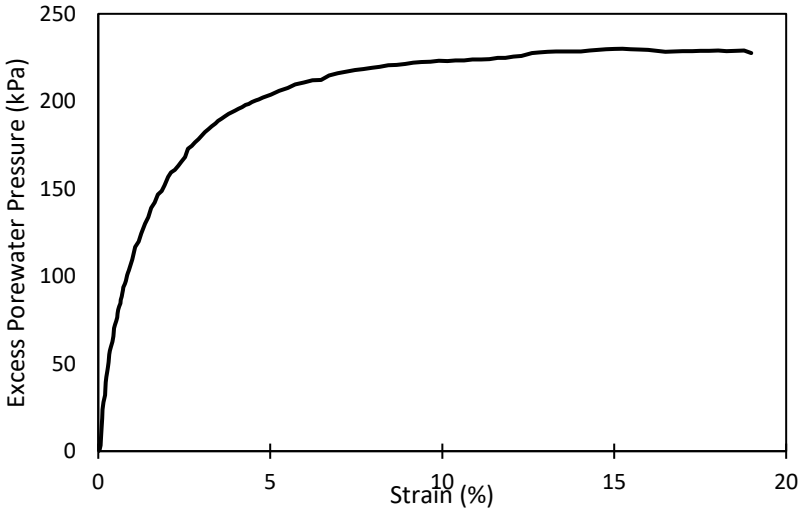
Excess Porewater Pressure (kPa)
Strain (%)
0
50
100
150
200
250
0
5
10
15
20

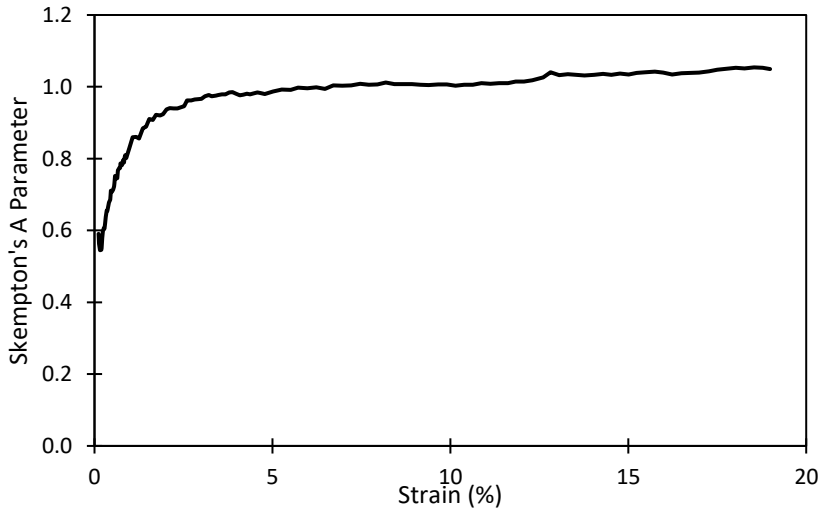
Skempton's A Parameter
Strain (%)
0.0
0.2
0.4
0.6
0.8
1.0
1.2
0
5
10
15
20

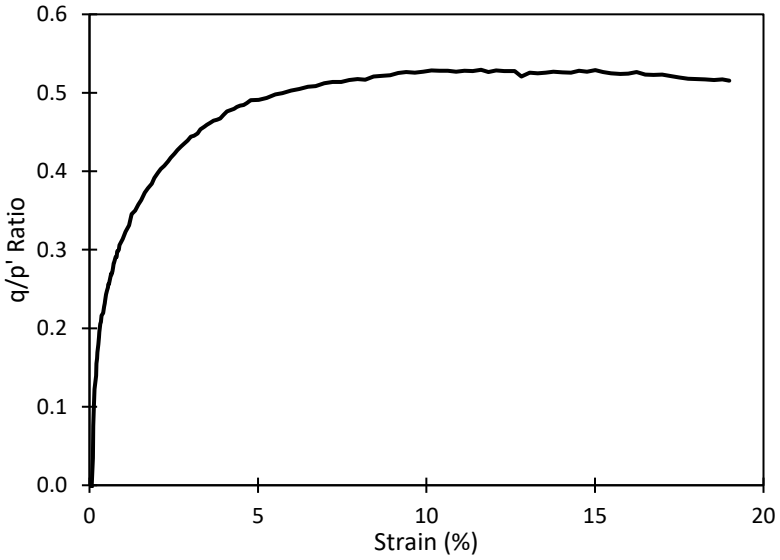

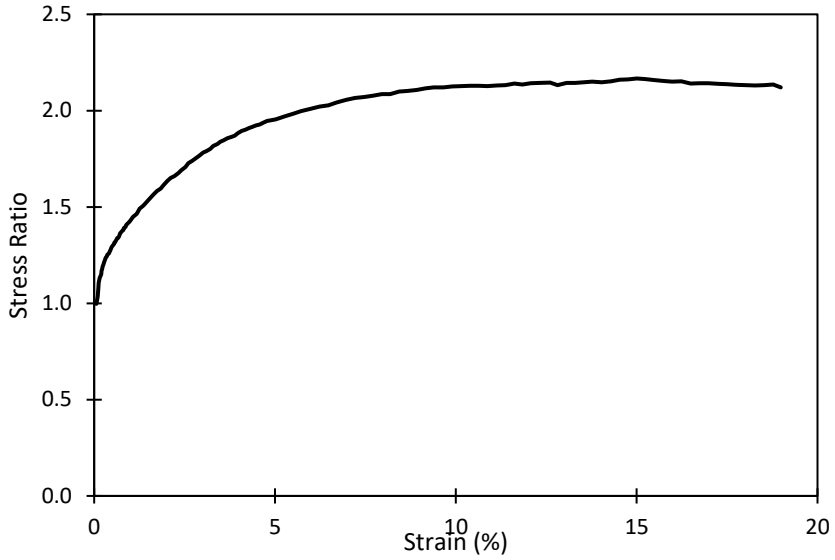

Sample no.	Target σ' (kPa)	Actual σ' (kPa)	Failure Criteria	ε at failure (%)	$\Delta\sigma_f$ (kPa)	$\sigma'3_f$ (kPa)	$\sigma'1_f$ (kPa)	U_{ef} (kPa)	p'_f (kPa)	M	Su (kPa)	Su/p'c	phi' (°)	Af
ReRb 400	400	420	Maximum Δσ	11.62	222.58	195.15	417.73	224.85	269.34	0.83	111.29	0.265	21.29	1.01
			Maximum σ'3/σ'1	15.01	222.36	190.56	412.92	229.94	264.68	0.84	111.18	0.265	21.62	1.03
			ε at end of test	18.98	216.72	193.29	410.02	224.85	265.53	0.82	108.36	0.258	21.05	1.04

In 100

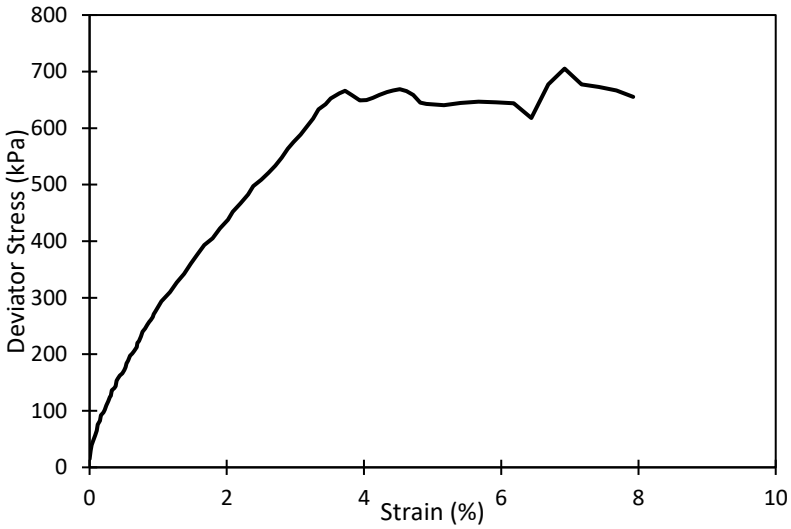
Deviator Stress (kPa)
800
700
600
500
400
300
200
100
0
0
2
4
6
8
10
Strain (%)

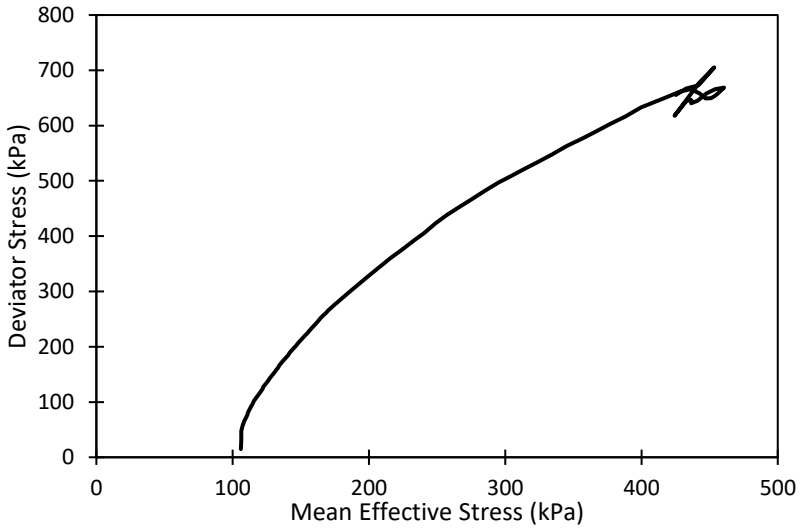
Deviator Stress (kPa)
800
700
600
500
400
300
200
100
0
0
100
200
300
400
500
Mean Effective Stress (kPa)

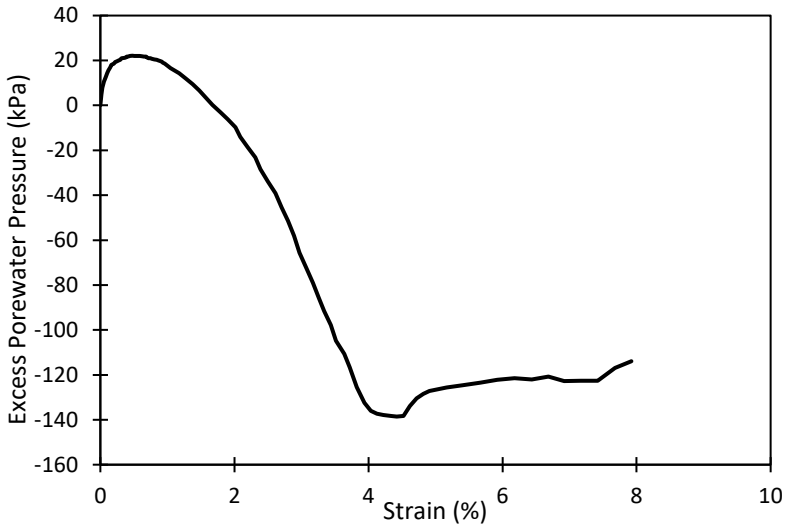
Excess Porewater Pressure (kPa)
40
20
0
-20
-40
-60
-80
-100
-120
-140
-160
0
2
4
6
8
10
Strain (%)

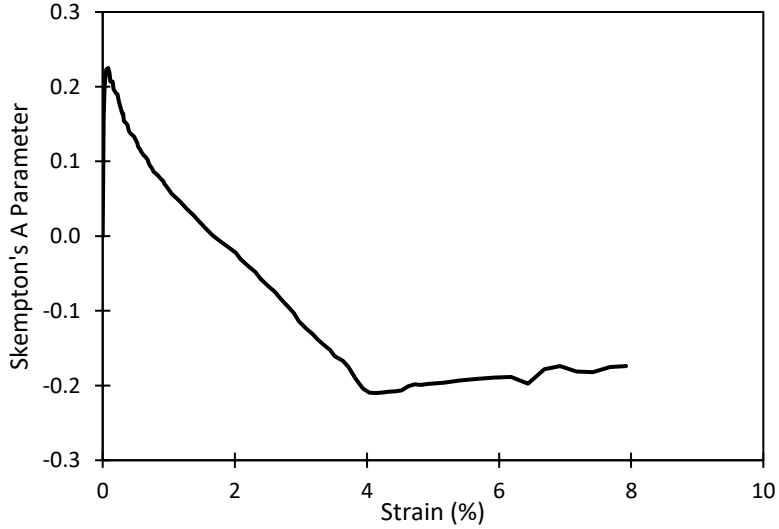
Skempton's A Parameter
0.3
0.2
0.1
0.0
-0.1
-0.2
-0.3
0
2
4
6
8
10
Strain (%)

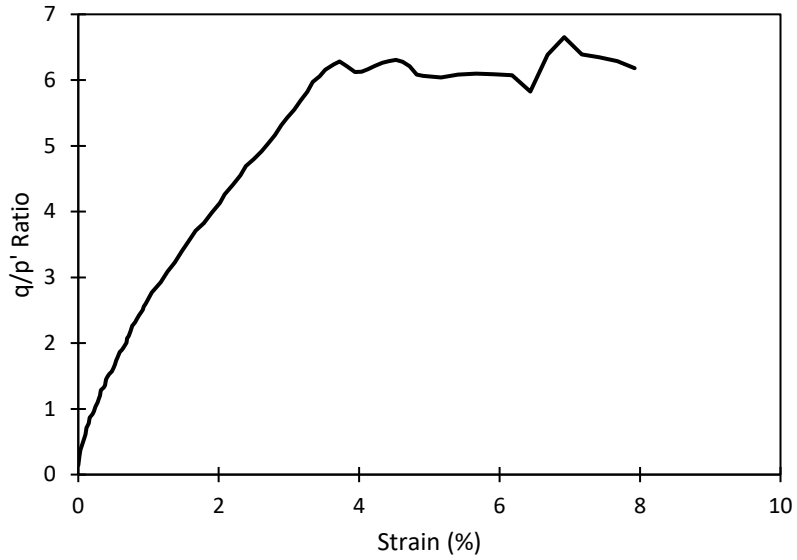
q/p' Ratio
Strain (%)
0
1
2
3
4
5
6
7
0
2
4
6
8
10

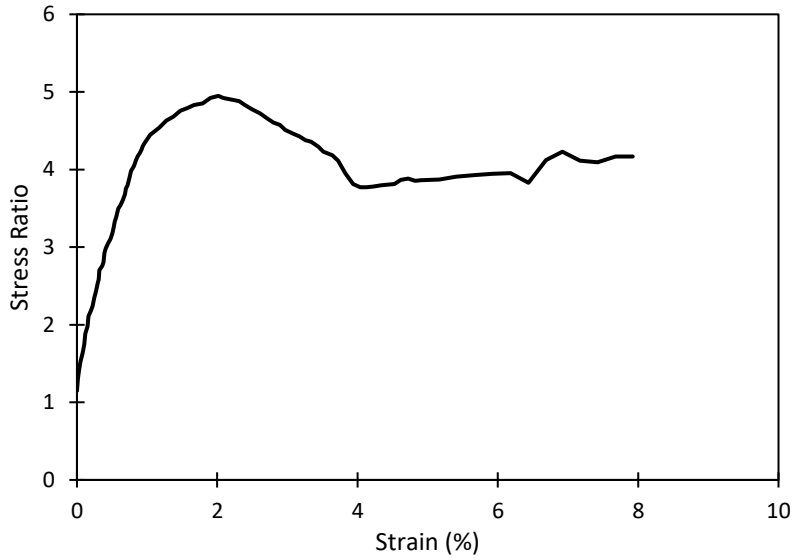
Stress Ratio
Strain (%)
0
1
2
3
4
5
6
0
2
4
6
8
10

In 100 -2

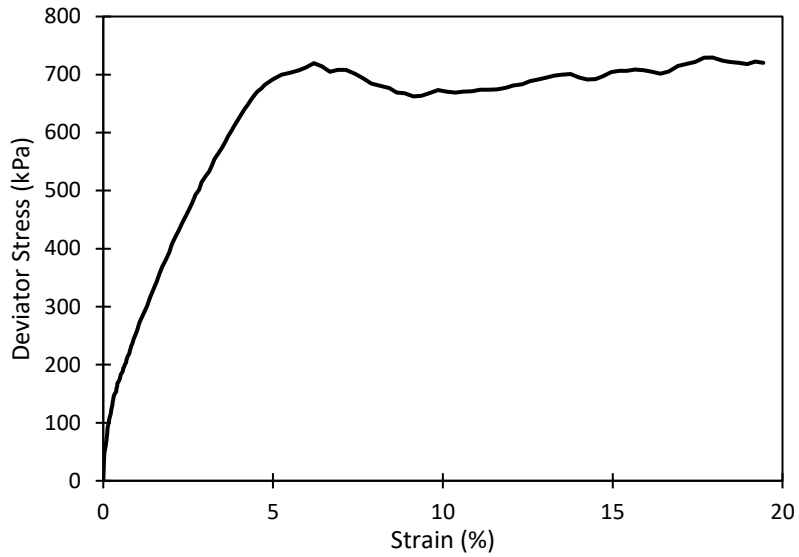
Deviator Stress (kPa)
Strain (%)
0
100
200
300
400
500
600
700
800
0
5
10
15
20

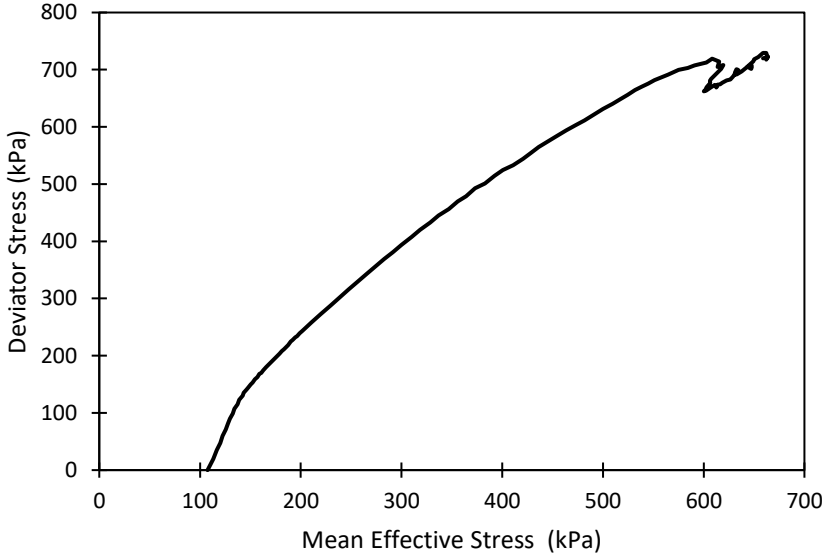
Deviator Stress (kPa)
Mean Effective Stress (kPa)
0
100
200
300
400
500
600
700
800

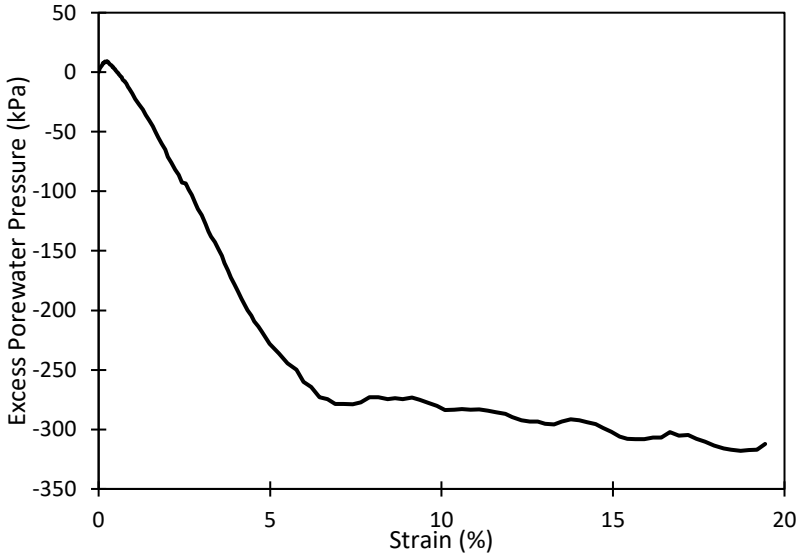
Excess Porewater Pressure (kPa)
Strain (%)
50
0
-50
-100
-150
-200
-250
-300
-350
0
5
10
15
20

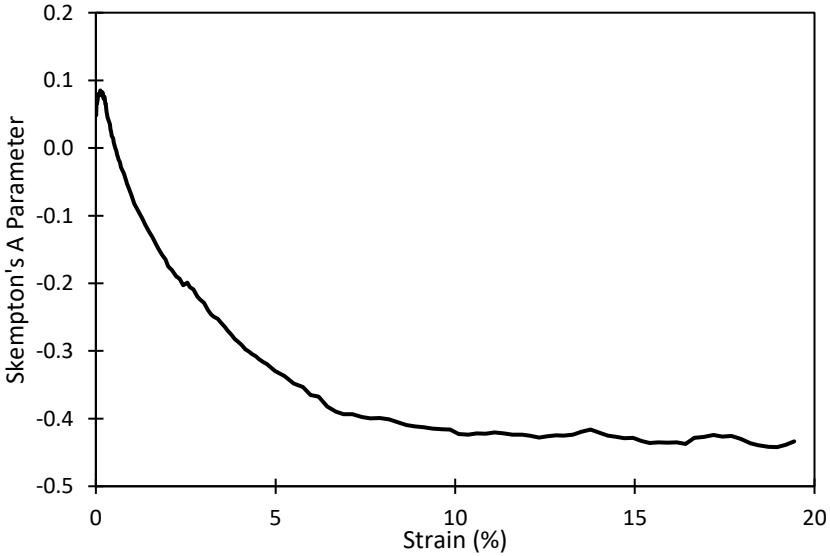
Skempton's A Parameter
Strain (%)
0.2
0.1
0.0
-0.1
-0.2
-0.3
-0.4
-0.5
0
5
10
15
20

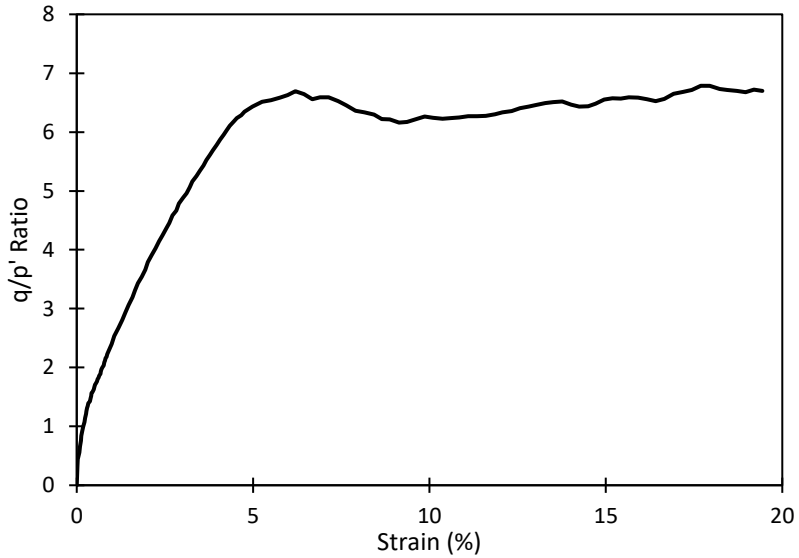
q/p' Ratio
Strain (%)
0
1
2
3
4
5
6
7
8
0
5
10
15
20

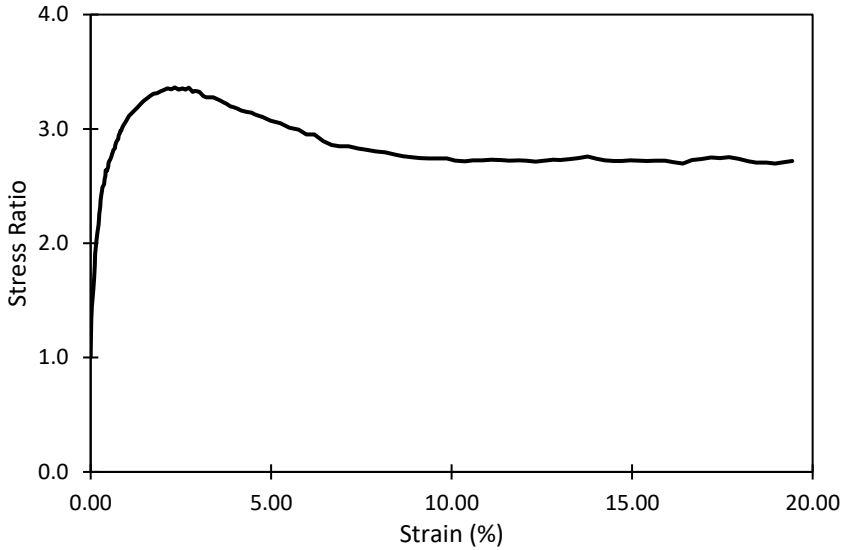
Stress Ratio
Strain (%)
0.0
1.0
2.0
3.0
4.0
0.00
5.00
10.00
15.00
20.00

In 200

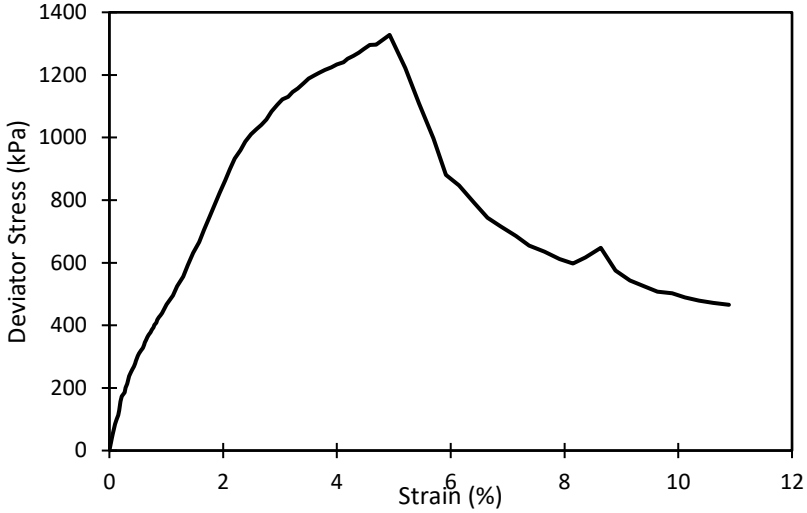
Deviator Stress (kPa)
1400
1200
1000
800
600
400
200
0
0
2
4
6
8
10
12
Strain (%)

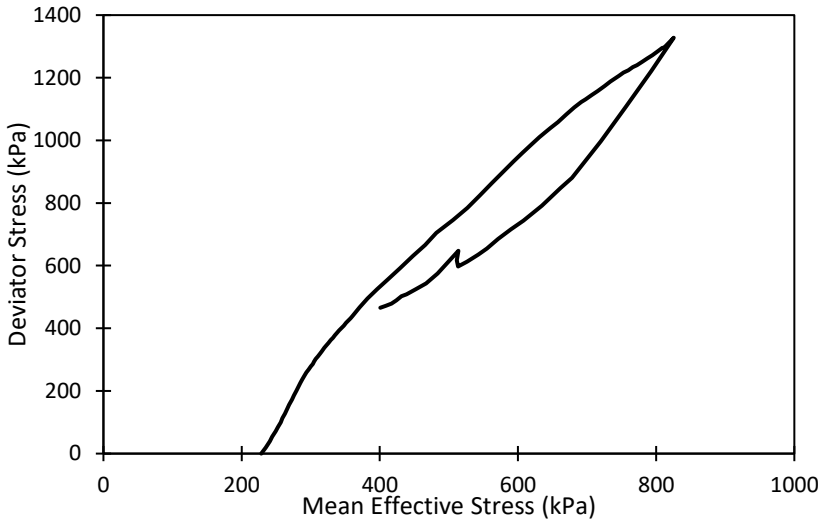
Deviator Stress (kPa)
1400
1200
1000
800
600
400
200
0
0
200
400
600
800
1000
Mean Effective Stress (kPa)

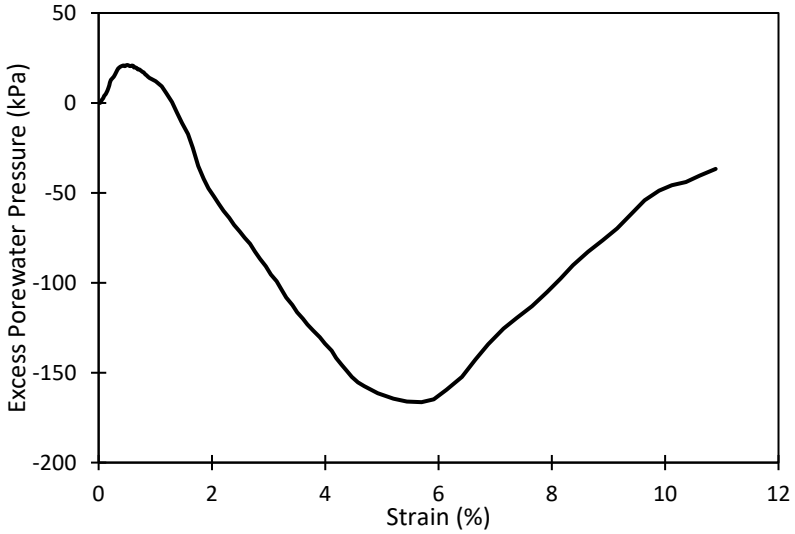
Excess Porewater Pressure (kPa)
50
0
-50
-100
-150
-200
0
2
4
6
8
10
12
Strain (%)

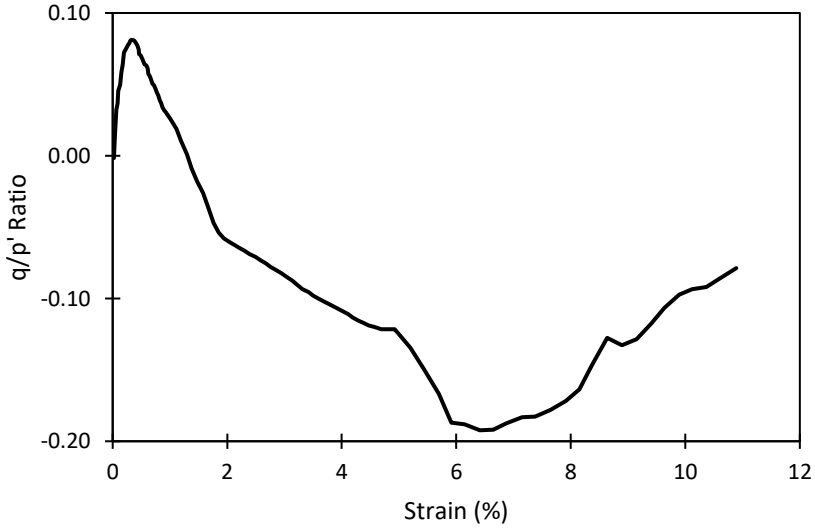
q/p' Ratio
0.10
0.00
-0.10
-0.20
0
2
4
6
8
10
12
Strain (%)

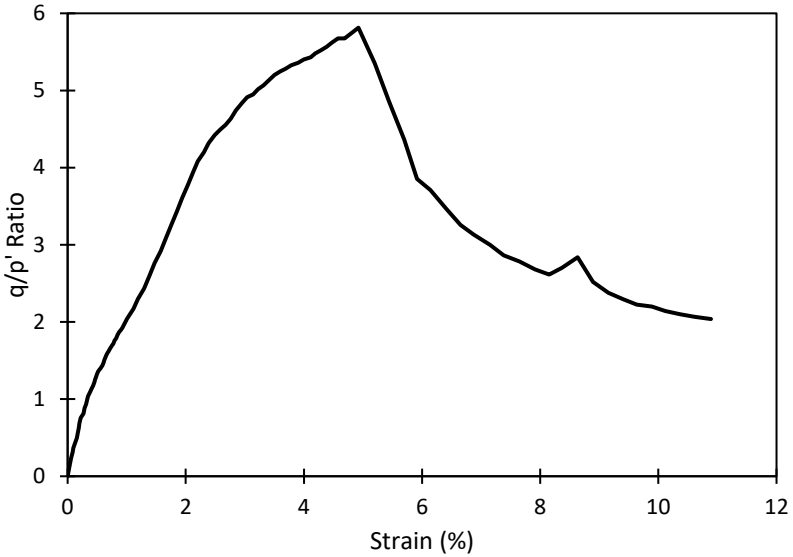
q/p' Ratio
Strain (%)
0
1
2
3
4
5
6
0
2
4
6
8
10
12

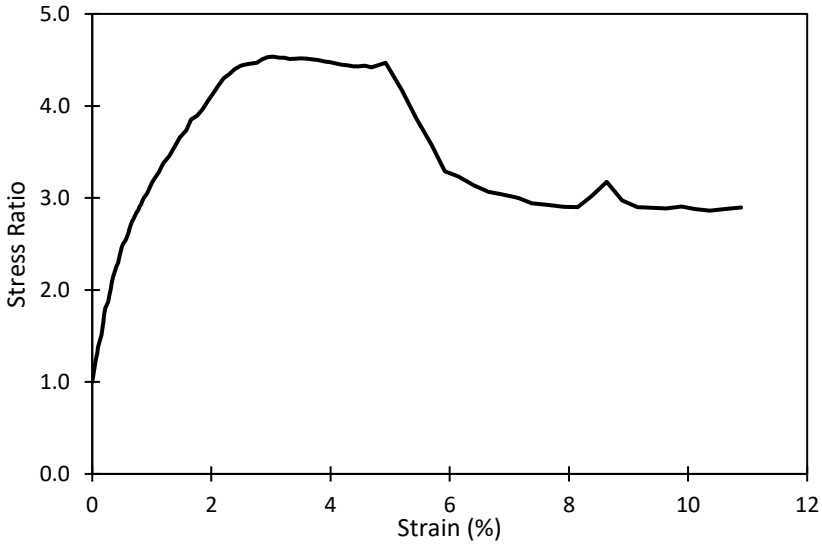
Stress Ratio
Strain (%)
0.0
1.0
2.0
3.0
4.0
5.0
0
2
4
6
8
10
12

APPENDIX B: RESULTS FROM 1-DIMENSION CONSOLIDATION TESTS

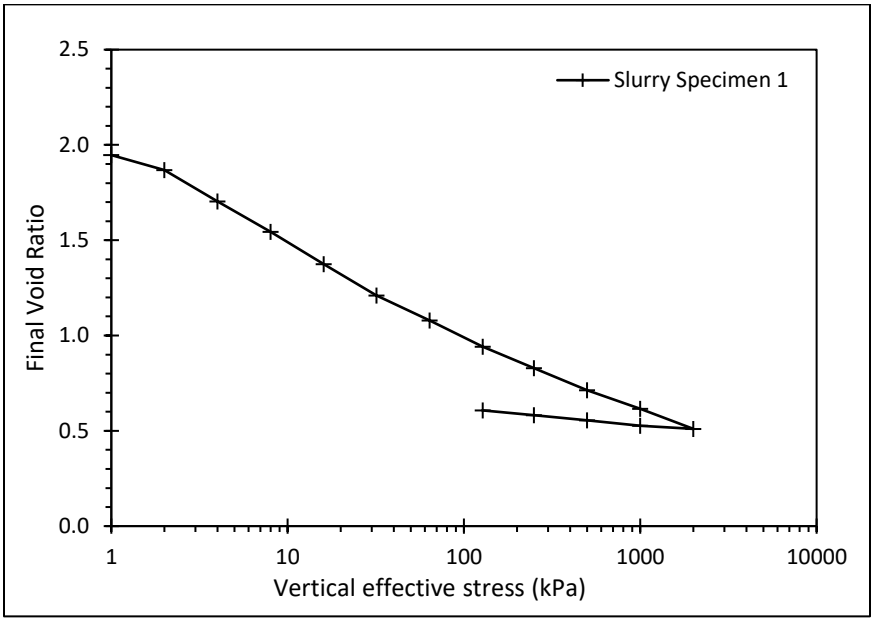

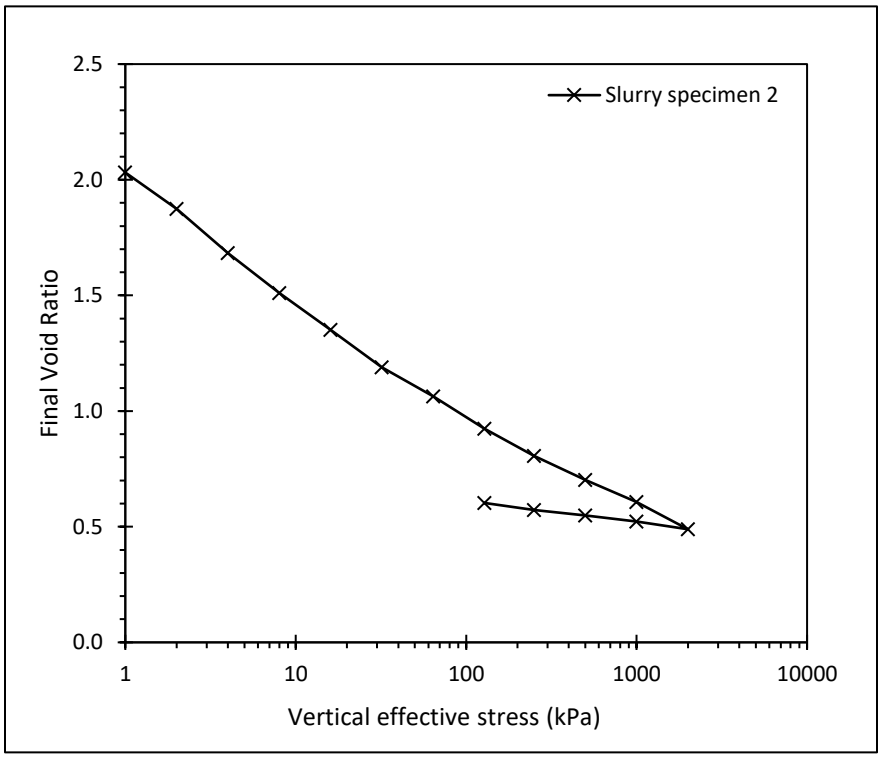

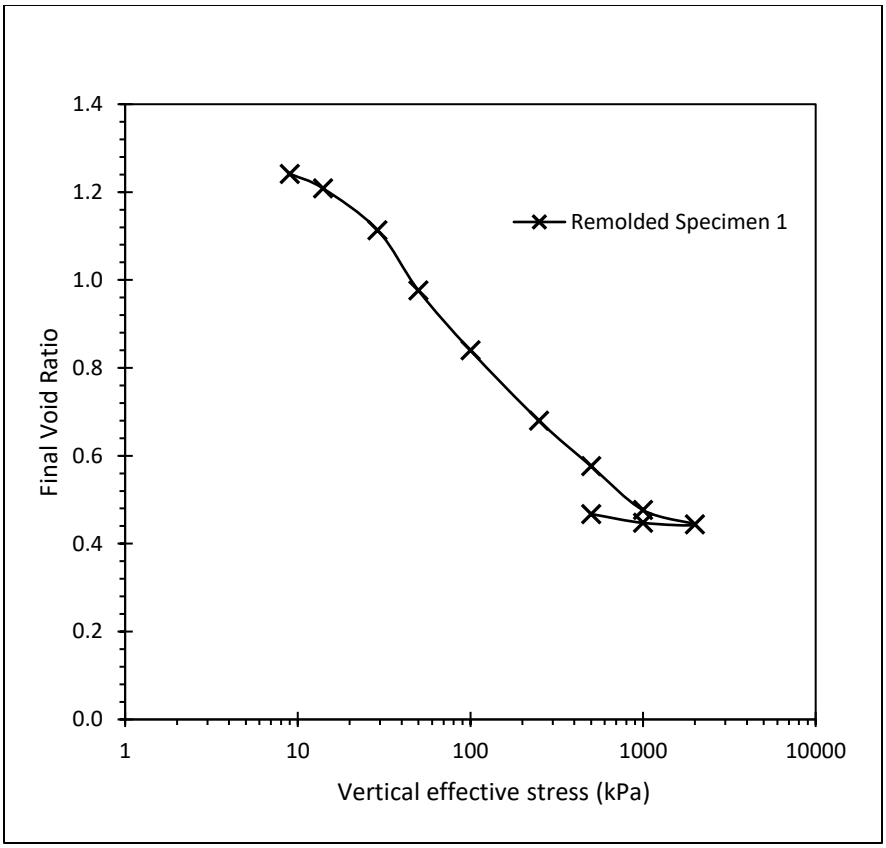
1.4
1.2
1.0
0.8
0.6
0.4
0.2
0.0
Final Void Ratio
Remolded Specimen 1
1
10
100
1000
10000
Vertical effective stress (kPa)

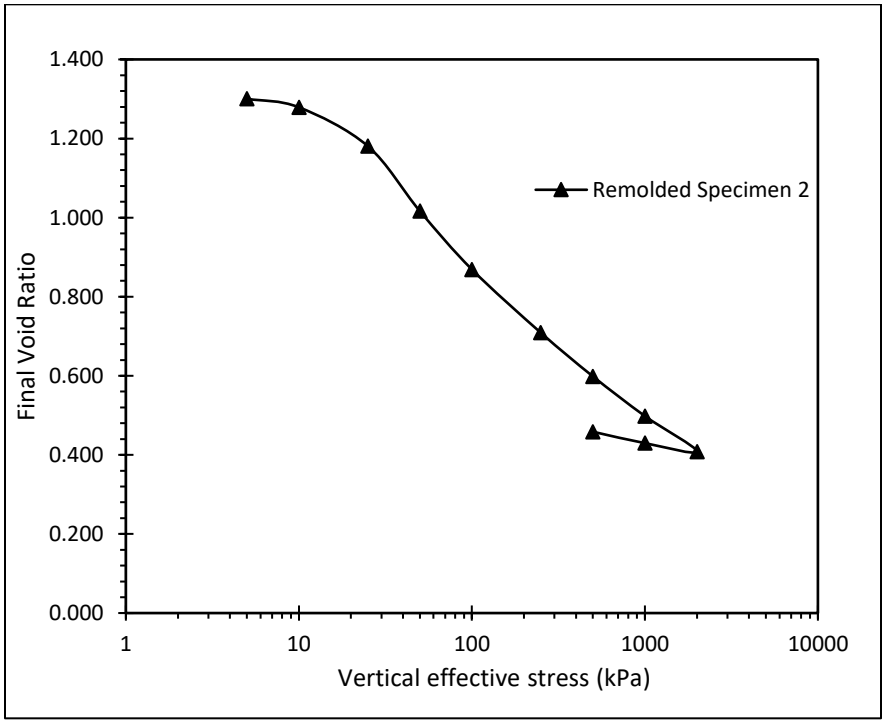
1.400
1.200
1.000
0.800
0.600
0.400
0.200
0.000
Final Void Ratio
Remolded Specimen 2
1
10
100
1000
10000
Vertical effective stress (kPa)

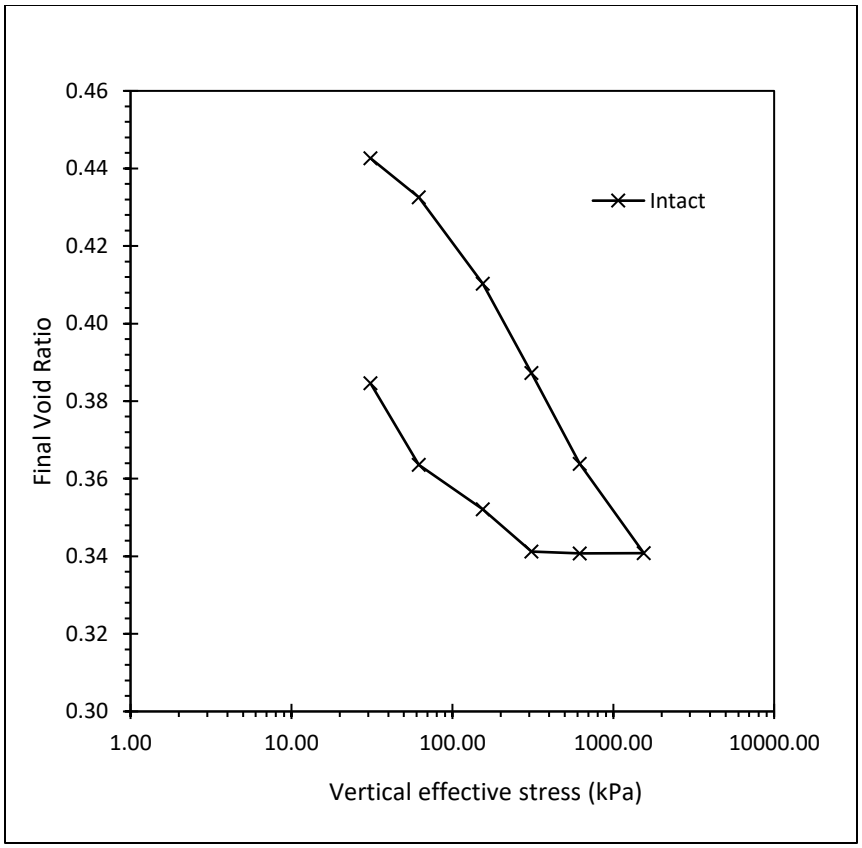
0.46
0.44
0.42
0.40
0.38
0.36
0.34
0.32
0.30
Final Void Ratio
Intact
1.00
10.00
100.00
1000.00
10000.00
Vertical effective stress (kPa)

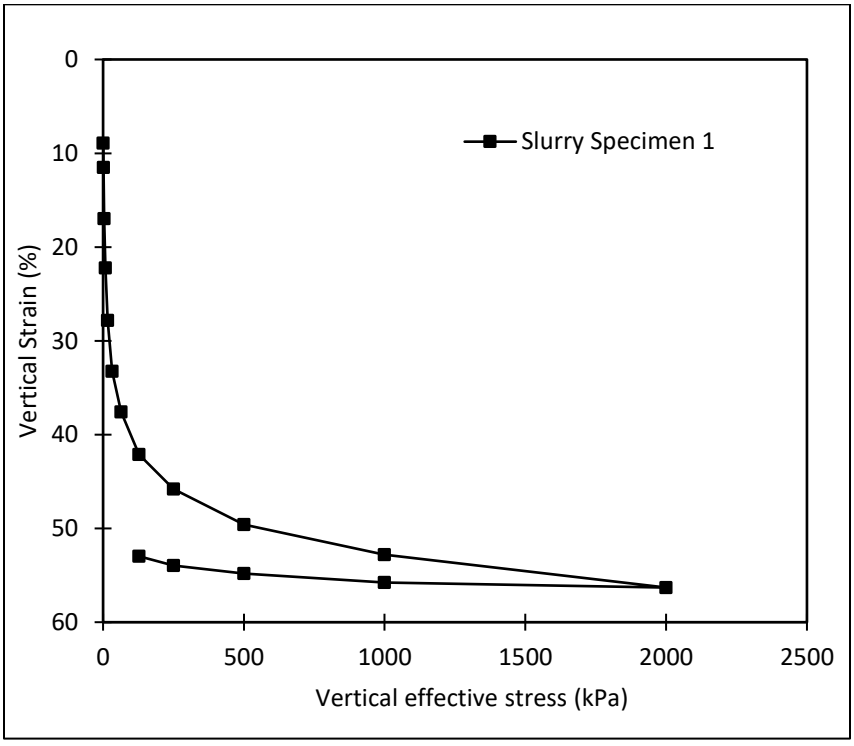
0
10
20
30
40
50
60
Vertical Strain (%)
Slurry Specimen 1
0
500
1000
1500
2000
2500
Vertical effective stress (kPa)

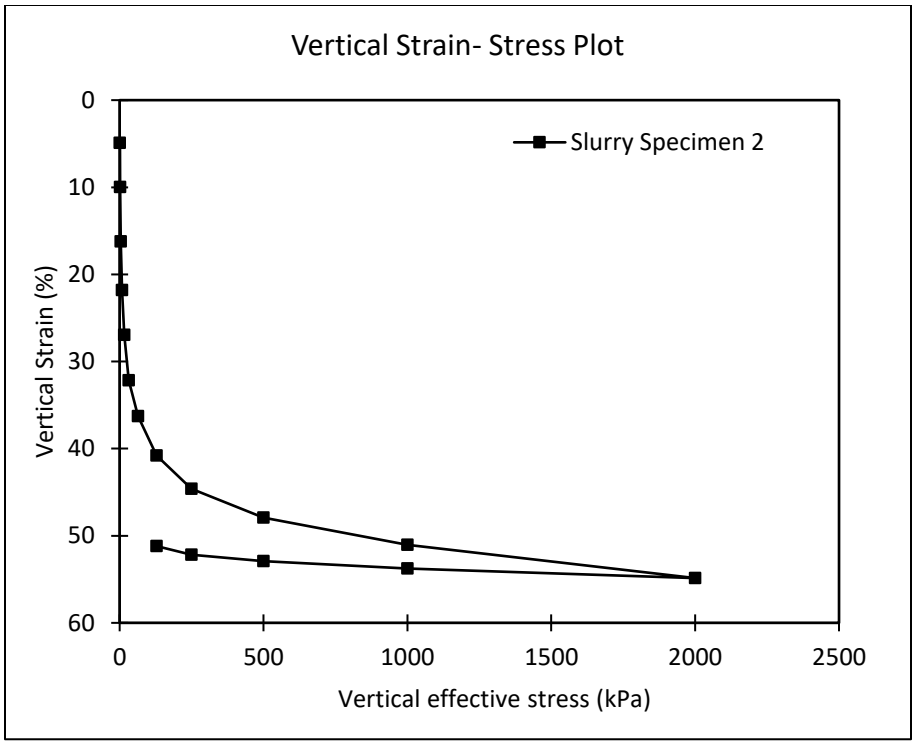
Vertical Strain- Stress Plot
Slurry Specimen 2
Vertical Strain (%)
0
10
20
30
40
50
60
0
500
1000
1500
2000
2500
Vertical effective stress (kPa)

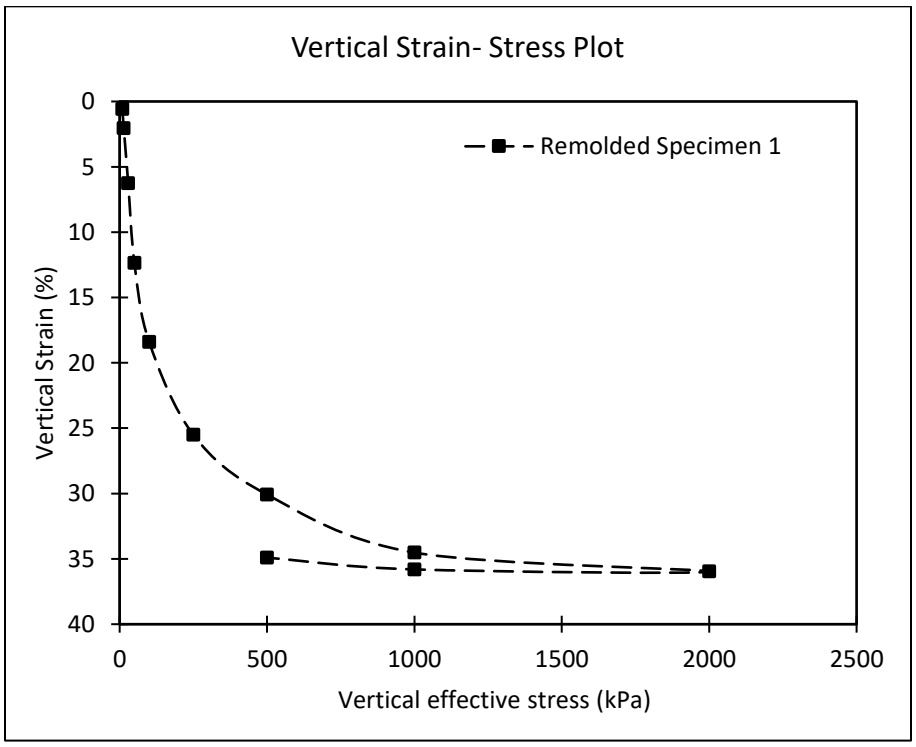
Vertical Strain- Stress Plot
Remolded Specimen 1
Vertical Strain (%)
0
5
10
15
20
25
30
35
40
0
500
1000
1500
2000
2500
Vertical effective stress (kPa)

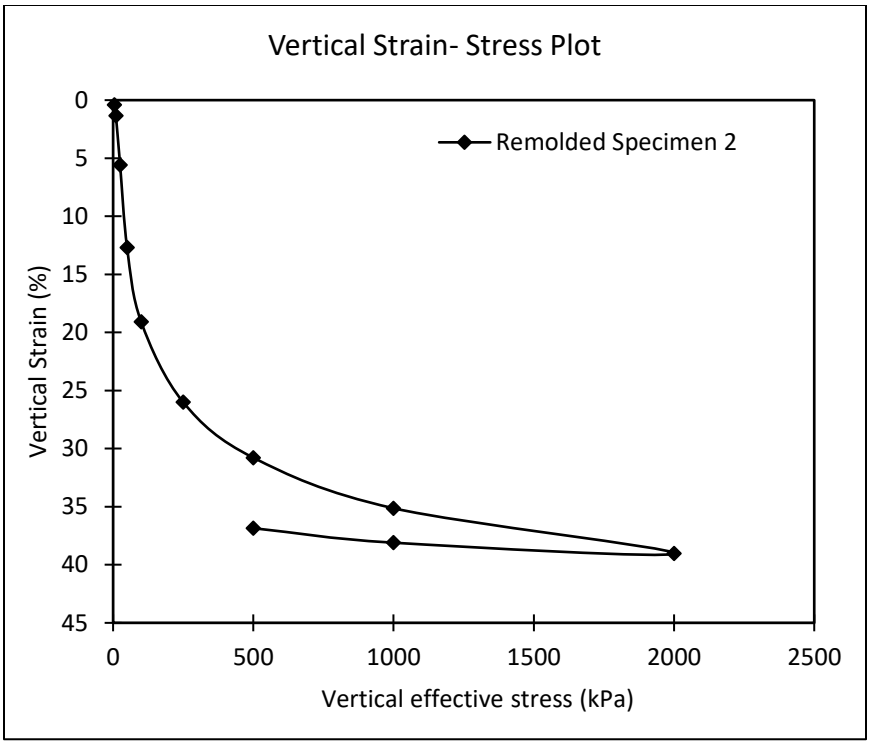
Vertical Strain- Stress Plot
Remolded Specimen 2
Vertical Strain (%)
0
5
10
15
20
25
30
35
40
45
0
500
1000
1500
2000
2500
Vertical effective stress (kPa)

APPENDIX C: PHOTOGRAPHS

Intact Redbed Claystone Prior to Wetting

Disintegrated Claystone after Wetting

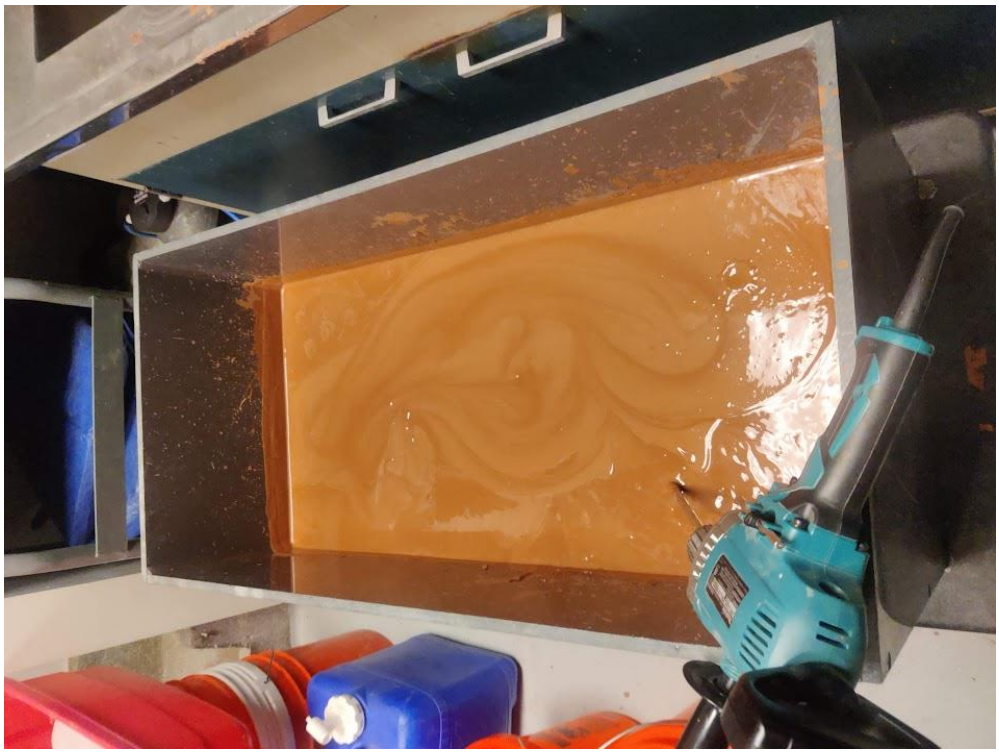

"Blenderizing" the disintegrated rock to form slurry

Transfer of claystone slurry to buckets

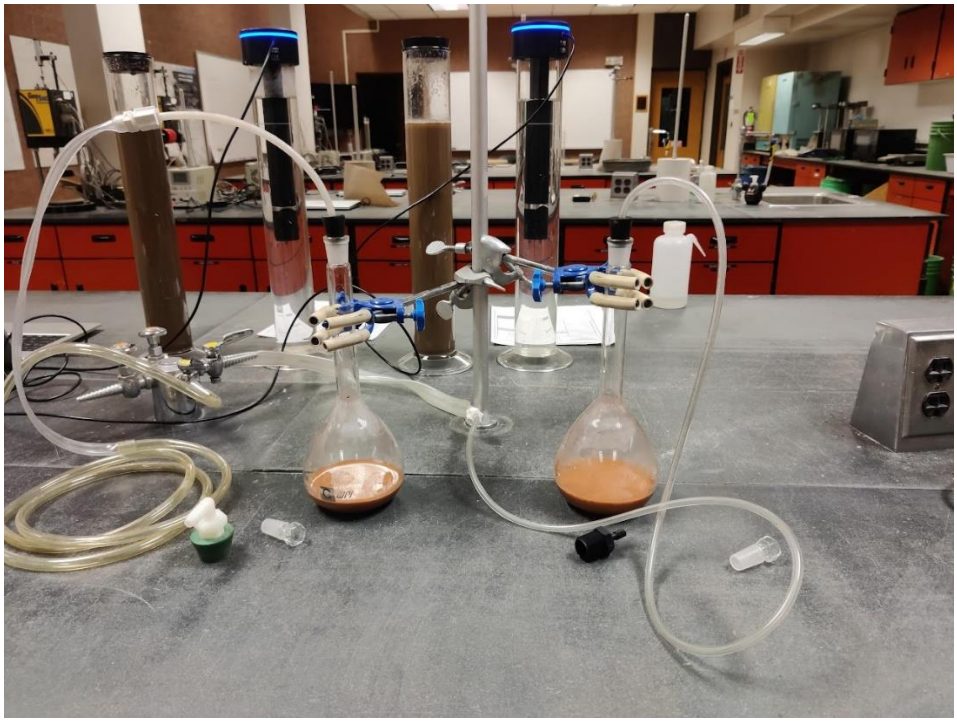

Calculating specific gravity using pycnometers

Carving intact rock to obtain specimen for triaxial specimen

Sanding down the intact rock to cylindrical shape

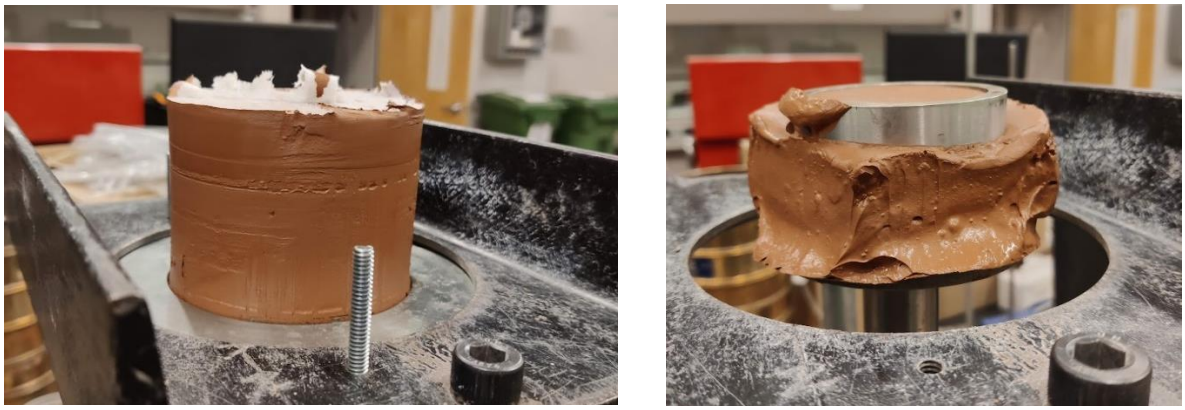

Remolded claystone for 1-dimensional consolidation test in the Geojac

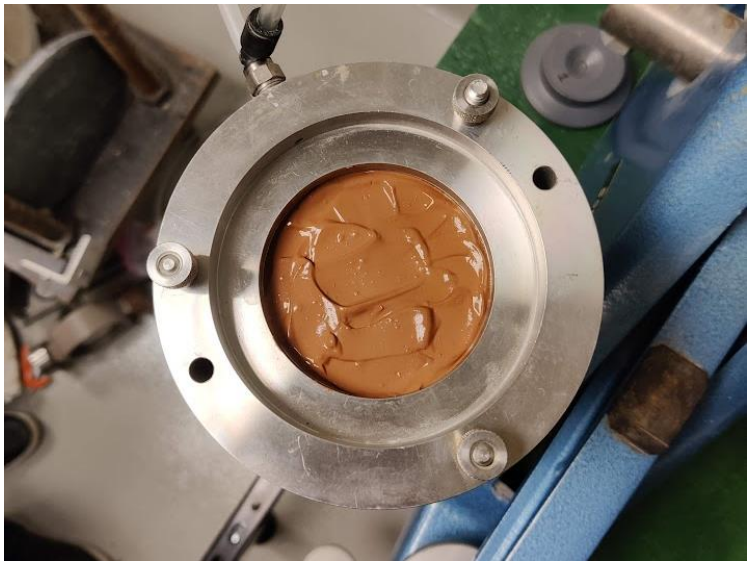

Slurry claystone for 1-dimensional in conventional oedometer

1-Dimensional consolidation test of remolded sample in Geojac

Conventional Oedometer

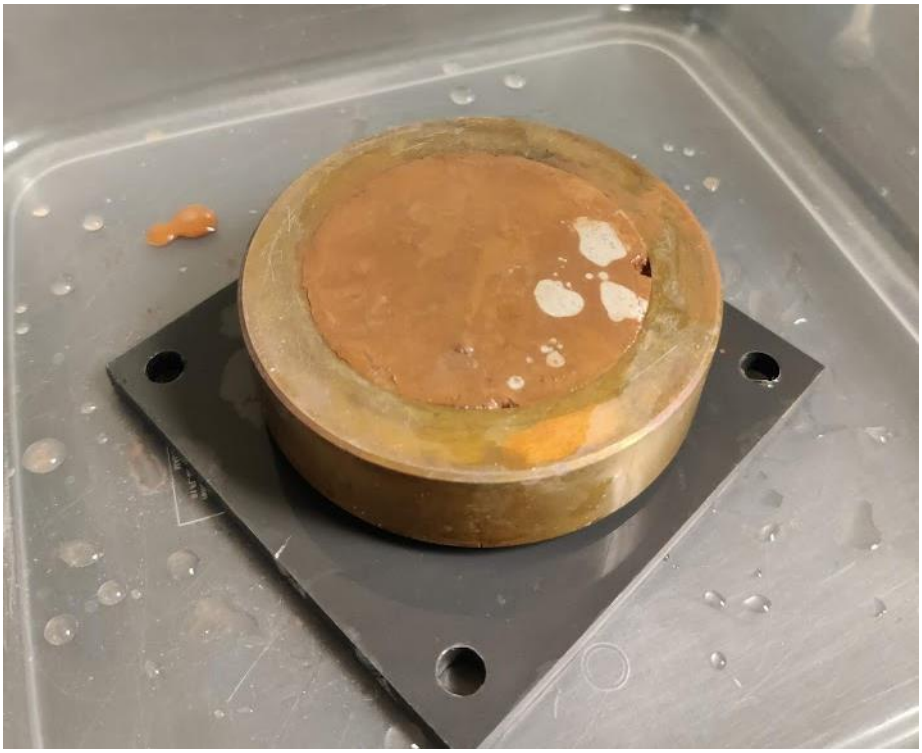

Intact sample for 1-Dimensional Consolidation Testing in a floating ring setup.